MITOCHONDRIAL TARGETING IN PHOTODYNAMIC THERAPY. METABOLIC AND DRUG STRUCTURE REQUIREMENTS FOR SPECIFIC MITOCHONDRIAL LOCALIZATION. A PILOT INVESTIGATION.

by

Melissa R. Pergande

A Thesis Submitted in

Partial Fulfillment of the

Requirements for the Degree of

Master of Science

in Chemistry

at

The University of Wisconsin-Milwaukee

December 2012

ABSTRACT

MITOCHONDRIAL TARGETING IN PHOTODYNAMIC THERAPY. METABOLIC AND DRUG STRUCTURE REQUIREMENTS FOR SPECIFIC MITOCHONDRIAL LOCALIZATION. A PILOT INVESTIGATION.

by

Melissa R. Pergande

The University of Wisconsin-Milwaukee, 2012
Under the Supervision of Dr. Guilherme L. Indig

Photodynamic therapy (PTD) has shown promise in the treatment of certain types of cancer (Davis et al. 1985, Chen 1988). One appealing strategy under consideration to selectively target tumor cells in PDT is that of mitochondrial targeting (Chen 1988, Chen 1989). The concept of mitochondrial targeting has its origin in the pioneering observation by Chen and colleagues that an enhanced mitochondrial transmembrane potential ($\Delta\Psi_{mito}$) is a prevalent tumor cell phenotype (Davis et al. 1985, Chen 1988). Because the plasma transmembrane potential is negative on the inner side of the cell, and the mitochondrial transmembrane potential is negative on the matrix side of this organelle, a variety of extensively conjugated cationinc molecules (i.e., cationic dyes) tend to accumulate in energized cell mitochondria with a high degree of specificity. In keeping with the larger transmembrane potentials typically observed in tumor cells, a number of cationic dyes were already found both to accumulate in larger quantities and be retained

for longer periods in the mitochondria of these cells as compared to normal cells (Chen 1988, Chen 1989). In these last cases, the respective (photo) toxic effects observed toward tumor cells were considerably higher than the effects observed toward normal cells (Belostotsky et al. 2011). Thus, a differential in dye loading and retention, when observed between normal and tumor cells, can provide an opportunity for the selective destruction of the latter cells via mitochondrial targeting.

The rational development of novel PDT agents for mitochondrial targeting is currently limited by the lack of a reliable model describing how the molecular structure of cationic dyes control the degree of specificity with which these agents localize in energized cell mitochondria, and may preferably accumulate in tumor cells as compared to normal cells. Likewise, the reasons why mitochondrial transmembrane potentials are typically higher in tumor cells are yet to be understood. The objectives of this project were two-fold. First, to investigate how the molecular structure and charge in a series of rhodamine dyes affects their subcellular distribution/mitochondrial localization. Second, to explore whether mitochondrial transmembrane potentials may be affected by enhanced glutaminolysis when the supply of glucose is limited. To this end, we have used a non-transformed cell line (CV-1, African green monkey kidney cells) as a biological model. Glutaminolysis is an anaplerotic pathway thought to be highly active in tumor cells.

Our findings have provided further evidence which support previous inferences on the structural requirements for rapid and selective mitochondrial localization. First, the PDT agent must be a cationic species at physiological pH. Zwitterionic species do not show these desirable properties. Second, cationic dyes showing lipophilic character similar to that of the prototypical mitochondrial marker Rhodamine-123 can be expected

to localize in energized cell mitochondria with a high degree of specificity, although such specificity is presumably lost when the lipophilic character of the cationic agent is significantly higher than that of Rhodamine-123. These studies have also indicated that the mitochondrial transmembrane potentials of CV-1 cells apparently increase when these cells experience glucose starvation and derive their energy needs primarily from glutamine/glutaminolysis. The observed effects were modest though, and very severe morphological abnormalities were simultaneously noticed. Although these results appear to represent the first line of evidence on the possibility that the enhanced mitochondrial potential typically observed in tumor cells may (at least in part) be a result of enhanced glutaminolysis, further investigations will be required in order to better explore such possibility. In addition, while the development of a single cell model for use in studies dealing with mitochondrial targeting would be highly desirable, e.g., CV-1 cultures showing either high or normal mitochondrial potentials as modulated by the characteristics of the growth media, the morphological abnormalities observed in this study (for cells grown under conditions of glucose starvation) may represent a major limitation for the development of such a biological model.

TABLE OF CONTENTS

LIST OF FIGURES

1. Introduction

2. Material and Methods

3. Results and Discussion

LIST OF TABLES

2. Material and Methods

3. Results and Discussion

LIST OF ABBREVIATIONS

Abs λ_{Max}	Wavelength of maximum absorption
ATCC	American type culture collection
ATP	Adenosine-5'-triphosphate
CCD	Charge-coupled device
CV^{+}	Crystal Violet
CV-1	African green monkey kidney cells
DPBS	Dulbecco's phosphate buffered saline
DMEM	Dulbecco's minimum essential media
DMSO	Dimethyl sulfoxide
EPR	Enhanced permeability and retention
EV^{+}	Ethyl Violet
FBS	Fetal bovine serum
Fluor λ_{Max}	Wavelength of maximum fluorescence
HeLa	Cervical cancer cells
HPD	Haematoporphyrin derivative
HPLC	High performance liquid chromatography
HT-29	Colorectal adenocarcinoma cells
IC	Internal Conversion
IR	Infrared
ISC	Intersystem crossing
MRC5	Lung fibroblast cells

MES-SA	Uterine sarcoma cells
NMR	Nuclear magnetic resonance
PII	Photofrin II
PDT	Photodynamic therapy
Rh-110	Rhodamine-110
Rh-123	Rhodamine-123
Rh-123 Br_2	Rhodamine-123 Br_2
Rh6g	Rhodamine 6g
Rh6gFA	Rhodamine 6g free acid
RhB	Rhodamine B
RhBEE	Rhodamine B ethyl ester
Rh-Oct	Rhodamine *n*-octyl ester
Rh-OctBr_2	Rhodamine *n*-octyl ester Br_2
ROS	Reactive oxygen species
S	Substrate
S_0	Ground state
S_1, S_2, S_3	Excited singlet state
^{3}Sens*	Triplet photosensitizer
T_1	Triplet state
TLC	Thin layer chromatography
TAM^+	Triarylmethanes
VR	Vibrational relaxation

ACKNOWLEDGEMENTS

To Dr. Indig for giving me the opportunity, guidance, and resources to succeed;

To my friends Andrea, Angela E., Suzanne, Angela C., and Athena who provide constant encouragement and understanding;

To my family members, especially my mother, without whom I could have never completed this journey;

You have all contributed to this work with your support and patience.

1. Introduction

Cancer is a specific group of diseases that cause normal, healthy cells to transform and grow uncontrollably. These normal-to-cancer transitions are thought to be due to certain genetic factors or exposure to mutagens. Consequently, this uncontrollable cellular growth can cause malignant tumors to develop. Unfortunately, over time many of these cellular transitions can become potentially fatal. According to the World Health Organization, 7.6 million people worldwide died (13% of all deaths) from cancer in 2008 (Ferlay et al. 2010). Consequently, certain chemotherapy and anti-cancer drugs have been developed that target the most rapidly dividing cells in the body in order to slow down the progression of these diseases. Often, this includes both normal and transformed cells. Therefore, different therapies that can be used to selectively target and kill cancer cells, while sparing the surrounding normal cells, continues to be a topic of interest. One such treatment modality that has shown promise is that of mitochondrial targeting in Photodynamic therapy.

1.1 Photodynamic Therapy

Photodynamic therapy (PDT) is the photoinduced destruction of living cells by the combined action of three essential components: a PDT agent (photosensitizer) (typically a dye showing strong absorption bands in the visible and/or near-infrared regions of the spectrum), light, and dissolved molecular oxygen (Khan et al. 1995). This therapeutic approach was first scientifically documented by Raab in 1896 when studying the effects of acridine on paramecia (algae) cultures (Schastak et al. 2008); however, it was not referred to as PDT until much later. Subsequently, in 1903 Finsen was awarded the

Nobel Prize for his work using this therapeutic approach to clinically treat diseases such as: lupus, cutaneous tuberculosis, and smallpox lesions (Dolmans et al. 2003). Since the pioneering work of the above scientists, the concept of PDT has evolved as a promising treatment for cancer. Some of the highlights in this progression include the work of von Tappeiner and Jesiokek. Notably, these authors are credited with the very first attempt to utilize this method as a clinical treatment for tumors (von Tappeiner and Jesionek 1903, Moan and Peng 2003). Later, in 1960 Lipson and colleagues were able to demonstrate that haematoporphyrin derivative (HPD) efficiently localized in tumors and emitted fluorescence, thus allowing for the photo detection of certain tumors (Lipson et al. 1961). Interestingly, the first successful treatment against cancer (skin) was not documented until 1978 when Dougherty and colleagues published results in which 111 of 113 cutaneous and subcutaneous malignant tumors were observed to be partially or completely responsive to this modality of treatment (Dougherty et al. 1978). It was in that same year that Kelly and colleagues initiated the first clinical trial of HPD to treat bladder cancer (Dolmans et al. 2003). Currently, PDT is still proposed as a method of treatment for various types of cancer including the purging of residual tumor cells from autologous bone marrow grafts in patients with leukemia, lymphoma, or metastatic neuroblastoma (Huang et al. 2003, Bergmann et al. 2008, Kessel and Oleinick 2009). Therefore, the vast potential of phototherapy has been known for over a hundred years, but the journey in successfully targeting and killing cancer cells has been gradual.

The therapeutic approach of PDT owes its success to the highly cytotoxic effects that are produced by a variety of reactive oxygen species (ROSs). This clinical treatment process is initiated by administering a certain photosensitizer into the bloodstream

intravenously or topically to the skin depending on the location of the tissue being treated. It is important to note that photosensitizers themselves are relatively unactive (prodrugs) until activated to their active state. This is done by the use of visible or near infrared light, one that is appropriate for exciting the photosensitizer to produce ROSs (Soukos et al. 1996). After the absorption of light (photons), the photosensitizer is excited from its ground state (S_0) to a short-lived excited singlet state (S_1, S_2, S_3, etc) (**Figure 1.1**). Notably, Kasha's rule states that regardless of which singlet state is originally generated upon photon absorption (i.e., S_1, S_2, S_3, etc) in condensed media, within just a few femtoseconds the population of excited states will be entirely located in the respective first electronically excited singlet state (S_1) (Kasha 1968). Subsequently, the excited photosensitizer can return to its respective ground state (S_0) either by emitting a photon (fluorescence) or through internal conversion with energy lost as heat. Alternatively, the first electronically excited singlet state (S_1) can cross, to its respective first longer-lived excited triplet state (T_1) via intersystem crossing; this involves a change in the spin of an electron. Here, the excited triplet photosensitizer (^{3}Sens*) can engage either in electron (type I) or energy (type II) transfer reactions (**Figure 1.2**). The type I reaction involves the unidirectional electron transfer between the triplet photosensitizer (^{3}Sens*) and substrate (S), such as a phospholipid in a cell membrane, to form a radical pair which can further react with dissolved molecular oxygen to produce a variety of cytotoxic ROSs including: superoxide, hydroxyl, and peroxyl radicals as well as hydrogen peroxide (Khan and Wilson 1995). In addition, these ROSs can "dismutate" to produce other ROSs (Khan and Wilson 1995). The type II reactions involve the energy transfer from the triplet photosensitizer (^{3}Sens*) to molecular oxygen thus forming

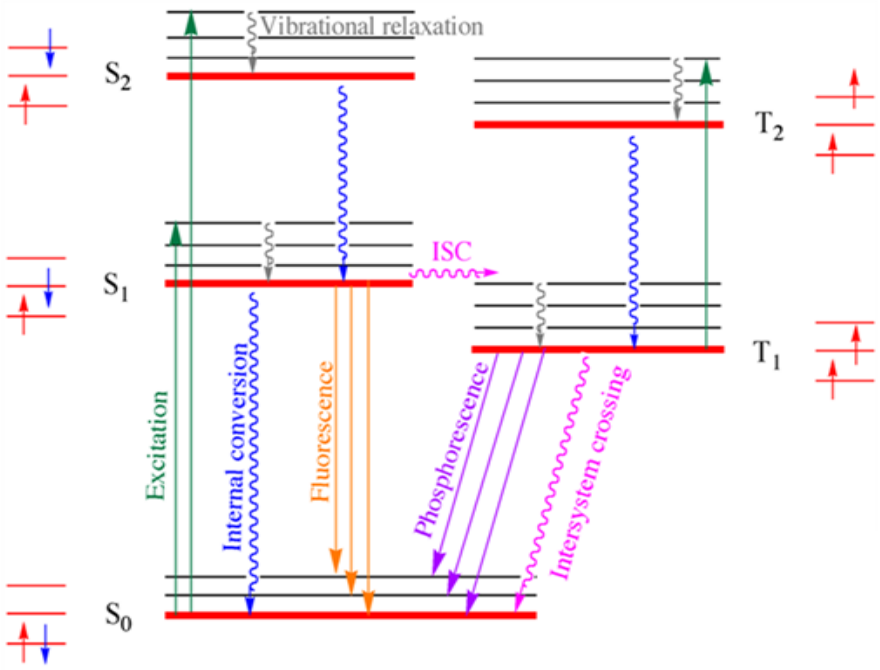

Figure 1.1 Jablonski diagram showing absorption, along with non-radiative (VR, IC and ISC), and radiative (fluorescence and phosphorescence) processes of deactivation of electronically excited states (VR=vibrational relaxation, IC=internal conversion, ISC=intersystem crossing).

$$^{3}\text{Sens}^{*} + \text{S} \rightarrow \text{Radical Pair} \xrightarrow{O_2} \text{Reactive Oxygen Species} \qquad \text{Type I}$$

$$^{3}\text{Sens}^{*} + O_2 \rightarrow {}^{1}O_2^{*} \qquad \text{Type II}$$

Figure 1.2 Type I and Type II photochemical reactions.

the ROS, singlet oxygen ($^1O_2$*). This later PDT mechanism regenerates the ground state photosensitizer, which can be subsequently used in cycles of photosensitization, and for this reason it is thought that type II reactions are more desirable in PDT. Intuitively, both the type I and type II reactions can occur simultaneously (i.e., in competition) in biological systems. Interestingly, only cells found in the immediate area of the reaction are directly affected due to the short half-lives of the various ROSs produced. For example, the half-life of singlet oxygen produced in biological systems is <0.04 μs, and its radius of action is <0.02 μm (Moan and Berg 1991). Nonetheless, through both mechanisms (type I and type II), PDT is able to induce the desired cytotoxic effects to the cells being targeted.

Photofrin II (PII) (**Figure 1.3**) is one of the most extensively used photosensitizers employed in PDT for the treatment of cancers due to it high accumulation in tumors (Dougherty et al. 1998, Dougherty 1992). It is a purified version of an oligomerized hematoporphyrin derivative (Bartlett 2002) which primarily targets the destruction of the tumor vasculature via the enhanced permeability and retention (EPR) effect rather than by direct cell kill (Maeda 2001). That is, it works by shutting down the tumor's blood supply thereby destroying the vasculature and thus promoting destruction to large areas of solid tumors. Although PII is the most commonly used photosensitizer to date, it has several limitations and undesirable properties which have limited its overall effectiveness. Interestingly, PII and other common photosensitizers are highly phototoxic in the presence of molecular oxygen, but do not work well in hypoxic areas of solid tumors (Dougherty 1988). In addition, PII and other anionic porphyrins are not as effective in the poorly vascularized internal regions of the tumor primarily because

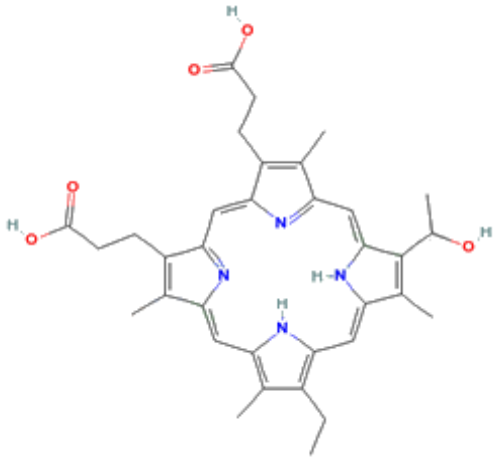

Figure 1.3 Molecular structure of Photofrin II (PII).

they work by targeting the destruction of the vasculature rather than direct cell kill (Bartlett 2002). In addition, porphyrins are not exclusively tumor targeting and display long persistence in normal tissues, including the skin. Therefore, patients often need to limit their exposure to sunlight after receiving treatment. Lastly, PII has an ideal absorption maximum of 630 nm, however, its molar absorption coefficient at this wavelength is low (ε = 1170 $M^{-1}cm^{-1}$) (Dougherty 1992, Stewart et al. 1998). Consequently, high concentrations of the photosensitizer and light must be delivered to the tumor. Since tumor localization of the photosensitizer is an important factor in the overall effectiveness of PDT, there remains an interest in developing novel photosensitizers that primarily target tumor cells with increased specificity. One appealing strategy under consideration to selectively target tumor cells in PDT is that of mitochondrial targeting.

1.1.1 Mitochondrial targeting in PDT

The concept of mitochondrial targeting has its origin in the pioneering observation by Chen and colleagues that an enhanced mitochondrial transmembrane potential ($\Delta\Psi_{mito}$) is a prevalent tumor cell phenotype (Chen 1988, Chen 1989). These authors investigated over 200 distinct cell lines (tumor and normal varieties) and demonstrated that the mitochondrial transmembrane potential is typically 60 mV higher in tumor cells than in normal cells, where only approximately 2% do not show this characteristic phenotype (Davis et al. 1985, Chen 1988). In addition, it has been observed that certain conjugated cationic molecules, dyes (potential photosensitizers) displaying the appropriate structural features, accumulate in the mitochondria of tumor cells with a high degree of specificity due to this enhanced transmembrane potential (Belostotsky et al. 2011). Notably, these cationic compounds are electrophoretically driven through the membranes and localize efficiently in the mitochondria because the plasma transmembrane potential is negative on the inner side of the cell and the inner mitochondrial transmembrane potential is negative on the matrix side of the organelle. Therefore, the idea of the selective targeting and destruction of tumor cells via mitochondrial targeting in PDT is based on the observation that a number of cationic dyes tend to naturally accumulate in larger amounts and are retained for longer periods in the mitochondria of tumor cells compared to normal cells (Bernal et al. 1993, Kandela et al. 2002).

The selective accumulation of such suitable cationic molecules may be adequately predicted using the Nernst formalism (**Figure 1.4**). Interestingly, the plasma transmembrane potential is typically -60 mV while the mitochondrial transmembrane potential is typically -120 mV for normal cells and -180 mV for tumor cells (Chen 1988).

$$[A+]_{cytoplasm} = [A+]_{outside\ the\ cell} \times 10^{-\{\Delta\Psi plasma/(2.3RT/nF)\}} \quad (1)$$

$$[A+]_{mito} = [A+]_{cytoplasm} \times 10^{-\{\Delta\Psi mito/(2.3RT/nF)\}} \quad (2)$$

$$[A+]_{mito} = [A+]_{outside\ the\ cell} \times 10^{-\{(\Delta\Psi plasma+\Delta\Psi mito)/(2.3RT/nF)\}} \quad (3)$$

Figure 1.4 Nernst equations. $\Delta\Psi$ *plasma* represents the plasma transmembrane potential (typically near -60 mV), $\Delta\Psi$ *mito* represents the mitochondrial transmembrane potential (typically –180 mV for tumor cells and –120 mV for normal cells), *R* represents the thermodynamic constant for ideal gases, *T* the absolute temperature, *n* the valence of the ion crossing the membrane, and *F* the Faraday constant. For monovalent ions, the parameter *2.3 RT/nF* assumes the value of ~ 61 mV at 37 ^{o}C (Belostotsky et al. 2011).

Equations 1-3 can be used to calculate the ratio of cationic molecules that could potentially accumulate in the mitochondria when employing the same concentration in both a tumor and normal cell line (Trapp and Horobin 2005, Belostotsky et al. 2011). When using the above numbers, the Nernst formalism predicts that the mitochondria of tumor cells can be theoretically loaded with as many as 10 times more of these selective molecules. Therefore, in addition to the observations of Chen and others (discussed above), the difference in dye loading, as predicted by the classical Nernst formalism, reinforces the premise that tumor cells can be selectively targeted with increased specificity via mitochondrial targeting and selective tumor cell kill induced.

In order for the successful mitochondrial localization of these selected cationic dyes to occur, the mechanism of mitochondrial targeting must be the dominant means of subcellular distribution. For example, one such mechanism that might preclude mitochondrial localization is that of lipophilic partitioning. Reasonably, the lipophilic

character of the cationic dye must be low enough that it is unable to compete with the mechanism of transmembrane potential-driven mitochondrial localization. If the latter is not the case, the increased loading of the cationic dye observed between tumor and normal cells, respectively, can be expected to significantly decrease or be entirely lost (Belostotsky et al. 2011); consequently, no tumor cell selectivity would be expected to occur. Comparatively, staining of other organelles would be expected to take place with the same efficiency as well (Indig et al. 2000, Kandela et al. 2002, Kandela et al. 2003, Lacerda et al 2005). Therefore, the desired distribution of cationic dyes into the mitochondria of tumor cells will be theoretically possible only if the contributions arising from the transmembrane potential-driven mechanism are greater than those arising from the mechanism of lipophilic partitioning or any other competing subcellular distribution mechanism (Belostotsky et al. 2011).

With this in mind, there are several cationic dyes that are known to naturally accumulate in the mitochondria of cells, however, only a small subset of these dyes is known to induce the desired photochemical destruction to tumor cells with a high degree of specificity (Indig 1999, Morgan et al. 2001). Some of these previously studied dyes include cationic triarylmethanes (TAM^+). For example, Crystal Violet (CV^+), a relatively low toxic dye (Indig 1999), has been employed in a variety of medicinal applications as: an antihelmintic, an antiseptic in burn patients, and for treatment of umbilical cords of newborns (Duxbury 1993), as well as an antifungal to treat both topical and vaginal infections caused by *Candida* (Remington's Pharmaceutical Sciences 1990, Bartlett 2002). Interestingly, it has been demonstrated that CV^+ localizes in the mitochondria and induces the desired phototoxic effects to tumor cells (HT-29) (Kandela et al. 2002).

Comparatively, Ethyl Violet (EV^+) is known to induce cytotoxic effects; however, Indig and colleagues demonstrated that it does not induce the destruction of tumor cells with a high degree of selectivity because not only does it localize in the mitochondria, but it is observed to accumulate in the lysosomes of both normal (CV-1) and tumor (MES-SA) cells (Kandela et al. 2002). In this case, any cell death induced by EV^+ is not primarily controlled by mitochondrial damage, rather by a more complex combination of subcellular toxic events (Kandela et al. 2002). Remarkably, the studies involving CV^+ and EV^+ are of vast importance because they reveal that only dyes that exclusively localize in the mitochondria can mediate the destruction of tumor cells with desirable degrees of selectivity. In addition, these authors demonstrated that only dyes showing a lipophilic/hydrophilic character similar to that of the prototypical mitochondrial-specific dye, Rhodamine-123 (Rh-123), are efficiently taken up by tumor cells in large quantities and display selective tumor cell kill.

Rh-123 is a member of another class of dyes (rhodamines) known to accumulate in the mitochondria of cells. It is highly fluorescent and commonly employed as a molecular probe in fluorescence microscopy. Also, it was the first dye identified by Chen and colleagues as a mitochondrial-specific agent (Summerhayes et al. 1982, Chen 1988, Chen 1989). These authors demonstrated that tumor cells uptake and retain more Rh-123 longer when compared to normal cells. Presumably, the mechanism of cellular uptake and subcellular localization (mitochondrial) of Rh-123 is controlled primarily by transmembrane potentials (Chen 1988, Chen 1989) where the dye has been observed to pass directly to the mitochondria with no staining of the plasma membrane, nuclear envelope, lysosomes, endoplasmic reticulum, or Golgi complex (Johnson et al. 1981).

Therefore, Rh-123's characteristic positive charge most likely allows for easy mitochondrial uptake and retention. Interestingly, most lipophilic, cationic molecules are toxic to cells due to their increased retention, however, studies of a vast number of cationic dyes revealed that Rh-123 specifically showed low cytotoxicity when CV-1 cells were grown in a 10 μM solution of the dye for two weeks (Lampidis et al. 1984, Chen 1988). Therefore, many research studies have demonstrated that Rh-123 is a great choice for studying living cells because it is low in cellular toxicity and allows for easy visualization using fluorescence microscopy.

The most important aspect of mitochondrial targeting, from a therapeutic viewpoint in PDT, is the fact that most mitochondrial damage can lead, and often does, to apoptosis. Ideally, any potential PDT drug candidate must show the following desirable properties to be considered an ideal agent in order to induce such desired effects: (i) strong absorption in the visible and near-IR regions of the electromagnetic spectrum, (ii) display good yields of triplet formation upon electronic excitation, (iii) effective singlet oxygen generation from the respective triplets, (iv) carry a positive charge (cationic photosensitizers typically show superior tumor cell selective properties), and (v) display a high degree of selectivity toward the targeted tumors (Sorokina 2009). Interestingly, in 2008, Rh-123 Br_2 received an orphan drug designation from the United States Food and Drug Administration for purging tumor cells from bone marrow grafts which would be used in bone marrow transplants (Villeneuve 1999, Brasseur et al. 2000, Belostotsky et al. 2011). Here, the spin-orbital coupling is enhanced by the electronic perturbation that is promoted by the substitution of bromine atoms to the parent compound (Rh-123). This leads to an increase in the intersystem crossing rate constant which results in an increase

in population of its respective triplet species. To our knowledge, Rhodamine-123 Br_2 is the only cationic mitochondrial photosensitizer to reach phase III clinical trials for cancer therapy. In summary, the mitochondrial accumulation of suitable cationic dyes, displaying the above properties, is thought to be responsible for the selective destruction of certain tumor cells at the mitochondrial level.

With this in mind, the objectives of this study were twofold. First, explore how and to which extent the molecular structure of a series of rhodamine dyes affects their subcellular localization in a chosen model non-transformed cell line (CV-1). This was motivated by the fact that it has been previously hypothesized that selective tumor cell kill can be achieved on the basis of the differences in the mitochondrial transmembrane potential typically observed between normal and tumor cell lines. Second, because all previous studies dealing with mitochondrial targeting have involved tumor and normal (non-transformed) cells of different origins (Modica-Napolitano and Aprille 2001, Belostotsky et al. 2011), we have attempted to harmonize the cell model used in these studies, in order to explore whether by inducing an increase in the mitochondrial transmembrane potential, CV-1 cells (normal vs. increased mitochondrial transmembrane varieties, respectively) could be used as an appropriate model to investigate the effects of mitochondrial targeting on selective cell kill. Here, our motivation has its origins in previous studies described by Rossignol and colleagues on the effects of energy substrate availability (glucose vs. glutamine) which aimed to study the response of the limitation of glucose in various tumor cells. These authors demonstrated that by limiting glucose and promoting oxidative phosphorylation via the anaplerotic glutamine pathway, both a non-transformed cell line (lung fibroblast, MRC5) and a tumor cell line (HeLa), were able to

adapt to these changes at the mitochondrial level (i.e., structurally) (Rossignol et al. 2004). Therefore, we have explored the spectroscopic properties of various rhodamine dye derivatives, determined which of these derivatives is exclusively mitochondrial localizing in our chosen non-transformed cell line, and explored whether CV-1 cells could potentially be used as a model to investigate the effects on selective cell kill via mitochondrial targeting.

Glucose and Glutamine as Energy Substrates

Glucose is thought to be the preferred energy substrate needed by most cells. Under aerobic conditions, mammalian cells metabolize this energy substrate through a series of catabolic reactions in the three stages of cellular respiration (**Figure 1.5**) in order to transduce energy (i.e., to promote ATP synthesis). In the first stage, glucose is converted into pyruvate (in the cytoplasm) via glycolysis (**Figure 1.6**). Subsequently, pyruvate is converted to acetyl Co-A which transfers its acetyl group to oxaloacetate to generate citric acid. This last reaction represents the major feeding pathway along the citric cycle (**Figure 1.7**). In the third stage, the NADH and $FADH_2$ molecules generated by the citric acid cycle are fed into the respiratory chain (electron transport chain) (**Figure 1.8**); it is this stage that is especially significant in the production of ATP for the cell and is best explained by the chemiosmotic theory proposed by Peter Mitchell in 1961 (Mitchell 1979). Here, the exergonic energy that results as a consequence of the flow of electrons through the respiratory chain is coupled to the simultaneous pumping of protons across the inner mitochondrial membrane (i.e., from the matrix to the intermembrane compartment). Accordingly, there are two major consequences that occur due to this

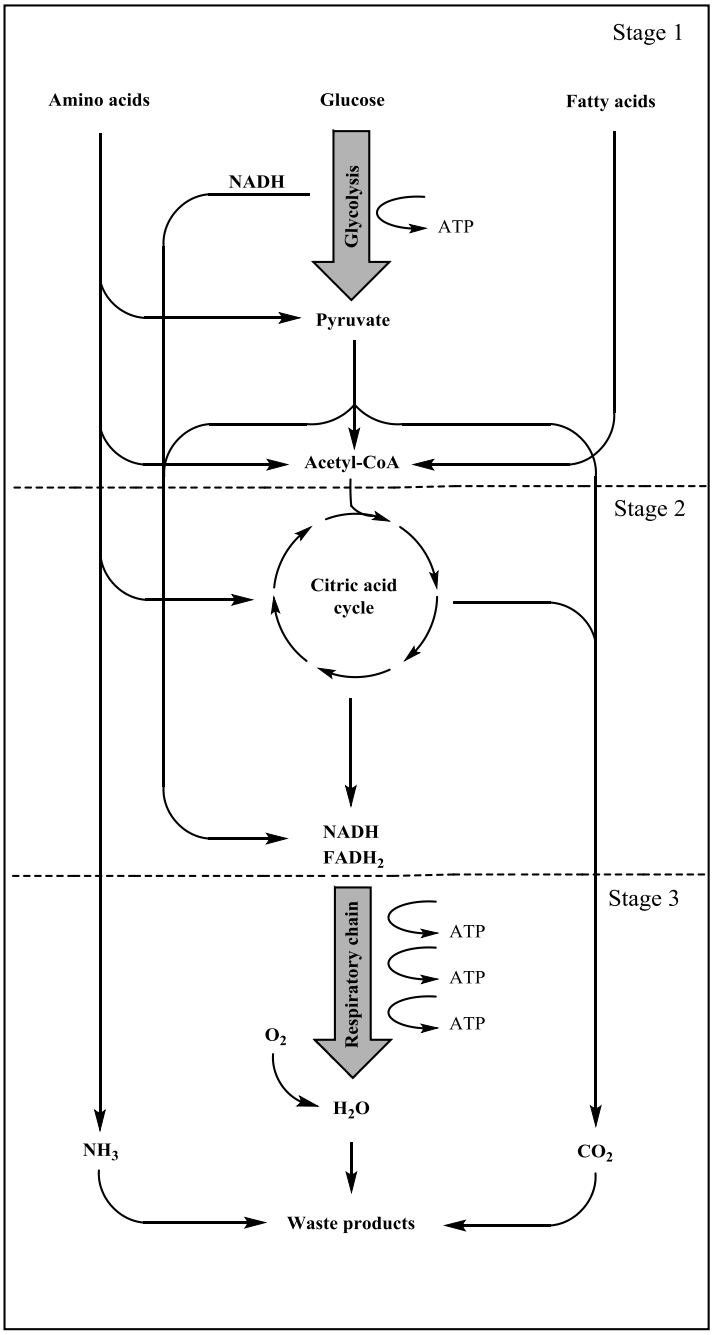

Figure 1.5 The three stages of cellular respiration (Nelson and Cox 2008).

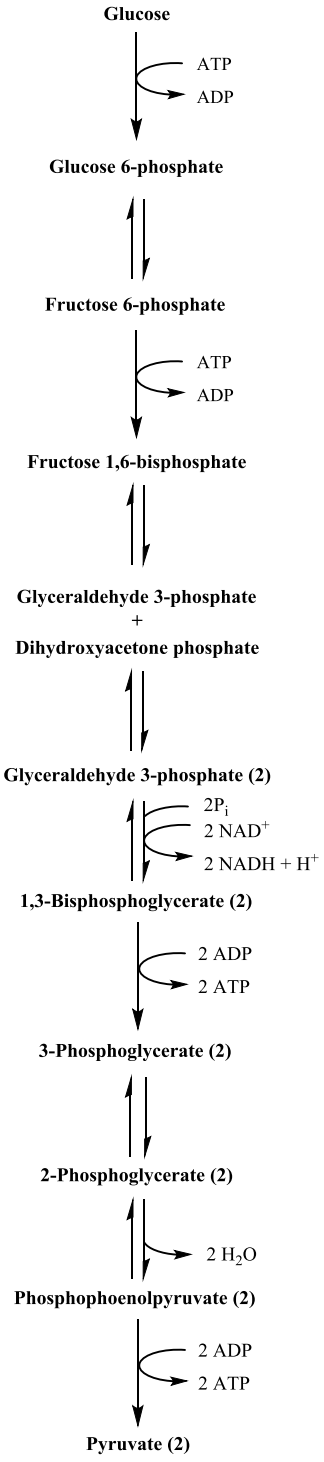

Figure 1.6 The glycolytic pathway (Nelson and Cox 2008).

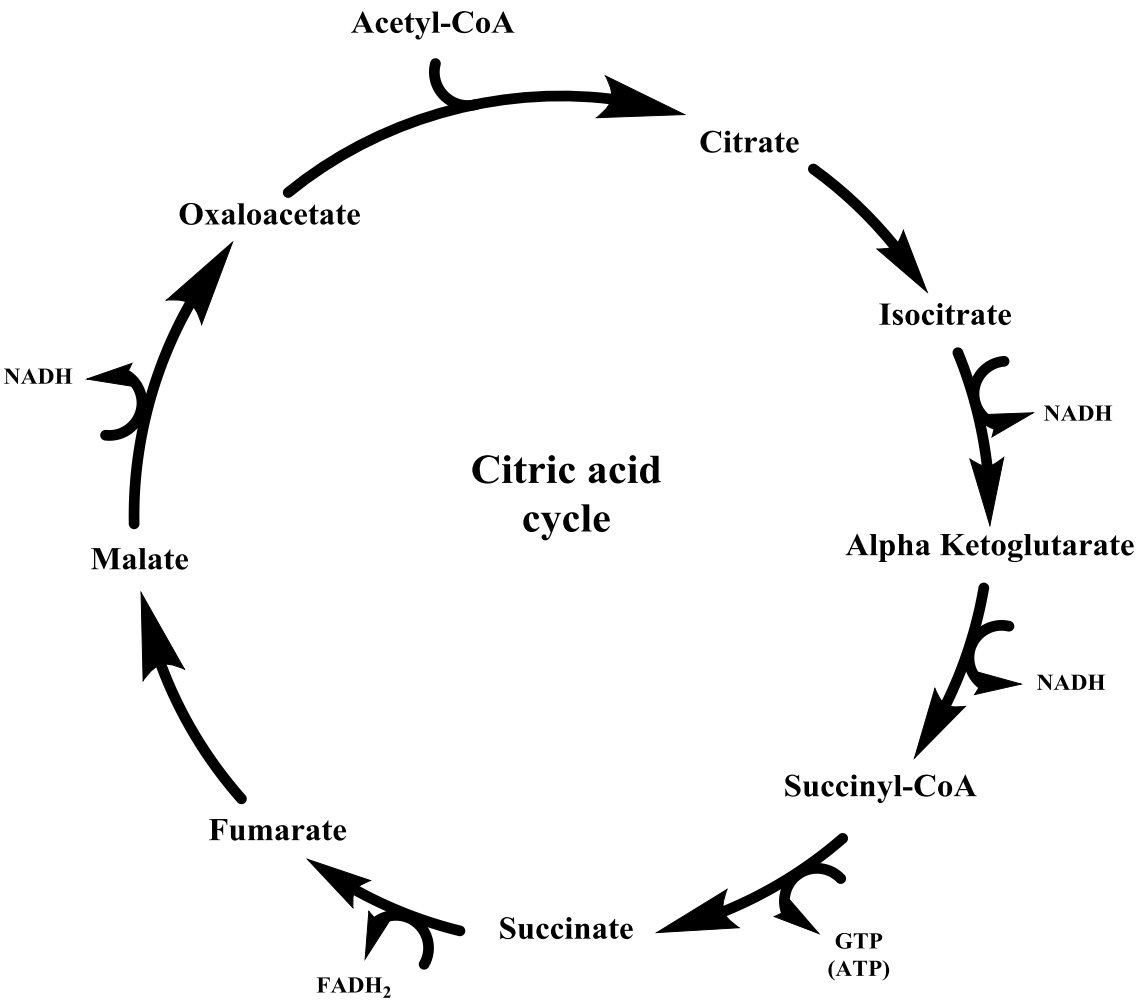

Figure 1.7 The citric acid cycle (Nelson and Cox 2008).

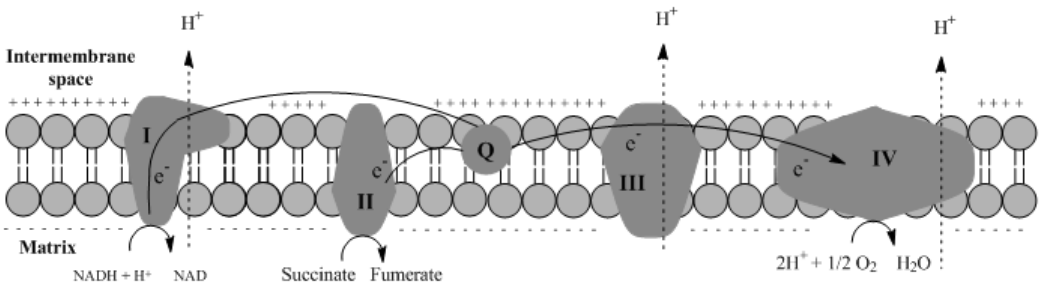

Figure 1.8 The electron transport chain (Nelson and Cox 2008).

movement of protons: (i) a pH (i.e., proton) gradient is generated across the inner mitochondrial membrane where the proton concentration is lower in the matrix compared to the cytoplasm and (ii) a voltage gradient (mitochondrial transmembrane potential) is generated across the inner mitochondrial membrane where it is negative on the inside due to the efflux of protons from the matrix side to the intermembrane mitochondrial space. Together these two forces result in a net free energy (proton-motive force) (**Figure 1.9**). Because the membrane is impermeable to protons, the protons that re-enter the matrix must pass through a proton channel lined with enzymes, the ATP synthase (F_0F_1) complex. Consequently, ATP is made using the proton-motive force as a source of energy. Through these unique reactions, mammalian cells can acquire the majority of the energy that is required for cellular growth and survival from the metabolism of the main energy substrate, glucose. However, when the availability of glucose is low, glutamine can act as a relevant substrate.

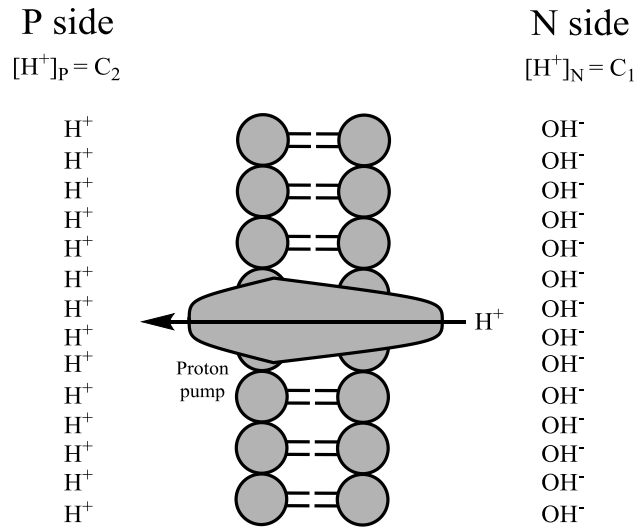

Figure 1.9 The proton-motive force. Shown here, the inner mitochondrial membrane separates two compartments of different $[H^+]$, resulting in differences in chemical concentration (ΔpH) and charge distribution ($\Delta\psi$) across the membrane. The net effect is the proton-motive force (ΔG). Here, R represents the thermodynamic constant for ideal gases, T the absolute temperature, C_2/C_1 the concentration ratio of ions on their respective side of the membrane, Z the absolute value of its electrical charge (1 for a proton), and F the Faraday constant (Nelson and Cox 2008).

Glutamine is a versatile amino acid that plays fundamental roles in the maintenance and vitality of all cells. It is the most abundant amino acid in the body, where 60% of all unbound amino acids are glutamine, the main storage being located in the musculature (Nelson and Cox 2008). Commonly, it is used in the building of muscle tissue, maintenance of optimal immune function, and is needed for the repair and maintenance of intestinal tissue (Young and Ajami 2001). In addition to these regular maintenance roles, glutamine can also be employed as a particularly convenient

alternative energy substrate when the supply of glucose is limited, which can be the case with many fast growing tumors. For example, Rossignol and collegues demonstrated that HeLa cells can achieve 98% of their ATP predominantly by the oxidation of glutamine alone (Rossignol et al. 2004). Interestingly, these authors also observed that while doing so HeLa cells, as well as osteosarcoma cells, adapted their mitochondrial network structurally and functionally in order to derive energy from glutamine. Intuitively, the utilization of glutamine as an energy substrate may correlate between these observed structural changes because the anaplerotic metabolism of glutamine (**Figure 1.10**) takes place in the mitochondria where the enzymes needed for its metabolism (glutaminase and glutamate dehydrogenase) are located (Kovacevic and McGivan 1983, Matsuno et al. 1987). In this organelle, glutamine is first converted to glutamate by the amidohydrolase enzyme, glutaminase. Next, glutamate is converted into α-ketoglutarate by glutamate dehydrogenase and subsequently entered into the citric acid cycle (**Figure 1.7**) and ultimately the electron transport chain (**Figure 1.8**) thus providing the cell with an alternative energy source. Therefore, due to the increased needs of energy for growth and survival, certain tumor cell lines have been observed to obtain significant energy by metabolizing additional energy substrates, such as glutamine, when the availability of glucose is limited.

Researchers have also observed that certain tumor cells cannot survive in the absence of glutamine and therefore, exhibit a "glutamine addiction" (Wise et al. 2008). Classical studies conducted by Eagle in determining the optimal media formulary for certain mammalian cell lines, revealed that glutamine was generally needed in concentrations much higher than other amino acids (Eagle 1955). Interestingly, Eagle

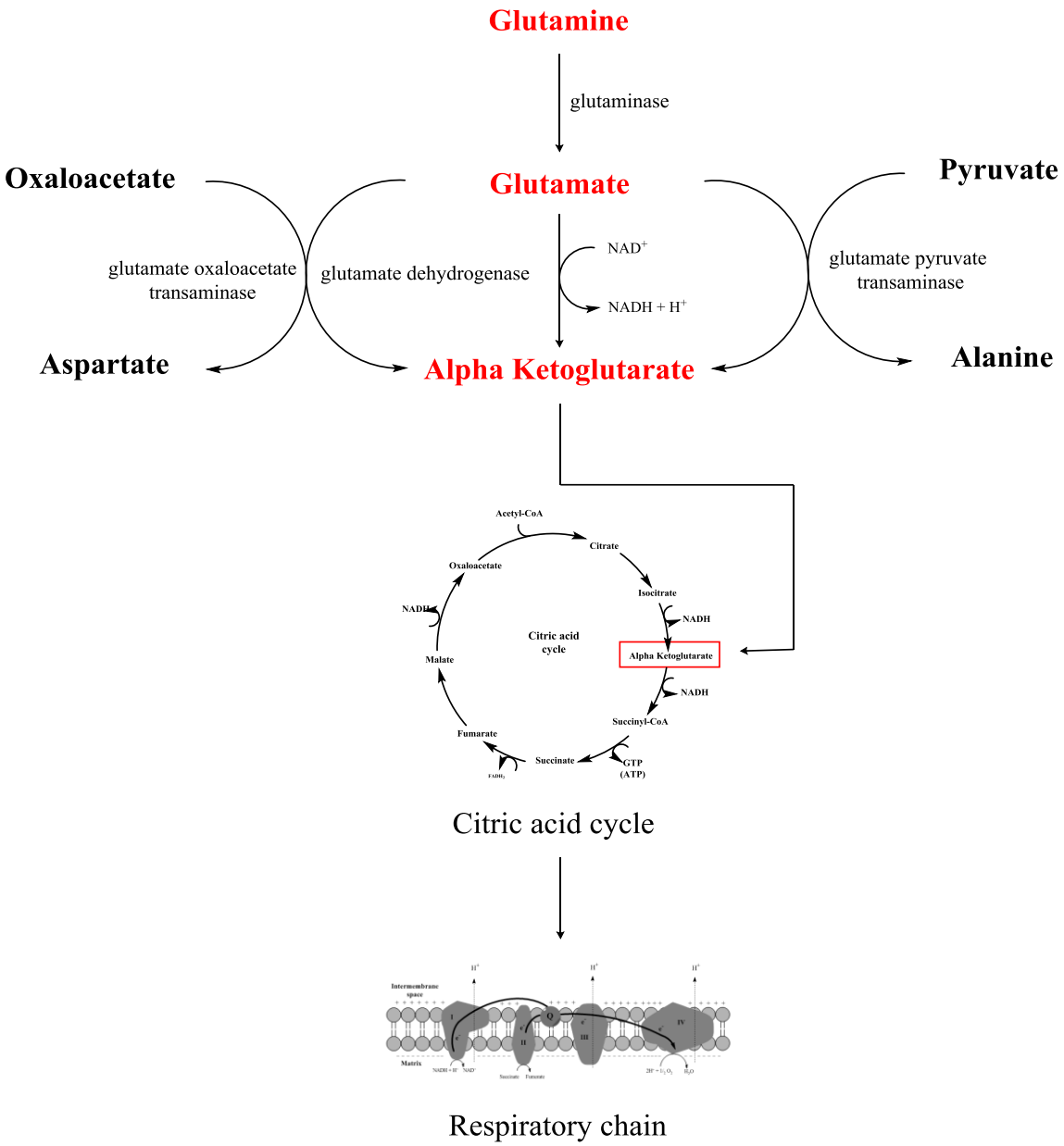

Figure 1.10 The catabolism of glutamine to the citric acid cycle intermediate, α-ketoglutarate (Eigenbrodt and Mazurek 2011).

also observed that glutamine plays an essential metabolic role in certain tumor cells (HeLa) that glutamic acid could not satisfy, where up to 20 times as much glutamic acid compared to glutamine was required to obtain comparative growth. More recently, even in the presence of ample glucose, pancreatic cancer cells deprived of glutamine displayed no cellular proliferation (Kaadige et al. 2009). Therefore, glutamine has proven to be not only be an alternative energy substrate for fast growing cells, but essential even in high glucose media.

The objective of the last part of our study was to explore the effects of energy substrate availability in our chosen non-transformed cell model (CV-1). This was done in order to explore whether or not an enhanced mitochondrial transmembrane potential could be induced by the stimulation of the anaplerotic pathway of glutaminolysis. Ultimately, this pilot study will provide useful information for the future development of a single, same cell model in which the effects of mitochondrial targeting on selective cell kill could be explored. In order to satisfy this objective, the main energy substrate glucose was removed from the cell culture media and replaced with an ample supply of glutamine. Ideally, this would suppress the metabolic process of glycolysis and force the cells to achieve the majority of their energy primarily from the catabolism of glutamine. In theory, this method would increase the contribution of oxidative phosphorylation, in cell energy transduction (compared to glycolysis) while potentially inducing an increase in the mitochondrial transmembrane potential. Ideally, such increase in inner mitochondrial potential would permit the use of a single cell line (here the CV-1 cell line) in studies dealing with the question of how and to which extent molecular structure may affect the specificity with which more cationic species accumulate in the mitochondria of

tumor cells.

2. Material and Methods

2.1 Materials

2.1.1 Chemical Reagents, Biologicals, and Disposables

Rhodamine-110 (Rh-110), Rhodamine-123 (Rh-123), Rhodamine B (RhB) and Rhodamine 6g (Rh6g) were obtained from Acros Organics (Morris Plains, NJ). Ethyl alcohol, methyl alcohol, sodium hydroxide, hydrochloric acid, acetone, filter paper (#2 qualitative), sulfuric acid, ammonium chloride, 3Å molecular sieves, ethyl acetate, silica gel TLC plates, neutral aluminum oxide TLC plates, dichloromethane, Penicillin-Streptomycin (10,000 I.U./ml Penicillin and 10,000ug/ml Streptomycin), fetal bovine serum (FBS), dialyzed fetal bovine serum, Trypan Blue biological stain, glutamine, glucose, 0.25% trypsin-0.03% EDTA, and 0.25% trypsin-0.03% EDTA in saline (without glucose), ethyl alcohol, hydrochloric acid, and sodium hydroxide were purchased from Fisher Scientific (Pittsburgh, PA). Sodium bicarbonate, neutral aluminum oxide Dulbecco's Phosphate Buffered Saline without calcium and magnesium (DPBS), Dulbecco's Phosphate Buffered Saline with calcium and magnesium were obtained from Sigma-Aldrich Chemical Co. (St. Louis, MO). Anhydrous ethanol for spectroscopic experiments was acquired from Electron Microscopy Sciences (Hatfield, PA). Rhodamine *n*-octyl ester (Rh-Oct) was previously synthesized in our laboratory via Fisher esterification of Rh-110, using *n*-octyl alcohol and anhydrous hydrochloric acid (Belostotsky et al. 2011). In addition, Rhodamine-123 Br_2 (Rh-123Br_2) and Rhodamine *n*-octyl ester Br_2 (Rh-OctBr_2) were also previously synthesized in our laboratory via electrophilic aromatic halogenation of the parent dyes: Rh-123 and Rh-Oct (Sorokina 2009). African green monkey kidney (CV-1) cells (ATCC, CCL-70) and Amphotericin B

(25μg/mL) were obtained from the American Type Culture Collection (Manassas, VA). All Dulbecco's Minimum Essential Media (DMEM) used in this study: high glucose with glutamine (#11965), high glutamine without glucose (#11966), and high glucose without glutamine (#11960) were obtained from Invitrogen (Carlsbad, CA). Carbon dioxide gas was purchased from Praxair (Danbury, CT). MitoTracker Deep Red 633 was obtained from Molecular Probes (Eugene, OR). Water was distilled, deionized, and filtered before use (Millipore Milli-Q system; resistivity, 18 $M\Omega cm^{-1}$). All chemicals were high purity grade, and, unless otherwise stated, used as received. Disposables such as: 33mm neck bottle filters (0.22μm), sterile centrifuge tubes, 35mm diameter culture dishes containing glass coverslip bottoms, serological pipettes, $75cm^2$ culture flasks, pipette tips, and gloves were all obtained from Fisher Scientific (Pittsburgh, PA).

2.1.2 Instruments

Spectroscopic measurements were carried out on a Shimadzu UV-2101 PC spectrophotometer (Kyoto, Japan). The fluorescence emission and quantum yield experiments were performed using a Timemaster Strobemaster fluorometer from Photon Technology International, Inc. (South Brunswick, NJ) which has been factory-calibrated to provide corrected emission spectra. Acquired spectra were plotted and analyzed using a graphing software package (Igor Pro 6) from Wave Metrics Inc. (Portland, OR). Analysis and characterization of synthesized dyes was performed by High Performance Liquid Chromatography (HPLC), mass spectrometry, and ^1H NMR. HPLC analyses were performed on a HP1100 system from Agilent Technology (Palo Alto, CA) equipped with an auto-injector, auto-collector, and diode array detector. Mass spectrometry data was

acquired using a VG AutoSpec mass spectrometer (UK, Manchester). NMR spectra were acquired on a 300MHz spectrometer model Spectrospin DPX300 from Bruker (Billerica, MA). Microscopy experiments were carried out on an inverted microscope model Eclipse TE2000-U from Nikon equipped with an epi-florescence module model TE 2000T-Fl (Nikon) and a back-illuminated CCD camera model Cascade 512B from Photometrics (Tucson, AZ). Image acquisition and analysis were carried out using a software package (MetaMorph) from Universal Imaging Corp. (Downingtown, PA). In addition, microscopy objectives, model Plan Fluor (10x, NA =0.3) and an oil immersion objective model Plan Apo (60x, NA = 1.4), as well as the appropriate sets of long-pass dichroic and band-pass filters: 528 $\pm$ 19 nm region (490 $\pm$ 10 nm excitation) and 685 $\pm$ 20 nm region (635 $\pm$ 10 nm excitation) (Chroma, Rockingham, VT) were used to aid in microscopy experiments.

2.2 Methods

2.2.1 Buffer Preparation

Powdered DPBS was taken from refrigeration and allowed to warm to room temperature. Next, the complete buffer was prepared according to the manufactures specification using autoclaved, ultra pure Milli-Q water, a 3L Erlenmeyer flask, a large octagonal stir bar, and a magnetic stir plate and subsequently allowed to mix at room temperature until all the solid was dissolved. Next, a pH electrode was inserted and used to monitor the pH while adjusting it to 7.2 $\pm$ 0.2 with a few micro liters of 1M HCl or 1M NaOH. After adjusting the pH, the completed buffer was filtered using a 33mm bottle-top filter (0.22μM) into sterile 500mL glass bottles. In addition, the DPBS with calcium and

magnesium was prepared in the same manner as stated above.

2.2.2 Media Preparation

Dulbecco's Modified Eagle Media (DMEM) was supplemented with precise quantities of glucose and glutamine in order to form 4 different DMEM media. Next, media #1 (4500 mg/L glucose and 584 mg/L glutamine), media #2 (0 mg/L glucose and 4234 mg/L glutamine), media #3 (4500 mg/L of glucose and 4234 mg/L glutamine), and media #4 (4500 mg/L of glucose and 0 mg/L glutamine) were supplemented with 10% FBS, 2% Penicillin-Streptomycin solution, and 0.2% Amphotericin B. In the case of media #2, dialyzed FBS was used to avoid the addition of serum sugar. Subsequently, a pH electrode was inserted and used to monitor the pH while adjusting each of the DMEM media solutions to 7.2 ± 0.2 with a few micro liters of 1M HCl or 1M NaOH if needed. In addition, all the media solutions contained the pH indicator phenol red which was used to visually verify physiological pH during all experiments. Furthermore, the formulary for each prepared media can be seen in **Table 2.1.** Lastly, all media solutions were filtered into sterile 500mL glass bottles using a 33mm bottle-top filter (0.22μM) prior to use.

Components	Media #1	Media #2	Media #3	Media #4
Amino Acids				
Glycine	30 mg/L	30 mg/L	30 mg/L	30 mg/L
L-Arginine hydrochloride	84 mg/L	84 mg/L	84 mg/L	84 mg/L
L-Cysteine·2HCl	63 mg/L	63 mg/L	63 mg/L	63 mg/L
L-Glutamine	584 mg/L	4234 mg/L	4234 mg/L	0 mg/L
L-Histidine hydrochloride·H_2O	42 mg/L	42 mg/L	42 mg/L	42 mg/L
L-Isoleucine	105 mg/L	105 mg/L	105 mg/L	105 mg/L
L-Leucine	105 mg/L	105 mg/L	105 mg/L	105 mg/L
L-Lysine hydrochloride	146 mg/L	146 mg/L	146 mg/L	146 mg/L
L-Methionine	30 mg/L	30 mg/L	30 mg/L	30 mg/L
L-Phenylalanine	66 mg/L	66 mg/L	66 mg/L	66 mg/L
L-Serine	42 mg/L	42 mg/L	42 mg/L	42 mg/L
L-Threonine	95 mg/L	95 mg/L	95 mg/L	95 mg/L
L-Tryptophan	16 mg/L	16 mg/L	16 mg/L	16 mg/L
L-Tyrosine disodium salt dihydrate (2Na·$2H_20$)	104 mg/L	104 mg/L	104 mg/L	104 mg/L
L-Valine	94 mg/L	94 mg/L	94 mg/L	94 mg/L
Vitamins				
Choline chloride	4 mg/L	4 mg/L	4 mg/L	4 mg/L
D-Calcium pantothenate	4 mg/L	4 mg/L	4 mg/L	4 mg/L
Folic Acid	4 mg/L	4 mg/L	4 mg/L	4 mg/L
Niacinamide	4 mg/L	4 mg/L	4 mg/L	4 mg/L
Pyridoxine hydrochloride	4 mg/L	4 mg/L	4 mg/L	4 mg/L
Riboflavin	0.4 mg/L	0.4 mg/L	0.4 mg/L	0.4 mg/L
Thiamine hydrochloride	4 mg/L	4 mg/L	4 mg/L	4 mg/L
i-Inositol	7.2 mg/L	7.2 mg/L	7.2 mg/L	7.2 mg/L
Inorganic Salts				
Calcium Chloride ($CaCl_2$) (anhyd.)	200 mg/L	200 mg/L	200 mg/L	200 mg/L
Ferric Nitrate ($Fe(NO_3)3"9H_2O$)	0.1 mg/L	0.1 mg/L	0.1 mg/L	0.1 mg/L
Magnesium Sulfate ($MgSO_4$) (anhydrous)	97.67 mg/L	97.67 mg/L	97.67 mg/L	97.67 mg/L
Potassium Chloride (KCl)	400 mg/L	400 mg/L	400 mg/L	400 mg/L
Sodium Bicarbonate ($NaHCO_3$)	3700 mg/L	3700 mg/L	3700 mg/L	3700 mg/L
Sodium Chloride (NaCl)	6400 mg/L	6400 mg/L	6400 mg/L	6400 mg/L
Sodium Phosphate monobasic ($NaH_2PO_4·H_2O$)	125 mg/L	125 mg/L	125 mg/L	125 mg/L
Other Components				
Phenol Red	15 mg/L	15 mg/L	15 mg/L	15 mg/L
D-Glucose (Dextrose)	4500 mg/L	0 mg/L	4500 mg/L	4500 mg/L

Table 2.1 Formulary of all media used: media #1 (optimal glucose/optimal glutamine), media #2 (no glucose/ high glutamine), media #3 (optimal glucose/high glutamine), and media #4 (optimal glucose/no glutamine).

2.2.3 Synthesis of Rhodamine 6g Free Acid

The Rh6g free acid derivative was synthesized by the saponification of its respective parent dye (**Figure 2.1**). The reaction was carried out by dissolving 0.475g of Rh6g in 100mL of distilled, deionized, and filtered water ($18M\Omega cm^{-1}$). Approximately 20mL of ethanol was added to the mixture until all of the Rh6g was dissolved. An initial standard 1mL aliquot of the mixture was taken for HPLC analysis. Next, 1mL of 1M sodium hydroxide was added to the reaction mixture and continuously stirred under heat with the assistance of an octagonal stirring bar, and a magnetic stirring plate for 24 hours. The progress of the reaction was monitored by HPLC (reverse phase C18 column; mobile phase: 75% methanol and 25% 100mM aqueous NH_4Cl) (see Results and Discussion). After the HPLC data indicated that the reaction was brought to completion (100% yield), the reaction was neutralized with hydrochloric acid. Next, any excess ethanol and water were removed by roto-evaporation. Afterwards, the dried product was dissolved in acetone and cooled to 5^oC for 24 hours. After 24 hours, any salt in the mixture was removed by cold filtration and the remaining elutant was subjected to roto-evaporation to remove all acetone. Lastly, the solid sample was dried under vacuum at 40^oC overnight. The identity of the newly synthesized Rh6g derivative was confirmed by mass spectrometry and ^1H NMR (see Results and Discussion).

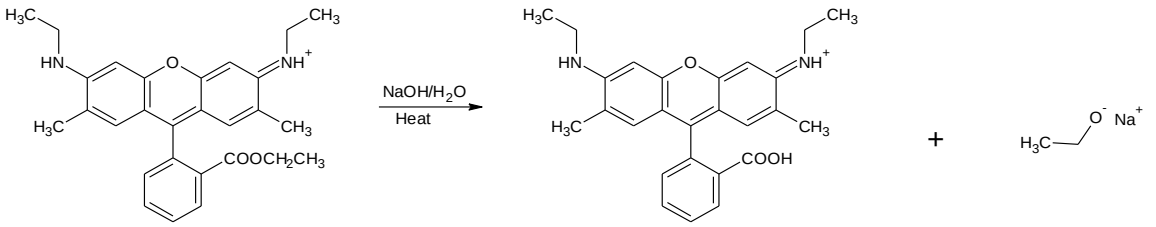

Figure 2.1 The saponification of Rhodamine 6g resulting in Rhodamine 6g free acid.

2.2.4 Synthesis of Rhodamine B Ethyl Ester

The RhB derivative was synthesized via Fischer esterification of the parent dye using ethyl alcohol (**Figure 2.2**). The reaction was carried out by dissolving 0.712g of RhB in 75mL of anhydrous ethanol (acquired by the use of heat activated 3Å molecular sieves). An initial standard 1 mL aliquot was taken for HPLC analysis (reverse phase C18 column; mobile phase: 75% methanol and 25% 100mM aqueous NH_4Cl). Next, the mixture was exposed to anhydrous gaseous HCl (50 mmol) which was generated slowly by the addition of hydrochloric acid (36%) to concentrated sulfuric acid. After the HPLC data indicated that the reaction was brought to completion (92% yield), ethyl acetate was added in excess to decrease possible hydrolysis of the newly synthesized product. Subsequently, the reaction mixture was neutralized by the addition of sodium bicarbonate until no more CO_2 bubbles were seen (approximately 20g). The remaining mixture was cooled to 5^oC and any excess sodium bicarbonate, as well as the sodium chloride byproduct, was removed by cold filtration. After filtration, the excess ethanol and ethyl acetate were removed by roto-evaporation. Lastly, the solid sample was dried under vacuum at 40^oC overnight.

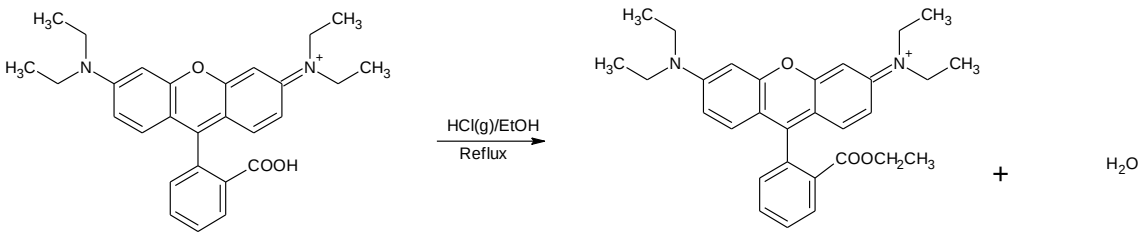

Figure 2.2 Fisher esterification of Rhodamine B resulting in Rhodamine B ethyl ester.

2.2.5 Purification of Rhodamine B Ethyl Ester

The desired product and starting material were separated using wet column chromatography. Analysis of silica gel and neutral alumina TLC plates were done to find optimal conditions for a separation mixture. To this end, neutral aluminum oxide (80–200 mesh) was made into a dichloromethane slurry and packed into a column under atmospheric pressure. The final crude product was dissolved in dichloromethane and loaded onto the column and the dye of interest removed by a 19:1 (v/v) mixture of dichloromethane: methanol mobile phase. A total of 18 fractions were collected and analyzed by HPLC (reverse phase C18 column; mobile phase: 90% methanol and 10% 100mM aqueous NH_4Cl). Pure fractions 2-4 were combined and dried by roto-evaporation and analyzed using the same HPLC condition as described above to confirm purity (see Results and Discussion). Lastly, the solid sample was dried under vacuum at 40^{o}C overnight. The identity of the newly synthesized RhB derivative was confirmed by mass spectrometry and ^{1}H NMR (see Results and Discussion).

2.2.6 Spectroscopic Experiments

Fresh stock solutions of Rh-123, Rh-110, Rh-Oct, Rh6g, RhB, Rh-123Br_2, and Rh-OctBr_2, as well as the newly synthesized free acid and ethyl ester derivatives of Rh6g and RhB, respectively (Rh6gFA and RhBEE), were prepared in anhydrous ethanol. The absorption spectrum of each dye was investigated in the 200-700nm range using an UV-visible spectrophotometer, and with a spectroscopic resolution of 1nm. Next, the newly acquired spectra were plotted via Igor graphing software and subsequently examined to find the maximum wavelength of each at their respective peak absorbance.

Similarly, 10mL of each dye solution was prepared by diluting the respective stock solutions with anhydrous ethanol so that each new solution had similar absorbances at the chosen excitation wavelength for fluorescence experiments. Furthermore, this dilution process was done in triplicates, using calibrated glassware, and making sure that the absorbance of each solution was kept below 0.05 at each dye's respective peak absorbance (investigated prior) in order to avoid inner-filter effects (Demas et al. 1971). Corrected fluorescence spectra were recorded using a Timemaster Strobemaster fluorometer. Lastly, the acquired fluorescence spectra were plotted via Igor graphing software. In addition, the fluorescence quantum yields were calculated (**Figure 2.3**) using Rh-123 (dissolved in ethyl alcohol) as the fluorescence standard ($\Phi_{Rh\text{-}123}$ =0.86) (Pal et al. 1996).

$$\Phi_X=\Phi_R(A_R/A_X)(B_X/B_R)(I_R/I_X)(n_X/n_R)^2$$

Figure 2.3 Equation used to calculate the fluorescence quantum yields (Demas et al. 1971, Indig et al. 1996). Here, Φ is the quantum yield, A is the absorbance of the solution at the excitation wavelength, B is the integrated area under the corrected emission spectrum, I is the relative intensity of the light at the excitation wavelength, and n is the refractive index of the solvent. The subscripts x and r refer to the unknown and reference solutions, respectively.

2.2.7 Rhodamine Dye and MitoTracker Deep Red 633 Preparation for Cell Culture Experiments

Fresh stock solutions of Rh-123, Rh-110, Rh-Oct, Rh6g, RhB, Rh-123Br_2, Rh-OctBr_2, as well as the newly synthesized free acid and ethyl ester derivatives, Rh6gFA and RhBEE, were prepared in anhydrous ethanol. The concentration of each of the stock solutions was determined using a UV-visible spectrophotometer (spectroscopic resolution of 1nm), the Beer-Lambert law (**Figure 2.4**), and each dye's respective molar extinction coefficient (**Table 2.2**) (Sorokina 2009); the molar extinction coefficients for RhBEE and Rh6gFA are the same as their respective parent dyes (Pal et al. 1996). Solutions of the rhodamine dyes used in the microscopy experiments were prepared in ethanol by diluting the stock solutions in a way that the final dye concentration in the cell culture media used for incubation would be 1µM and the final ethanol content at the 0.5% level. Lastly, a 1µM MitoTracker Deep Red 633 solution was freshly prepared in DMSO according to the manufacture's specification. Furthermore, the final DMSO content of the above solution was always maintained at the 0.02% level.

$$A = \varepsilon \cdot b \cdot c$$

Figure 2.4 The Beer-Lambert law used to calculate the concentration of the rhodamine dyes used in CV-1 cells for imaging. Here, ε is the molar absorbtivity with units of L $mol^{-1}cm^{-1}$, *b* is the path length in cm of the sample (specifically the path length of the cuvette in which the sample is contained), and *c* is the concentration of the compound in solution, expressed in mol L^{-1}.

Dye	**$\varepsilon_{\lambda max}$(EtOH) (x 10^3)**
Rh-123^+	8.52
RhB	10.6
$Rh6g^+$	11.6
Rh-Oct^+	8.52
Rh-$123Br_2^+$	7.25
Rh-$OctBr_2^+$	7.41

Table 2.2 Molar extinction coefficients (L $mol^{-1}cm^{-1}$) of rhodamine dyes in ethanol (Sorokina 2009).

2.2.8 The Biological Model

One million previously frozen CV-1 cells were taken from cryogenic storage and thawed in a 37^{o}C 50% ethyl alcohol and 50% water bath. Immediately after the cells were thawed, the cell culture was started by transferring the cells into a sterile 75cm^{2} canted neck cell culture flask with the use of a 1mL sterile serological pipette. Next, 15mL of media #1 was added to the flask. The flask was then sealed and placed in an incubator at 37^{o}C, 5% CO_2, and 86% humidity. After 24 hours, the culture flask was checked by microscopy in order to determine if the cells had adhered to the bottom. After determining that the cells had successfully attached, the old media was removed from the culture flask and replaced with 15mL of fresh media using sterile technique in order to remove any unattached, dead cells. The culture flasks were then monitored daily for growth. Typically, the old culture media was replaced with 15mL of fresh media solution every 2-3 days. In addition, the cells were allowed to grow until nearly 80% confluent (as evaluated by visual inspection). Subsequently, viability was verified by Trypan Blue staining and the cells were subcultured at a 1:3 subcultivation ratio twice before any experiments were preformed.

2.2.9 Cell Culture Maintenance and Sample Preparation

The cell culture media was replaced with fresh media solution every 2-3 days while the cells were growing in the incubator. Prior to changing the culture media or preparation of any samples for experimentation, the laminar flow hood was sterilized with a 70% ethyl alcohol solution followed by 30 minutes of exposure to UV light. The fresh media solution of choice was warmed in a 37^{o}C 50% ethyl alcohol and 50% water

bath while the UV light was sterilizing the hood. The old culture media was removed via a sterile serological pipette and replaced with 15mL of fresh, pre-warmed media solution with the aid of an additional sterile serological pipette.

The cell culture population was divided once the cells had become nearly 80% confluent (as evaluated by visual inspection), characteristically every 3 to 4 days. This process was initiated by removing the old culture media with a sterile serological pipette as previously described above. The pre-confluent monolayer was washed twice with 10-15mL of DPBS and discarded in order to remove any residual FBS. To detach the cells, 3mL of trypsin-EDTA solution was added to each 75cm^2 culture flask. After the enzyme solution was added, the culture flask was recapped and allowed to sit under the hood for 5 minutes. Next, the flask was removed from the hood and immediately viewed by microscopy in order to determine if the cells were small and sphere-like, indicating efficient trypsin activity. In addition, the cells ability to dissociate from the pre-confluent monolayer was tested by gently tapping the sides of the culture flask. Once confirmation that the cells were detaching from the surface was obtained, 10mL of fresh media solution was added to the flask via a sterile serological pipette in order to inhibit further trypsin activity. At this point, the same pipette was used to detach the cells by gently agitating the mixture up and down several times in order to break apart any cell clumps and consequently wash all cells off from the culture flask surface. Next, the detached cell culture population was divided and passed into new 75cm^2 culture flasks at a 1:3 subcultivation ratio as recommended by the ATCC. In addition, a 0.5mL aliquot was kept to verify viability of the cell culture using Trypan Blue staining. Lastly, 15mL of fresh media solution was added to each new flask and placed in the incubator.

In the case of sample preparation, all CV-1 cells were harvested in the exponential growth phase in their respective media solution as recommended by the ATCC. The plating process was initiated by removing the media solution and detaching the cells as previously described above. In addition, the cells were plated at a density of 30,000 cells per 3mL of growth media on small petri dishes containing a glass coverslip bottom (35mm diameter) and incubated 24 hours prior to examination.

2.2.10 Subcellular Localization Studies

Before acquiring microscopy images, the cells were incubated simultaneously for 1 hour in growth media #1 in the presence of the desired rhodamine dye (1μM for Rh-123, Rh-110, Rh-Oct, Rh-123Br_2, and Rh-OctBr_2 or 0.5μM for Rh6g, Rh6gFA, RhB, and RhBEE) and 1μM of MitoTracker Deep Red 633. After the initial incubation period, the cells were washed twice with 1-1.5mL DPBS and the fluorescence images recorded immediately in fresh DPBS solution containing calcium and magnesium.

2.2.11 Metabolism Studies

2.2.11.1 Comparison of Early Changes in Cellular Morphology and Mitochondrial Transmembrane Potential in CV-1 Cells Every 4 Hours for 0-48 Hours

CV-1 cells were harvested in exponential growth phase and detached as previously described in section 2.2.9. After detaching the cells, the cell culture solution was split into two separate 15mL centrifuge tubes. The cells in centrifuge tube #1 were used as the control. These cells were counted and viability verified by Trypan Blue staining and subsequently plated at a density of 30,000 cells per 3mL of media #1.

Centrifuge tube #2, containing the second half of the detached cell culture solution, was centrifuged at 4000 rpm for 5 minutes. After centrifugation, the media was immediately decanted in order to remove any old culture media and the pellet immediately resuspended in media #2 and centrifuged a second time under the same conditions as described above. Next, the media was decanted a second time and the pellet resuspended in a fresh aliquot of media #2. The newly suspended cells were then counted, their viability verified by Trypan Blue staining, and plated at a density of 30,000 cells per 3mL of their new media. Lastly, all of the dishes containing the newly plated cells were placed in the 37^{o}C incubator.

The dishes were examined every 4 hours for any early changes (for 48 hours) in cellular morphology and mitochondrial transmembrane potential when switched from media #1 to media #2. Before acquiring microscopy images, the cells were incubated for 10 minutes in the presence of growth media containing 10μM of Rh-123. After the initial incubation period, the cells were washed twice with 1-1.5mL DPBS and the fluorescence images recorded immediately in 3mL of fresh DPBS solution containing calcium and magnesium. Microscopy experiments were carried out on an inverted microscope model at 15x magnification in quintuplets and in a systematic manner in order to avoid biased imaging (**Figure 2.5**). Image acquisition and analysis were carried out using Metamorph software. Also, fluorescence from Rh-123 in glycerol was compared as a standard prior to imaging to check for any significant deviation of fluorescence intensity as a result of significant fluctuations in the mercury lamp during the experiment. Notably, the appropriate set of long-pass dichroic and band-pass filters were used to detect the fluorescence of Rh-123 in the 528 ± 19 nm region (490 ± 10 nm excitation). Lastly,

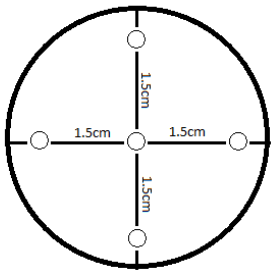

Figure 2.5 Diagram showing how each plate was imaged in quintuplets. Here, the large bold circle represents the perimeter of the plate and the small circles each represents the area studied by microscopy.

changes in cellular morphology and mitochondrial transmembrane potential were plotted and compared via Igor graphing software.

2.2.11.2 Comparison of Changes in Cellular Morphology and Mitochondrial Transmembrane Potential in CV-1 Cells Every 12 Hours for 0-72 Hours

CV-1 cells were harvested in exponential growth phase, viability verified, media type switched, and plated into small petri dishes as previously described in section 2.2.11.1. The dishes were examined every 12 hours (for 72 hours) for any changes in cellular morphology or mitochondrial transmembrane potential when switched from media #1 to media #2 in the same manner as described in section 2.2.11.1

.

2.2.11.3 Changes in Cellular Morphology in CV-1 Cells Over 36 Days

CV-1 cells were harvested in exponential growth phase, viability verified, and media type switched as previously described in section 2.2.11.1. In this case, the cells

were subcultured into 75cm^2 culture flasks in their new respective media. The culture flask were observed at 3, 9, 12, 15, 20, 31, and 36 days for changes in cellular morphology when switched from media #1 to media #2 in the same manner as described in section 2.2.11.1. Similarly, the culture flasks were viewed in quintuplets and in a systematic manner to avoid biased imaging (**Figure 2.6**). In addition, the old media was replaced with fresh media solution every 2 days and cell population maintained as previously described in section 2.2.9. Furthermore, when the culture flasks were not being examined or maintained they were placed in the 37^{o}C incubator.

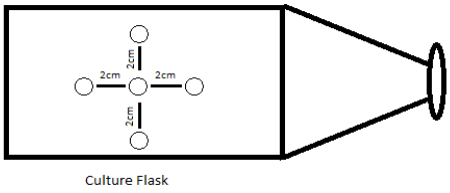

Figure 2.6 Diagram showing how each was imaged in quintuplets. Here, the small circles represent the area studied by microscopy.

2.2.11.4 Comparison of Mitochondrial Transmembrane Potential at 12 Days with Rh-123 and Rh-110

The results from the above experiment inspired the design of a subsequent experiment in which dye uptake could be compared in CV-1 cells when employing a

mitochondrial specific (Rh-123) and a non-mitochondrial specific (Rh-110) dye. In order to explore suspected changes in the mitochondrial transmembrane potential after 12 days in media #2, the cells were harvested in exponential growth phase, viability verified, and plated into small petri dishes as previously described in section 2.2.11.1. Here, the cells were examined for changes in rhodamine dye uptake when switched from media #1 to media #2 for 12 days by incubating them in the presence of either Rh-123 or Rh-110. In this specific experiment, a third media condition (media #3, optimal glucose and high glutamine) was also introduced. This was done in order to determine whether or not there would still remain an increase in dye uptake in the CV-1 cells cultured in a high glutamine media, even in the presence of optimal glucose conditions. Data was acquired in the same manner as above; however, in this case, the samples were incubated for 1 hour in the presence of 1μM Rh-123 or 1μM Rh-110 in order to give the Rh-110 dye enough time to be taken up by the cells.

2.2.11.5 Further Exploration of Cellular Morphology

In order to further explore the changes in cellular morphology related to the amount of glutamine in the culture media, CV-1 cells were harvested in exponential growth phase, viability verified, and media type switched as previously described in section 2.2.11.1. Next, a fourth growth condition was introduced where an aliquot of CV-1 cells were switched to media #4 (optimal glucose and no glutamine). These cells were subcultured into 75cm^2 culture flasks in their new media and observed at 1, 3, 6, 9, and 12 days for changes in cellular morphology in the same manner as previously described in section 2.2.11.3. In addition, the old media was replaced with fresh media

solution every 2 days and cellular population maintained as previously described in section 2.2.9. Lastly, the ability of the CV-1 cells to revert back to their normal, healthy growth pattern after being cultured in media #2 for 20 days was investigated. Here, an aliquot of cells grown for 20 days in media #2 (part 2.2.11.3) was switched back to media #1 using the same method as described in section 2.2.11.1. Subsequently, the cell culture was observed at 5, 10, and 12 days for changes in cellular morphology after being switched to media #1.

3. Results and Discussion

3.1. Synthesis, Purification and Characterization of Selective Rhodamine Dyes

For our investigation, we have chosen nine dyes from the rhodamine family motivated on the basis of their structural properties: Rhodamine-123 (Rh-123), Rhodamine-110 (Rh-110), Rhodamine *n*-octyl ester (Rh-Oct), Rhodamine 6g (Rh6g), Rhodamine 6g free acid (Rh6gFA), Rhodamine B (RhB), Rhodamine B ethyl ester (RhBEE), Rhodamine-123 Br_2 (Rh-123 Br_2), and Rhodamine *n*-octyl ester Br_2 (Rh-Oct Br_2) (**Figure 3.1**). The first part of this study included the synthesis and purification of the free acid (Rh6gFA) and ethyl ester (RHBEE) derivatives of Rh6g and RhB, respectively. The second part of this study included the spectroscopic and photophysical characterization of the above rhodamine dyes on the basis of structural changes. Information on specific combinations of long-pass dichroic and band-pass filters, as needed for fluorescence microscopy, was provided by this systematic evaluation.

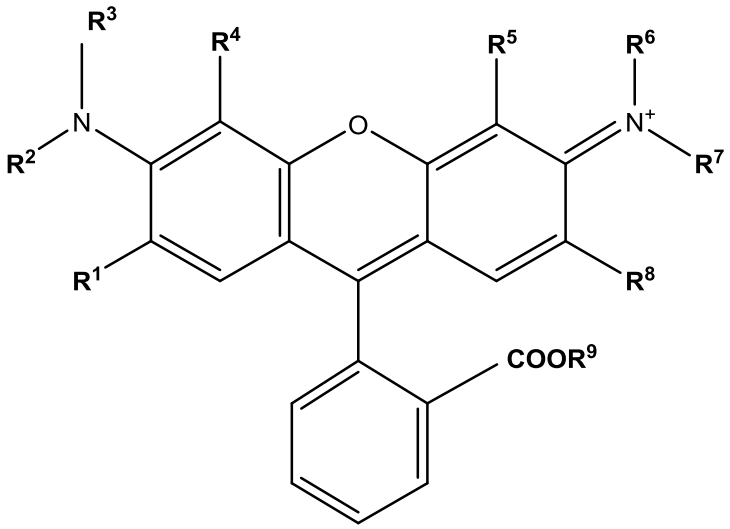

Dye	R^1	R^2	R^3	R^4	R^5	R^6	R^7	R^8	R^9
Rh-110	H	H	H	H	H	H	H	H	H
Rh-123^+	H	H	H	H	H	H	H	H	CH_3
Rh-Oct^+	H	H	H	H	H	H	H	H	C_8H_{17}
$Rh6g^+$	CH_3	H	CH_3	H	H	CH_3	H	CH_3	C_2H_5
Rh6gFA	CH_3	H	CH_3	H	H	CH_3	H	CH_3	H
RhB	H	C_2H_5	C_2H_5	H	H	C_2H_5	C_2H_5	H	H
$RhBEE^+$	H	C_2H_5	C_2H_5	H	H	C_2H_5	C_2H_5	H	C_2H_5
Rh-$123Br_2^+$	H	H	H	Br	Br	H	H	H	CH_3
Rh-$OctBr_2^+$	H	H	H	Br	Br	H	H	H	C_8H_{17}

Figure 3.1 Chemical structure of the rhodamine dyes investigated in this study.

3.1.2 Synthesis of Some Rhodamine Derivatives

3.1.2.1 Synthesis of Rhodamine 6g Free Acid

The free acid derivative of Rhodamine 6g (Rh6gFA) was synthesized by the saponification of the respective parent dye (**Figure 3.2**). Here, the loss of the ethyl group should be evident when the reactant and products are compared using HPLC analysis. Therefore, a standard aliquot of the mixture was taken for analysis before the addition of sodium hydroxide and the progress of the reaction was monitored by HPLC using a reverse phase C18 column (see Methods). **Figure 3.3** shows the normalized HPLC comparison of the parent dye to that of the synthesized derivative. Here, the starting material elutes from the reverse phase column at 2.8 minutes compared to the newly synthesized product which elutes at 2.3 minutes. This phenomenon suggests that the loss of the ethyl group was achieved through the saponification reaction resulting in the free acid derivative. In addition, mass spectrometry and ^{1}H NMR data for the Rh6g derivative described here is the following: Rh6gFA: EI+ (m/z) for $C_{26}H_{27}N_2O_3$, calculated 415.504, observed: 415.350, 416.360 (M+1); ^{1}H NMR (300 MHz, CD_3OD) δ 8.11 (1H, d, J = 6.9 Hz), 7.65 (2H, t, J = 6.9 Hz), 7.24 (1H, d, J = 7.2 Hz), 7.07 (2H, s), 6.89 (2H, s), 4.06 (1H,m), 3.53 (4H, d, J = 6.9 Hz), 2.15 (6H, s), 1.37 (6H, m).

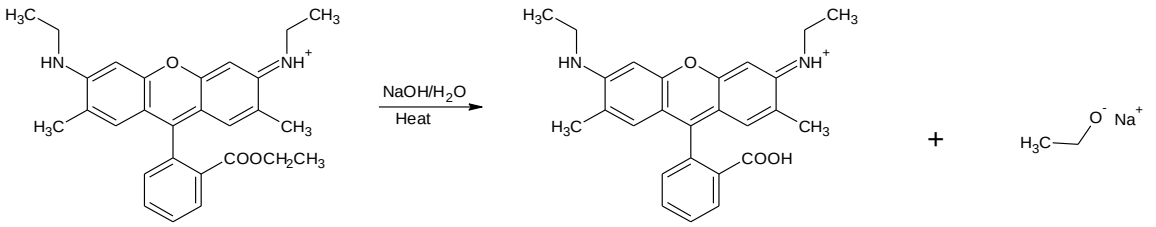

Figure 3.2 The saponification of Rhodamine 6g resulting in Rhodamine 6g free acid.

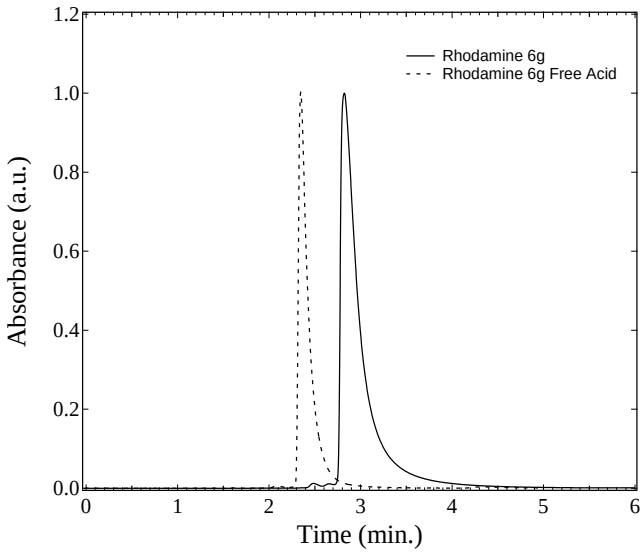

Figure 3.3 Normalized HPLC comparison for the synthesized Rhodamine 6g free acid derivative compared to the parent dye.

3.1.2.2 Synthesis of Rhodamine B Ethyl Ester

The ethyl ester derivative of Rhodamine B (RhBEE) was synthesized by Fisher esterification of its respective parent dye (**Figure 3.4**). Here, reaction progress was also tracked on basis of time-dependant HPLC analysis. Hence, a standard aliquot of the mixture was taken for analysis before exposure to gaseous HCl. The progress of the reaction was monitored by HPLC using a reverse phase C18 column (see Methods). **Figure 3.5** shows the normalized HPLC comparison of the parent dye to that of the collected pure fractions of the synthesized ethyl ester derivative. Here, the starting material elutes from the reverse phase column at 1.8 minutes whereas the newly synthesized product elutes at 2.4 minutes. Ultimately, this phenomenon suggests that the addition of the ethyl group was achieved through the Fisher esterification reaction resulting in the ethyl ester derivative. In addition, mass spectrometry and ^{1}H NMR data for the RhB derivative described here is the following: RhBEE: EI+ (m/z) for $C_{30}H_{35}N_2O_3$, calculated 471.621, observed: 472.609 (M+1), 443 (-CH_2CH_3), 399 (-$COOCH_2CH_3$) ; ^{1}H NMR (300 MHz, CD_3Cl_3) δ 8.32 (1H, d, J = 7.2 Hz), 7.86 (2H, m), 7.46 (1H, m), 7.09 (6H, m), 4.04 (2H, m), 3.70 (8H,d, J = 6.8 Hz), 1.32 (12H, t, J = 6.4 Hz), 0.99 (3H, t, J = 6.8 Hz).

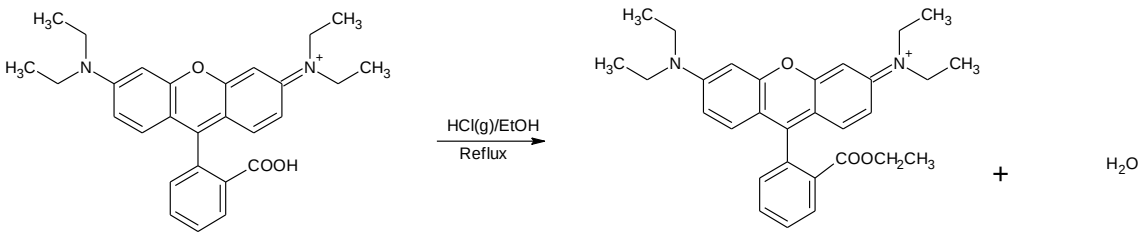

Figure 3.4 Fisher esterification of Rhodamine B resulting in Rhodamine B ethyl ester.

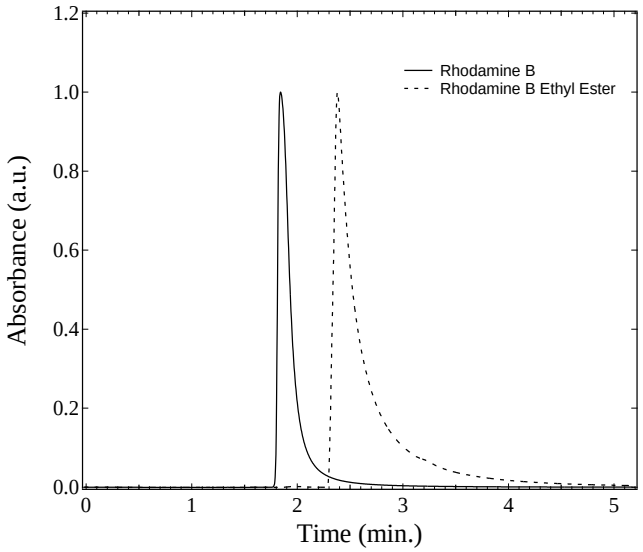

Figure 3.5 Normalized HPLC comparison for the synthesized Rhodamine ethyl ester derivative compared to the parent dye.

3.1.3 Spectroscopic Experiments

The absorption and florescence emission spectra of fresh stock solutions of Rh-110, Rh-123, Rh-Oct, Rh6g, Rh6gFA, RhB, RhBEE, Rh-123Br_2, and Rh-OctBr_2 were acquired in ethyl alcohol. **Figures 3.6-3.14** show the normalized absorption (left y-axes) and fluorescence emission (right y-axes) spectra of all of the rhodamine dyes used in this study. In addition, **Table 3.1** shows a summary of the wavelengths of maximum absorption and the wavelengths of maximum fluorescence as well as the calculated quantum yields for each of the selected rhodamine dyes (Rh-123 was used as the fluorescence standard ($\Phi_{Rh\text{-}123}$ =0.86) (Pal et al. 1996)). Here, we have investigated how and to which extent molecular structure affects the spectroscopic properties and quantum yields of the rhodamine dyes of interest.

The first of the dyes selected to be compared are very similar in structure except for the alkyl substitutions of the carbonyl group of the parent dye. **Figures 3.6-3.8** show the absorption and fluorescence emission spectra of Rh-110, Rh-123, and Rh-Oct, respectively. Comparatively, the esterification of the carbonyl group of Rh-110 (parent dye) via the alkyl substitution of a methyl (Rh-123) or an octyl (Rh-Oct) group leads to both a 4 nm red (bathochromic) shift in the wavelength of maximum dye absorption and a 9 nm red shift in the wavelength of maximum fluorescence. Analogously, virtually no changes in fluorescence quantum yields (**Table 3.1**) were observed among the above dyes upon the methyl ($\Phi_{Rh\text{-}123}$ =0.86) and octyl ($\Phi_{Rh\text{-}Oct}$ =0.86) alkyl substitution of the parent dye ($\Phi_{Rh\text{-}110}$ =0.95). Overall, the spectroscopic properties and quantum yields of these three dyes show very little differences upon the alkyl substitutions of the carbonyl group.

The second group of dyes (Rh6g and Rh6gFA) is also similar in structure and photophysical properties when compared. **Figure 3.9** and **3.10** show the absorption and fluorescence emission spectra of Rh6g and Rh6gFA, respectively. The product of hydrolysis (Rh6gFA) of the parent dye (Rh6g), leads to both a 12 nm blue (hypsochromic) shift in the wavelength of maximum dye absorption and a 9 nm blue shift in the wavelength of maximum fluorescence due to the removal of an ethyl group. Comparatively, the quantum yield (**Table 3.1**) only increases slightly with the removal of the ethyl alkyl group (Φ_{Rh6gFA} =0.81) from the parent dye (Φ_{Rh6g} =0.72). Similarly, the spectroscopic properties and quantum yields of these two dyes display very little differences with the removal of the ester group.

The same trend was observed when comparing the third group of dyes displaying similar structure, RhB (**Figure 3.11**) and its ethyl ester derivative (RhBEE) (**Figure 3.12**). That is, both a 5 nm red shift of maximum dye absorption and a 17 nm red shift of maximum fluorescence can be observed as a consequence of the Fisher esterification (RhBEE) of the parent dye (RhB). In addition, the quantum yield (**Table 3.1**) decreases with the ethyl esterification (Φ_{RhBEE} =0.29) of the parent dye (Φ_{RhB} =0.50). The comparison of the spectroscopic properties and quantum yields of this group of dyes also reveals little differences upon the esterification of the carbonyl group. Overall, these comparative studies have demonstrated that the esterification of rhodamine free acids lead to bathochromic shifts in the respective absorption and fluorescence emission spectra, along with a decrease in the respective fluorescence quantum yields.

All of the rhodamine dyes used in this study display similar spectroscopic profiles in ethyl alcohol. That is, each of the spectra acquired from the rhodamine dyes show a

similar shoulder at the left (blue side) of the absorption envelope. In addition, the above experimental results are in agreement with previous studies exploring the effects of structural changes of the parent dyes. In all cases, it was observed that there was a small decrease in the fluorescence quantum yields as well as a slight red shift in the wavelength of maximum dye absorption and the wavelength of maximum fluorescence emission upon the alkyl substitution of the carbonyl group. In the same manner, it was observed that there was a modest increase in the fluorescence quantum yields as well as a small blue shift in the wavelength of maximum dye absorption and the wavelength of maximum fluorescence emission upon the removal of the alkyl group from the ester linkage. Our experimental results are consistent with the results obtained in the classical studies in which the spectroscopic and photophysical properties of the above rhodamine dyes have been extensively investigated in relation to structural changes (Vogel and Rettig 1985, Arbeloa et al. 1989, Arbeloa et al. 1991).

In general, rhodamine dyes are well known for displaying high fluorescence quantum yields. For the compounds considered here, the wavelengths of maximum dye absorption vary from 508-556 nm and the respective wavelengths of maximum fluorescence emission vary from 519-575 nm. The alkylation of the amino groups is one of the main factors that can decrease the fluorescence quantum yields as well as cause small bathochromic shifts in the wavelength of maximum absorption and the wavelength of maximum fluorescence emission (Vogel and Rettig 1985). By analogy, our experimental results suggest that there is a significant decrease in the quantum yields between the different free acid dyes: Rh-110 ($\Phi_{Rh\text{-}110}$ =0.95), Rh6gFA (Φ_{Rh6g} =0.81), and RhB (Φ_{RhB} =0.50). Observably, the Rh-110 derivatives, Rh-123 and Rh-Oct, have no

ethyl alkyl substitutions of their amino groups. However, Rh6g and its derivative (Rh6gFA) have two ethyl amino groups and RhB and its derivative (RhBEE) have two diethyl amino groups, respectively. The trend observed for these last dyes, upon increasing the degree of alkylation of the amino groups, is due to a structural change within the respective molecules from a planar to pyramidal structures. That is, to the respective "open-closed umbrella-like motions" (Arbeloa et al.1991). Consequently, the structural change induced upon alkylation increases the rate constants of internal conversion from the first excited singlet state (S_1) to the ground state (S_0) and thus a decrease in the fluorescence quantum yields is observed (Pal et al. 1996, Vogel and Rettig 1985). Here, the ethyl substitution of the amino groups is thought to stabilize the positive charge on the N atom and subsequently increases the π-electron density of the xanthene-amine bond upon increasing the degree of alkylation of the amino groups (i.e. Rh6gFA vs. RhB) (Arbeloa et al.1991). The relatively modest changes in the spectral and photophysical properties observed in this study can be satisfactorily explained by the structural changes that take place as a result of the degree of the alkylation of the amino groups of our selected rhodamine dyes.

In addition, we have also investigated how and to which extent bromine atom substitution affects the spectroscopic properties of two selected rhodamines. Bromine atom substitution of organic dyes is known to result in increased ISC efficiency resulting in an increase in photochemical reactivity as compared to the respective parent compounds (Shea et al. 1989, Pal et al. 1996, Lacerda et al. 2005). High ISC efficiency is a strong requirement for any dye to be considered as a photosensitizer for PDT applications. For this reason, two dibrominated rhodamines were included in this study

(Rh-123Br_2 and Rh-OctBr_2). **Figures 3.13- 3.14** show the absorption and fluorescence emission spectra of the bromine derivatives of Rh-123 and Rh-Oct, respectively. The bromine substitution of Rh-123 leads to both a red shift of 6 nm in the wavelength of maximum absorption and a red shift of 11 nm in the wavelength of maximum fluorescence. Similarly, the bromine substitution of Rh-Oct leads to both a red shift of 7 nm in the wavelength of maximum absorption and a red shift of 11 nm in the wavelength of maximum fluorescence. There is very little difference in the maximum wavelength of absorption or maximum wavelength of fluorescence (**Table 3.1**) when comparing the dibrominated derivatives, Rh-123Br_2 and Rh-OctBr_2, although continuous shift toward the red region of the spectrum in the wavelengths of maximum absorption and fluorescence upon increasing the degree of bromine substitution of the parent rhodamine dye has been previously reported (about 4-5 nm per bromine atom substitution, Lacerda et al. 2005). On the other hand, very pronounced effects were observed in the fluorescence quantum yields (**Table 3.1**) upon the bromine substitution of the parent dyes: Rh-123 ($\Phi_{Rh\text{-}123}$ =0.86) and Rh-Oct ($\Phi_{Rh\text{-}Oct}$ =0.86) compared to Rh-123Br_2 ($\Phi_{Rh\text{-}123Br2}$ =0.38) and Rh-OctBr_2 ($\Phi_{Rh\text{-}OctBr2}$=0.40), respectively. These experimental results are consistent with previous observations and can be explained by the classical concept of heavy-atom effect on intersystem crossing (ISC) efficiency (Turro 1978).

The substitution of “heavy” atoms (i.e., atoms with a large atomic number, Z), such as bromine, increases the efficiency of intersystem crossing (ISC) to the triplet manifold by enhancing the spin-orbit coupling. Upon electronic excitation of these brominated dyes, a large fraction of the population of the respective first excited singlet state (S_1) species cross to their respective triplet (T_1) manifolds, via ISC. Consequently,

this phenomenon results in the increased triplet (T_1) population concomitantly with a decrease in the respective fluorescence quantum yields (Lacerda et al. 2005). The results obtained in this study are consistent with the heavy-atom theory and explain the decrease in fluorescence quantum yields that are observed upon bromination of the parent dyes. Here, the larger the heavy-atom perturbation, the larger the ISC rate constant, and subsequently, the larger the triplet population formed upon dye excitation (Turro 1978). Bromine atom substitution has become one of the most common strategies for increasing the photoreactivity of organic dyes for PDT. Iodine substitution has also been frequently used for such a purpose.

Our choice for rhodamines as model dyes for this study was largely motivated by previous work by Chen and colleagues. These authors examined over 200 cell lines and found that tumor cells typically uptake larger amounts of Rh-123 and retain this dye for longer periods as compared to most normal cell lines (Chen 1989). In addition, studies of a vast number of fluorescent, cationic dyes revealed that Rh-123 has relatively low phototoxic properties when used in mammalian cells (Chen 1988). These previous studies make Rh-123 an idea candidate for use in fluorescence microscopy. Because the absorption (Abs λ_{Max}) and fluorescence (Fluor λ_{Max}) properties of all rhodamine dyes studied here are not very different from each other, they can all be conveniently used as fluorescent probes employing the same set of optical filters for Rh-123 that are currently found in most fluorescence microscopes (Sikder et al. 2005). This fact facilitates the work needed to explore the structural determinates of successful mitochondrial localization in our model non-transformed cell line (CV-1).

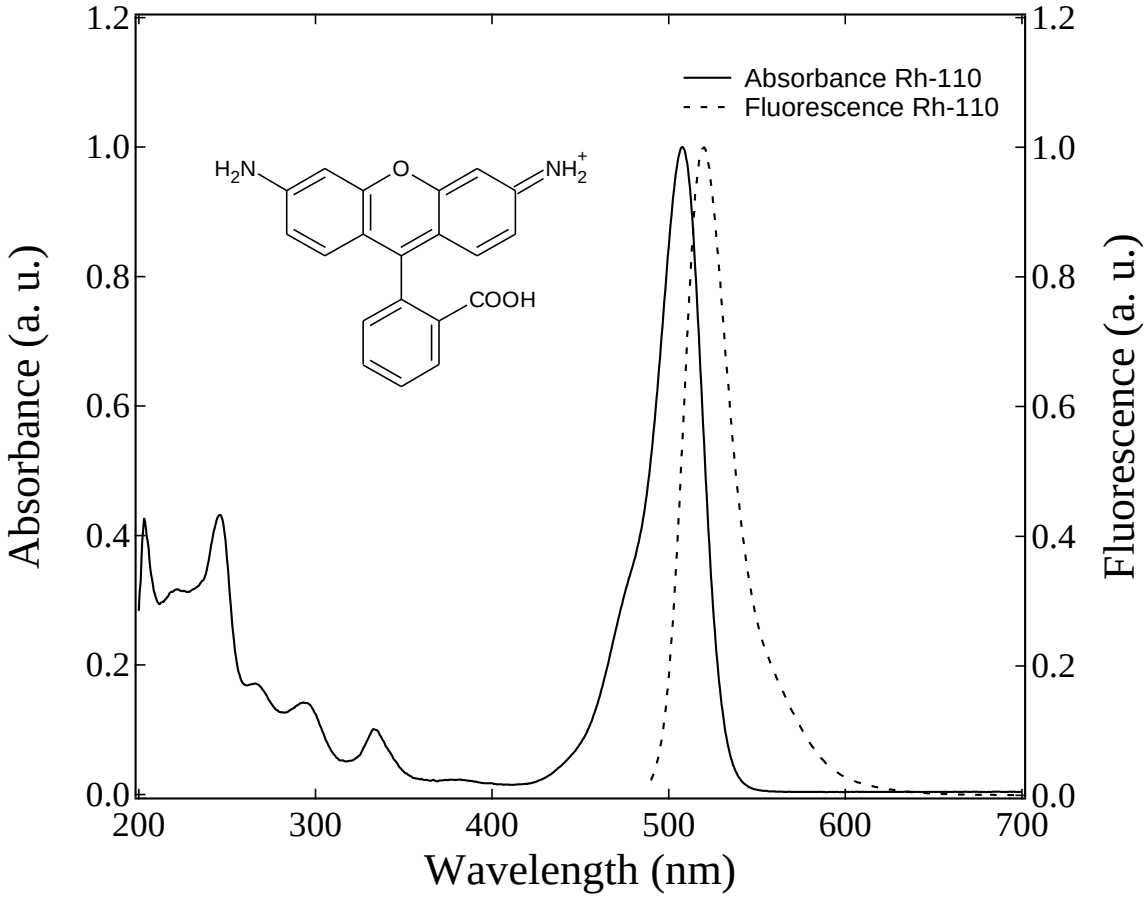

Figure 3.6 Normalized absorption (left y-axis) and fluorescence (right y-axis) spectra of Rhodamine-110 in ethanol.

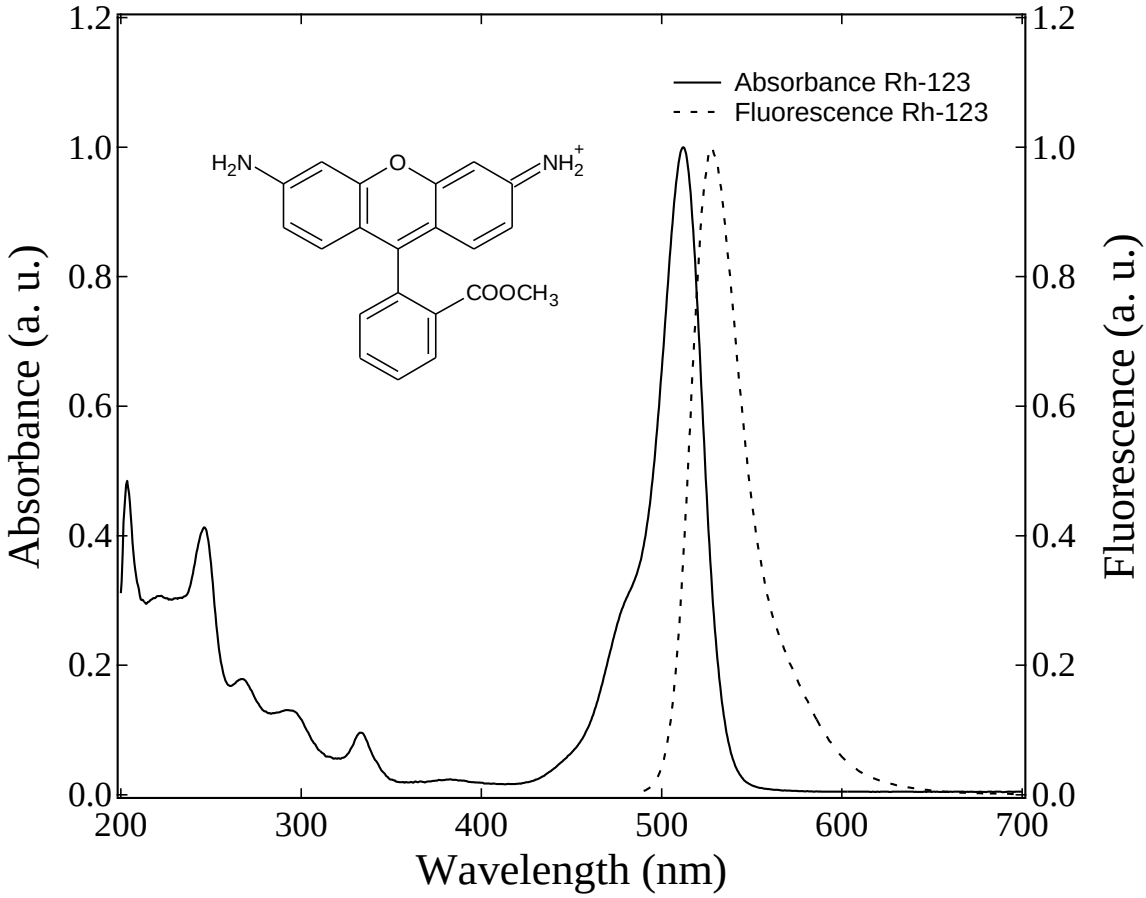

Figure 3.7 Normalized absorption (left y-axis) and fluorescence (right y-axis) spectra of Rhodamine-123 in ethanol.

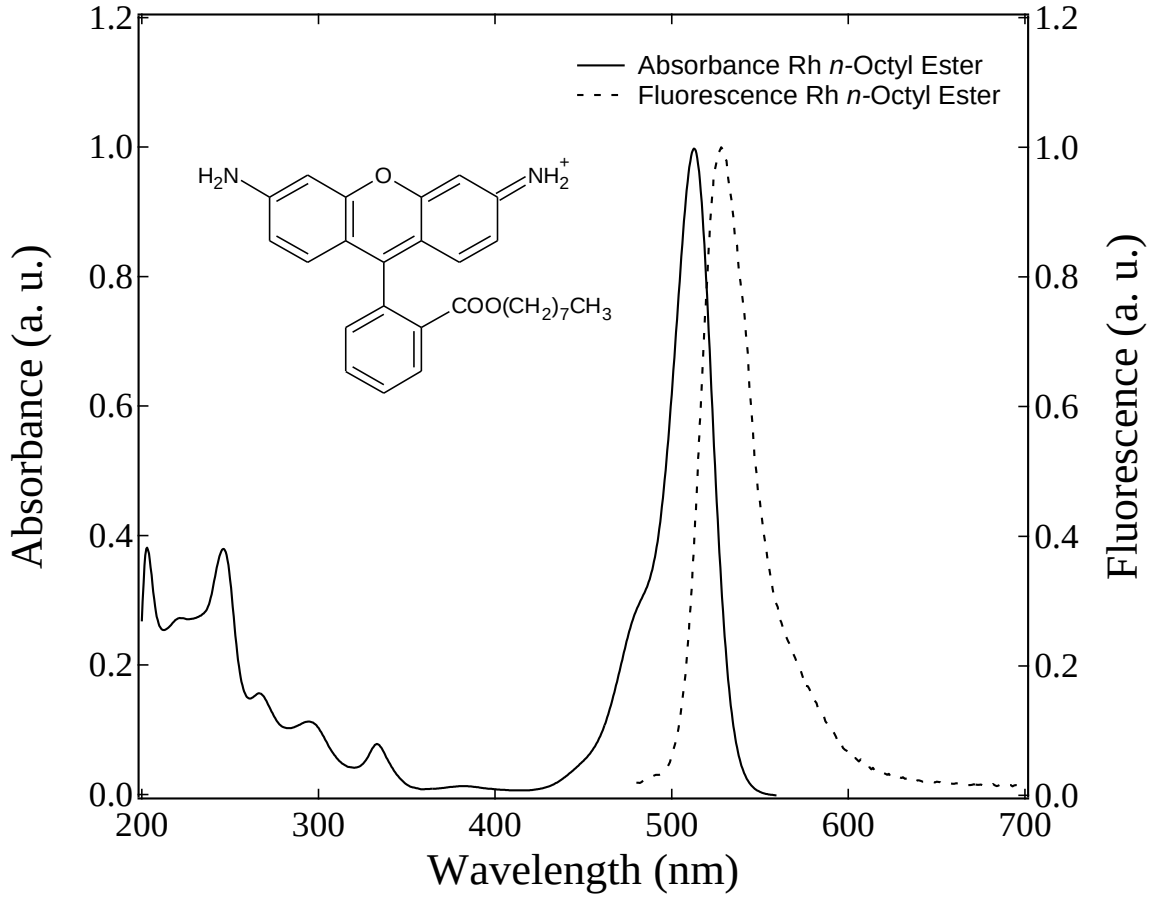

Figure 3.8 Normalized absorption (left y-axis) and fluorescence (right y-axis) spectra of Rhodamine n-octyl ester in ethanol.

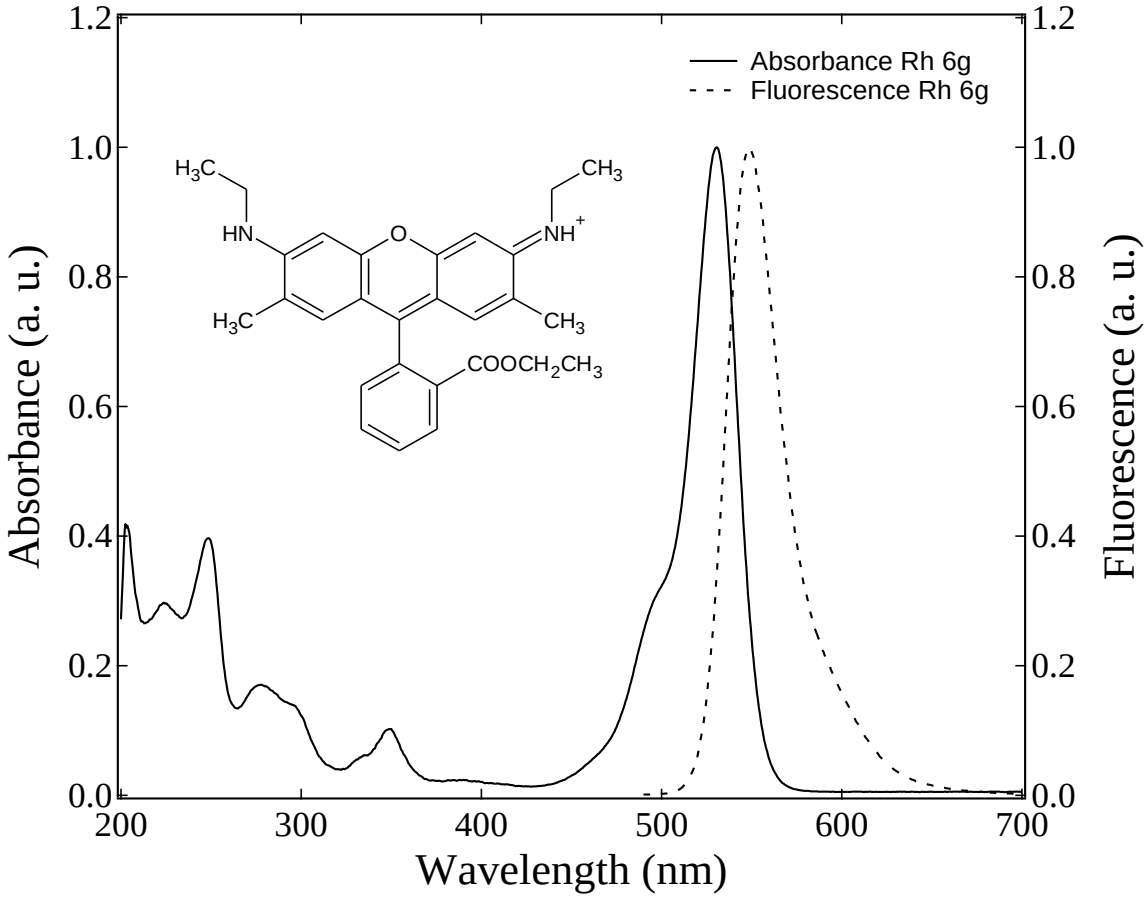

Figure 3.9 Normalized absorption (left y-axis) and fluorescence (right y-axis) spectra of Rhodamine 6g in ethanol.

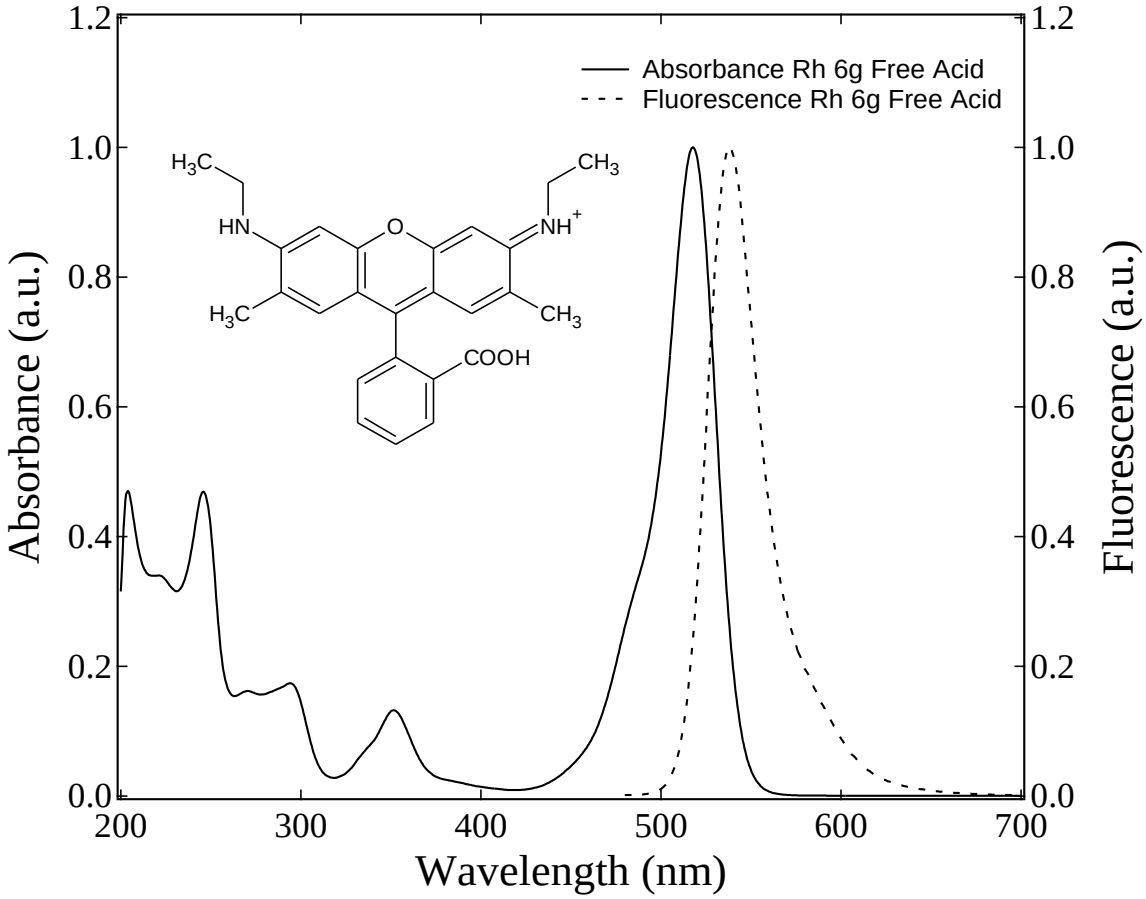

Figure 3.10 Normalized absorption (left y-axis) and fluorescence (right y-axis) spectra of Rhodamine 6g free acid in ethanol.

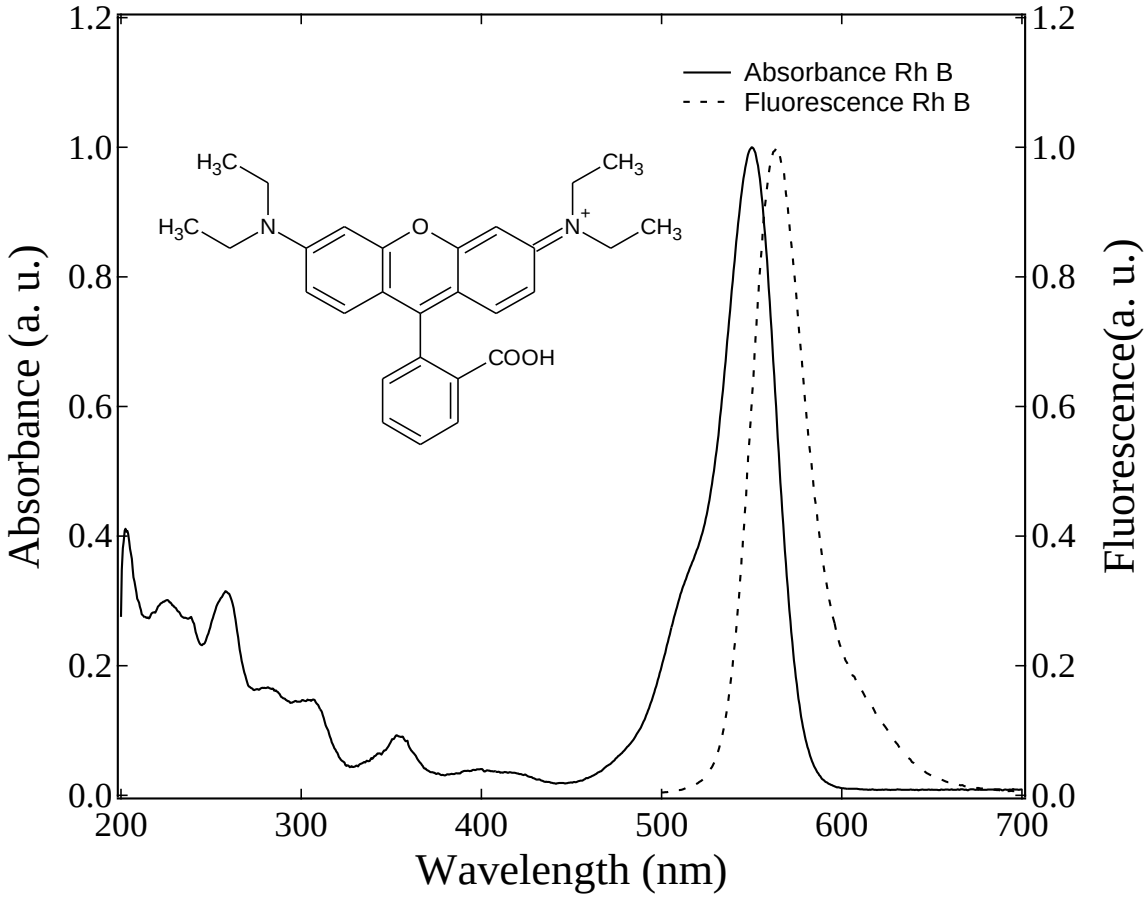

Figure 3.11 Normalized absorption (left y-axis) and fluorescence (right y-axis) spectra of Rhodamine B in ethanol.

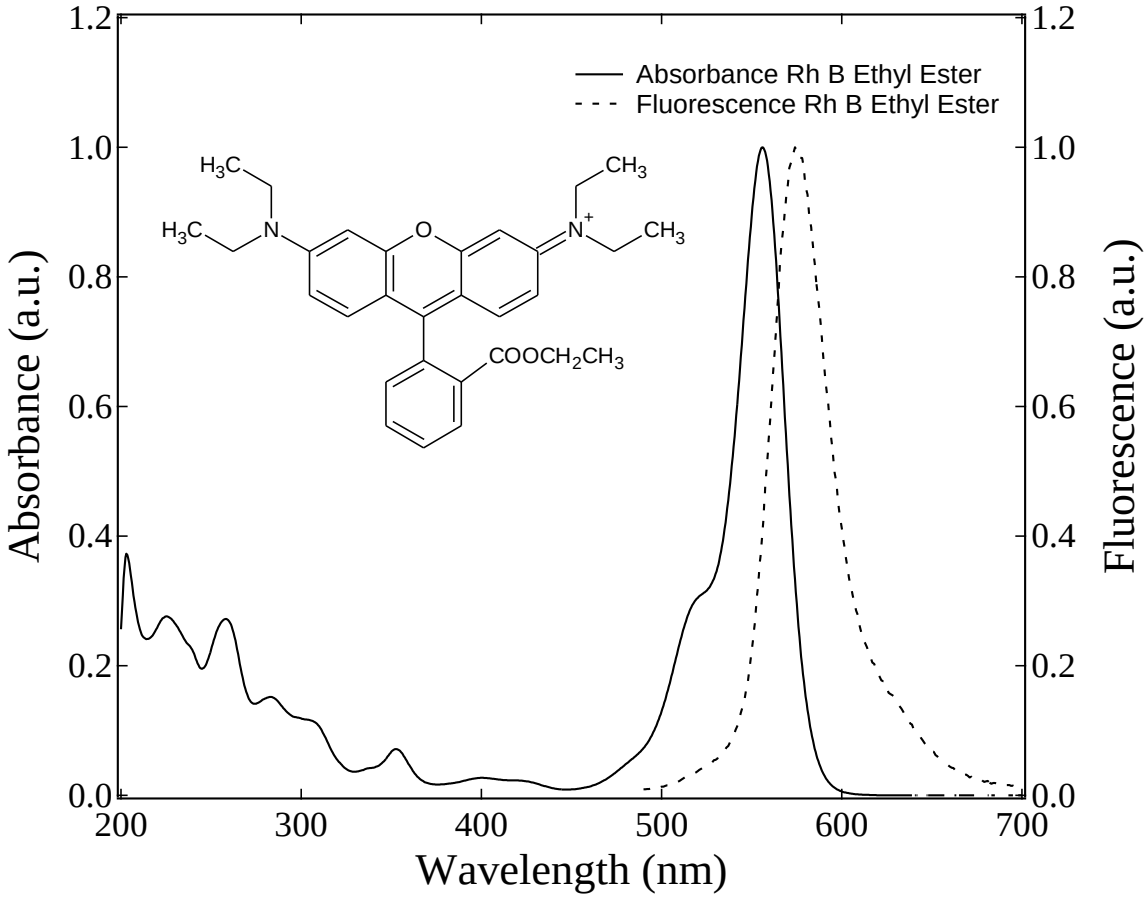

Figure 3.12 Normalized absorption (left y-axis) and fluorescence (right y-axis) spectra of Rhodamine B ethyl ester in ethanol.

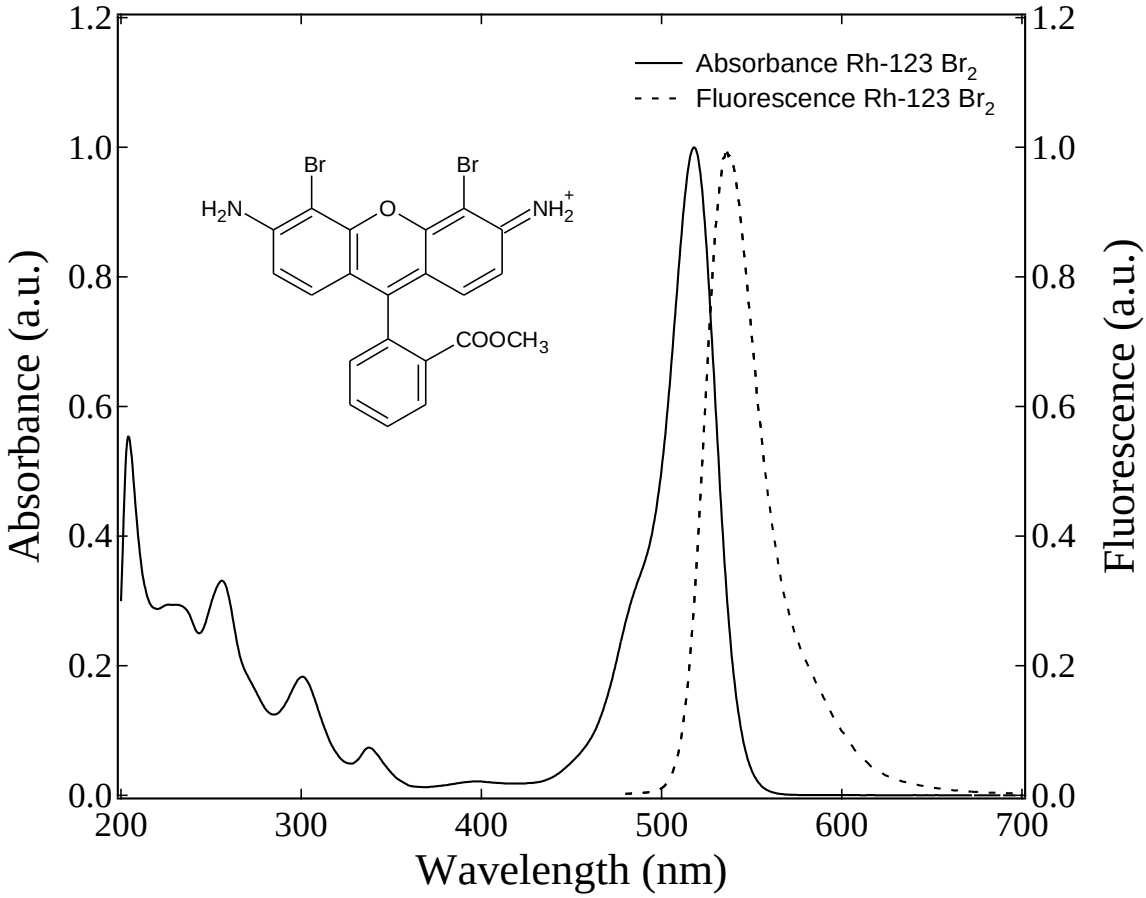

Figure 3.13 Normalized absorption (left y-axis) and fluorescence (right y-axis) spectra of Rhodamine-123 Br_2 in ethanol.

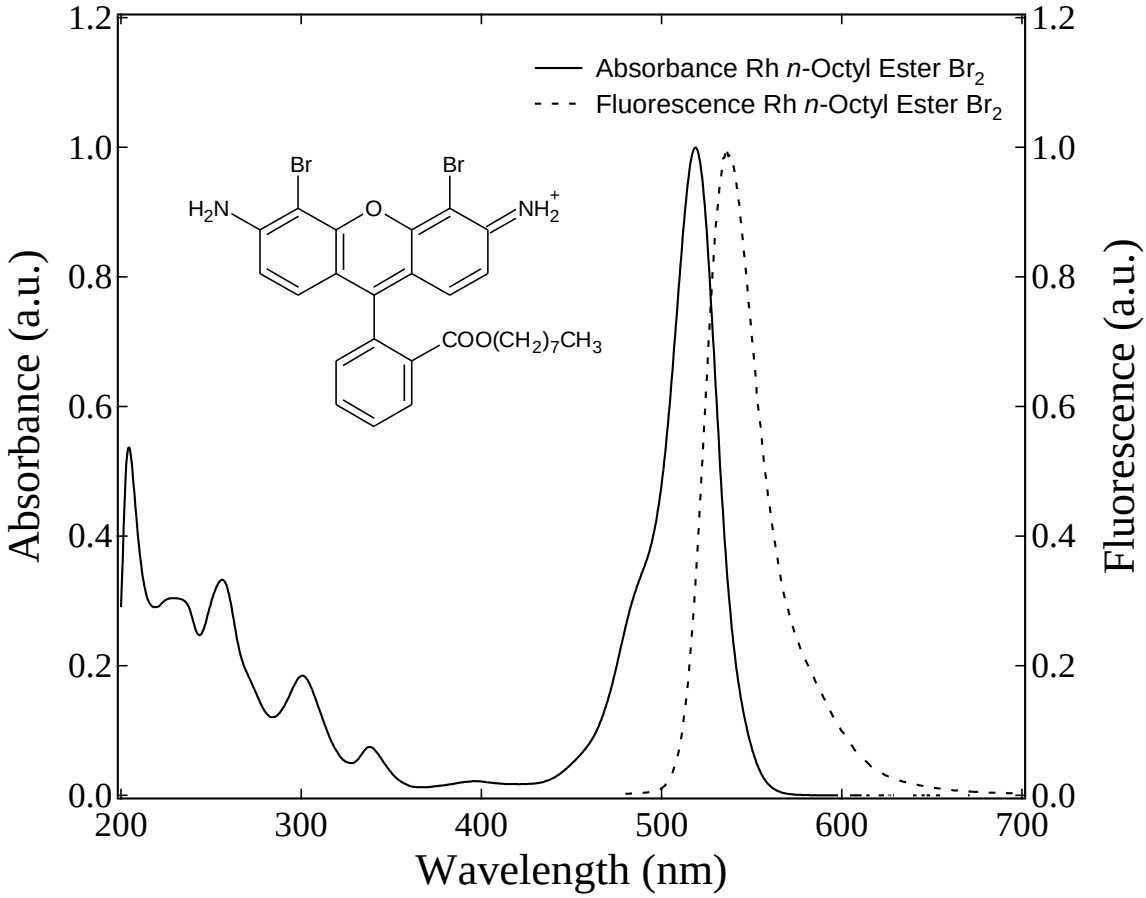

Figure 3.14 Normalized absorption (left y-axis) and fluorescence (right y-axis) spectra of Rhodamine *n*-octyl ester Br_2 in ethanol.

Dye	Abs λ_{max} (nm)	Fluor λ_{max} (nm)	φ_f
Rh-110	508	519	0.95 ± 0.05
Rh-123$^+$	512	528	0.86 (Std)
Rh-Oct$^+$	512	528	0.86 ± 0.01
Rh6g$^+$	530	548	0.72 ± 0.06
Rh6gFA	518	539	0.81 ± 0.02
RhB	551	558	0.50 ± 0.04
RhBEE$^+$	556	575	0.29 ± 0.01
Rh-123Br$_2^+$	518	539	0.38 ± 0.01
Rh-OctBr$_2^+$	519	539	0.40 ± 0.02

Table 3.1 Summary of spectroscopic properties and quantum yields for rhodamine dyes.

3.2 Subcellular Localization of Rhodamine Dyes

Tumor cell selectivity is a fundamental component in PDT. One proposed way of selective tumor cell killing is via mitochondria targeting with appropriate photosensitizers (Davis et al. 1985, Oseroff et al. 1986). In order for this targeting strategy to work, the mechanism of cellular uptake and subcellular distribution must be primarily controlled by the mitochondrial transmembrane potentials with just minor or negligible contributions arising from competing mechanisms such as lipophilic partitioning (Belostotsky et al. 2011). In this study, the rhodamine dyes from part 3.1 (Rh-123, Rh-Oct, Rh-110, Rh6g, Rh6gFA, RhB, RhBEE, Rh-123Br_2, and Rh-OctBr_2) were investigated in order to determine how the structure and charge of each affect the degree of specificity with which they localize in energized cell mitochondria of our non-transformed (CV-1) cells.

Figure 3.16 shows fluorescence images of CV-1 cells loaded simultaneously with MitoTracker Deep Red 633 (a mitochondrial specific fluorescence probe) and a rhodamine dye: Rh-123, Rh-Oct, or Rh-110. The merger of the two fluorescence images shows a nearly perfect overlap between the MitoTracker and the prototypical mitochondrial dye, Rh-123, as well as its octyl ester derivative, Rh-Oct. Therefore, not only Rh-123, a known mitochondrial localizing dye (Chen 1988, Chen 1989, Modica-Napolitano and Aprille 2001), but the more lipophilic Rh-123 derivative, Rh-Oct, also localizes in energized cell mitochondria with great specificity, and apparently even in larger quantities as compared to Rh-123. Here, it is reasonable to infer that the lipophilic character associated with the octyl ester derivative is still low enough to preclude any competitive phenomenon of lipophilic partitioning on subcellular localization. In addition, previous studies have shown that when the mitochondrial transmembrane

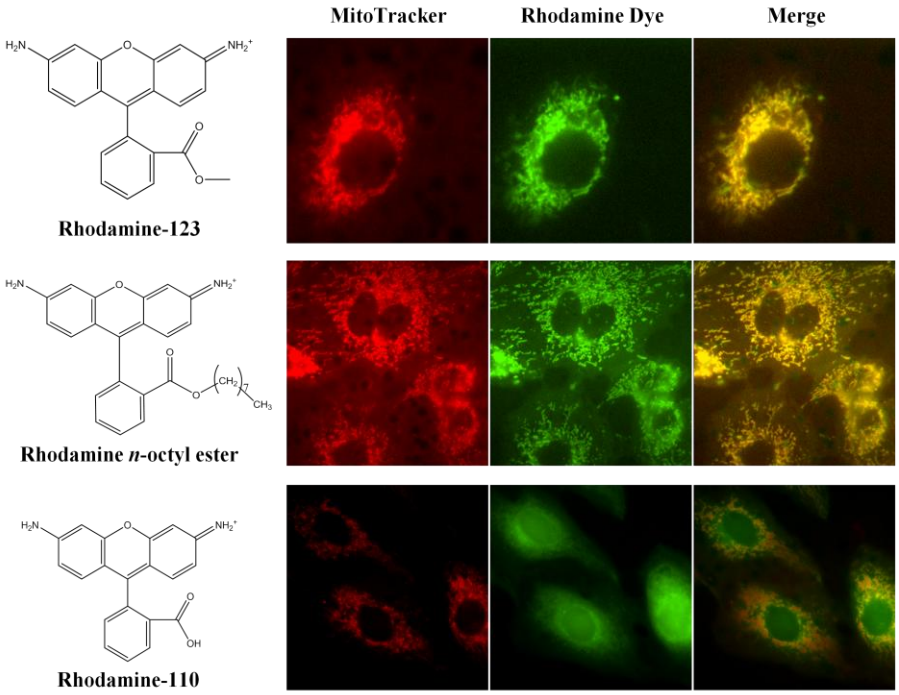

Figure 3.16 Fluorescence microscopy images (80x magnification) of CV-1 cells incubated simultaneously for 1 hour with 1 µM Rh-123, Rh *n*-octyl ester, or Rh-110 and 1 µM MitoTracker Deep Red 633. From left to right: fluorescence from MitoTracker (red), rhodamine dyes (green), and the merger of the two fluorescence images. In the right panels, yellow represents the subcellular regions in which the fluorescence from MitoTracker and the rhodamine dye overlap.

potential is depolarized, Rh-Oct leaks slowly from the mitochondria whereas its less lipophilic derivative, Rh-123, leaks rapidly from the mitochondria and the cell as a whole (Belostotsky et al. 2011). Consequently, Rh-123 dim cells, such as CV-1, become substantially easier to image (i.e., more fluorescent) with Rh-Oct due presumably to its greater lipophilic character. Therefore, Rh-Oct may find unprecedented application in studies focused on mitochondrial events that take place long after initial depolarization of the mitochondrial membrane, whereas Rh-123 is better suited for studies focused on the early events that take place during or immediately after depolarization.

On the other hand, **Figure 3.16** shows that when the fluorescence images of MitoTracker and Rh-110 are merged, the overlay of the two images indicates that the free acid derivative does not show mitochondrial localizing specificity. Instead, Rh-110 is diffuse and extends throughout the cytoplasm. This phenomenon is due to the loss of the ester alkyl substituent; the dye diffuses throughout the cytoplasm because it is primarily a zwitterion at physiological pH (pka of its carboxylic group ~ 4.3) (Jeannot et al. 1997, Belostotsky et al. 2011). The higher pH of the mitochondrial matrix (pH ~8.0) compared to that of the mitochondrial intermembrane space (pH ~7.2) tends to facilitate the accumulation of the zwitterionic form of Rh-110 in the mitochondrial matrix, but this process takes longer than the observation time used in our experiments (Jeannot et al. 1997). The concentration of Rh-110's cationic form in the cytoplasm/mitochondrial intermembrane space (pH ~7.2) is very low as it is estimated that at physiological pH, only about 1/1000 of Rh-110 molecules are in the protonated (cationic) form (Jeannot et al. 1997). In addition, previous experiments have demonstrated that the transmembrane transport process itself requires the protonated (cationic) form (Jeannot et al. 1997, Trapp

and Horobin 2005, Horobin et al. 2007). Therefore, only small quantities of Rh-110 are thought to cross the mitochondrial membrane through the same pathway used by other cationic rhodamine dyes when employing 1μM concentrations and 1h exposure times (Belostotsky et al. 2011). However, additional studies have shown that when using higher concentrations and longer cell exposure times (i.e., 10μM concentrations and 14h exposure times), Rh-110 will eventually find its way into the mitochondria (Jeannot et al. 1997). The cationic requirement of rhodamine dyes for the rapid and effective mitochondrial localization is further confirmed by our experimental results.

Figure 3.17 shows fluorescence images of CV-1 cells loaded simultaneously with MitoTracker Deep Red 633 and the known phototoxic dibrominated rhodamine dyes, Rh-123Br_2 and Rh-OctBr_2. Here, the merger of the two fluorescence images shows a nearly perfect overlap between the MitoTracker and the brominated dyes suggesting that these analogs of the ideal mitochondrial localizing dye, Rh-123, also localize in energized cell mitochondria of CV-1 cells with great specificity. In addition, previous studies have demonstrated that these brominated dyes accumulate in larger amounts and display desirable levels of phototoxicity towards tumor cells (Pal et al. 1996, Lacerda et al. 2005, Belostotsky et al. 2011). Therefore, any phototoxic agent displaying structural features and lipophilic character similar to those of the prototypical mitochondrial dye, Rh-123, should theoretically be able to localize in energized cell mitochondrial as well as induce the photochemical destruction of tumor cells with a high degree of selectivity.

Similarly, **Figure 3.18** shows fluorescence images of CV-1 cells loaded simultaneously with MitoTracker Deep Red 633 and either Rh6g, Rh6gFA, RhB, or RhBEE. Here, the mergers of the two fluorescence images of both Rh6g and RhBEE,

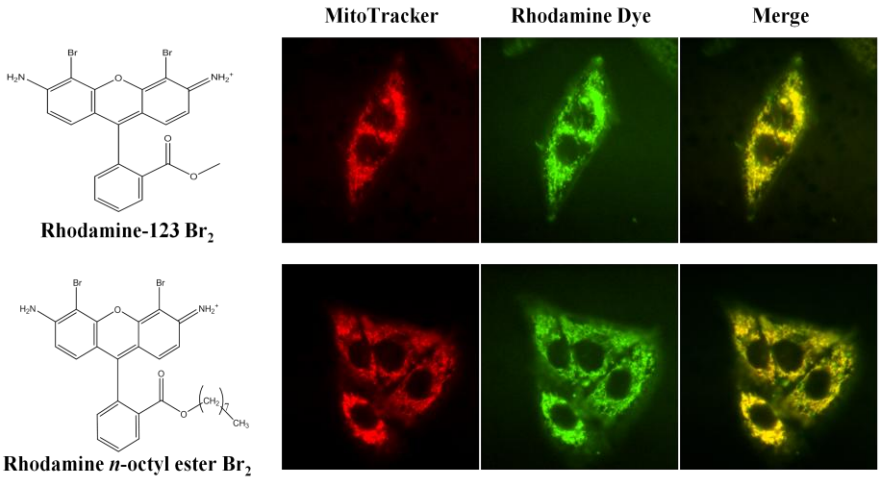

Figure 3.17 Fluorescence microscopy images (80x magnification) of CV-1 cells incubated simultaneously for 1 hour with either 1 µM Rh-123 Br_2, or Rh *n*-octyl ester Br_2 and 1 µM MitoTracker Deep Red 633. From left to right: fluorescence from MitoTracker (red), rhodamine dyes (green), and the merger of the two fluorescence images. In the right panels, yellow represents the subcellular regions in which the fluorescence from MitoTracker and the rhodamine dye overlap.

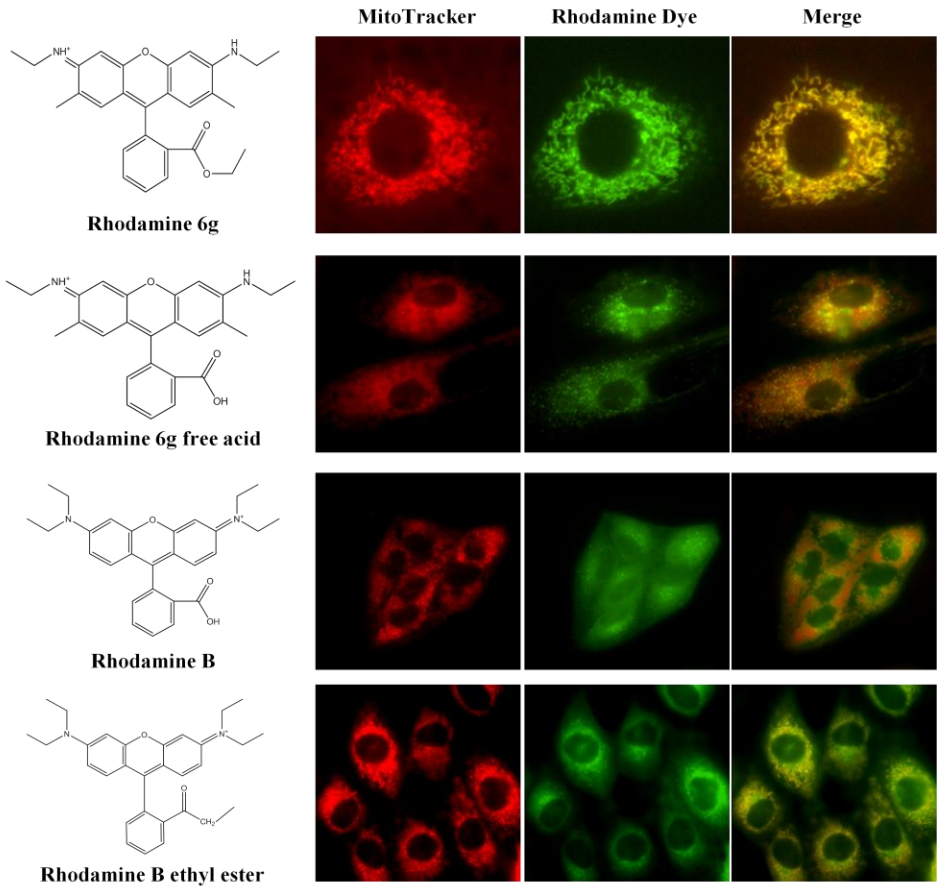

Figure 3.18 Fluorescence microscopy images (80x magnification) of CV-1 cells incubated simultaneously for 1 hour with either 0.5 µM Rh6g, 0.5 µM Rh6g free acid, 1 µM RhB, or 1 µM RhB ethyl ester and 1µM MitoTracker Deep Red 633. From left to right: fluorescence from MitoTracker (red), rhodamine dyes (green), and the merger of the two fluorescence images. In the right panels, yellow represents the subcellular regions in which the fluorescence from MitoTracker and the rhodamine dye overlap.

with their respective MitoTracker images, show a nearly perfect overlap suggesting that these two dyes are mitochondrial specific, similar to the ideal mitochondrial dye, Rh-123.

On the other hand, the mergers of the two fluorescence images of both Rh6gFA and RhB, with their respective MitoTracker images, reveal that there is not a perfect overlap. Here, the MitoTracker images display punctuated mitochondria whereas the rhodamine dye images reveal an even distribution of dye throughout the cytoplasm of the cell suggesting that these two free acid derivatives are not exclusively localized in the mitochondria. This lack of mitochondrial specificity is analogous to that observed with Rh-110. These dyes diffuse throughout the cytoplasm without mitochondrial localization due to the loss of the ester alkyl substituent (i.e. because they are zwitterionic at physiological pHs) (pKa of RhB's carboxylic group ~ 3.2, Woislawski 1953, Mchedlov-Petrossyan et al. 1994). These results further re-enforce the idea that the transmembrane transport process itself requires the protonated (cationic) form of the rhodamine dye (Jeannot et al. 1997, Trapp and Horobin 2005, Horobin et al. 2007). Further experiments would be needed to determine if these dyes will eventually find their way into the mitochondria when employing higher concentrations and longer cell exposure times similar to those previously used with Rh-110 (Jeannot et al. 1997). Based on these experimental results, it is reasonable to infer that in order for dyes to localize in the mitochondria with absolute specificity, the overall mechanism of cellular uptake and subcellular distribution of the above rhodamine dyes must be primarily controlled by the mitochondrial transmembrane potential and therefore, the rhodamine dye must be cationic, not zwitterionic.

Our results confirm the structural requirements for mitochondrial specificity in our chosen non-transformed cell line (CV-1), previously only described for high mitochondrial transmembrane potential tumor cell lines. The results observed in this experiment are consistent with the previously described idea that the transmembrane

transport process itself requires the cationic form for successful mitochondrial localization (i.e., Rh-123, Rh-Oct, Rh6g, RhBEE, Rh-123Br_2, and Rh-OctBr_2). In addition, our new zwitterionic dyes (Rh6gFA and RhB) and their respective cationic derivatives (Rh6g and RhBEE) are more lipophilic compared to Rh-110. Therefore, it can be concluded that the successful mitochondrial localization of our cationic dyes is controlled primarily by the mitochondrial transmembrane potentials and not due to the phenomenon of lipophilic partitioning. In the subsequent section, we have selected the classical mitochondrial dye, Rh-123, as our primary probe for the exploration of whether CV-1 cells could potentially be used as a single, same cell model in which the effects of the mitochondrial transmembrane potentials on selective cell kill could be explored.

3.3 Investigation of the Effect of Energy Substrate Availability on Cellular Morphology and Mitochondrial Transmembrane Potential in CV-1 Cells

An enhanced mitochondrial transmembrane potential is a common tumor cell phenotype. With the use of fluorescence microscopy, this characteristic transmembrane potential can be probed by many cationic dyes such as Rhodamine-123 (Rh-123). This dye efficiently localizes in the mitochondria and induces little phototoxicity when used in cell cultures. Here, we have explored the possibility that the mitochondrial transmembrane potential in our chosen non-transformed cell line (CV-1) could be enhanced to the levels typically found in tumor cells through the stimulation of specific anaplerotic pathways, such as glutaminolysis. Glutamine is a key metabolite required for a variety of diverse roles in mammalian cells including: the anabolic growth, biosynthesis of non-essential amino acids and protein translation (Wise and Thompson 2010, Young

and Ajami 2001). This pilot study was carried out in order to gain information on whether or not CV-1 cells could potentially be used as a single cell model in studies investigating selective cell kill via mitochondrial targeting in PDT.

3.3.1 Comparison of Early Changes in Cellular Morphology and Mitochondrial Transmembrane Potential in CV-1 Cells Every 4 Hours for 0-48 Hours

Early changes in cellular morphology and mitochondrial transmembrane potential were explored in "normal" CV-1 cells when switched from a media containing optimal amounts of the energy substrates glucose and glutamine (media #1) to a media containing no glucose and a high amount of glutamine (media #2). **Figure 3.19** shows the typical morphologies observed in the cell culture at 4, 8, and 12 hours after switching from media #1 to media #2. Noticeably, all of the cells display similar morphologies which are all commonly observed after initially plating CV-1 cells. In addition, all of the cells are growing at equal densities and it appears that they are all of similar size variations. Also, it is evident that there is no noticeable difference in the cellular morphology trend observed between either of the two growth conditions. In addition, the cellular morphologies can be clearly seen in the fluorescence images (**Figure 3.20**) when these cells were incubated with the prototypical mitochondrial probe, Rh-123, to test for increased dye uptake, indicative of an enhanced mitochondrial transmembrane potential. Analogously, **Figure 3.21** reveals no noticeable trend in the average integrated fluorescence intensity per cell, suggesting that the mitochondrial transmembrane potential

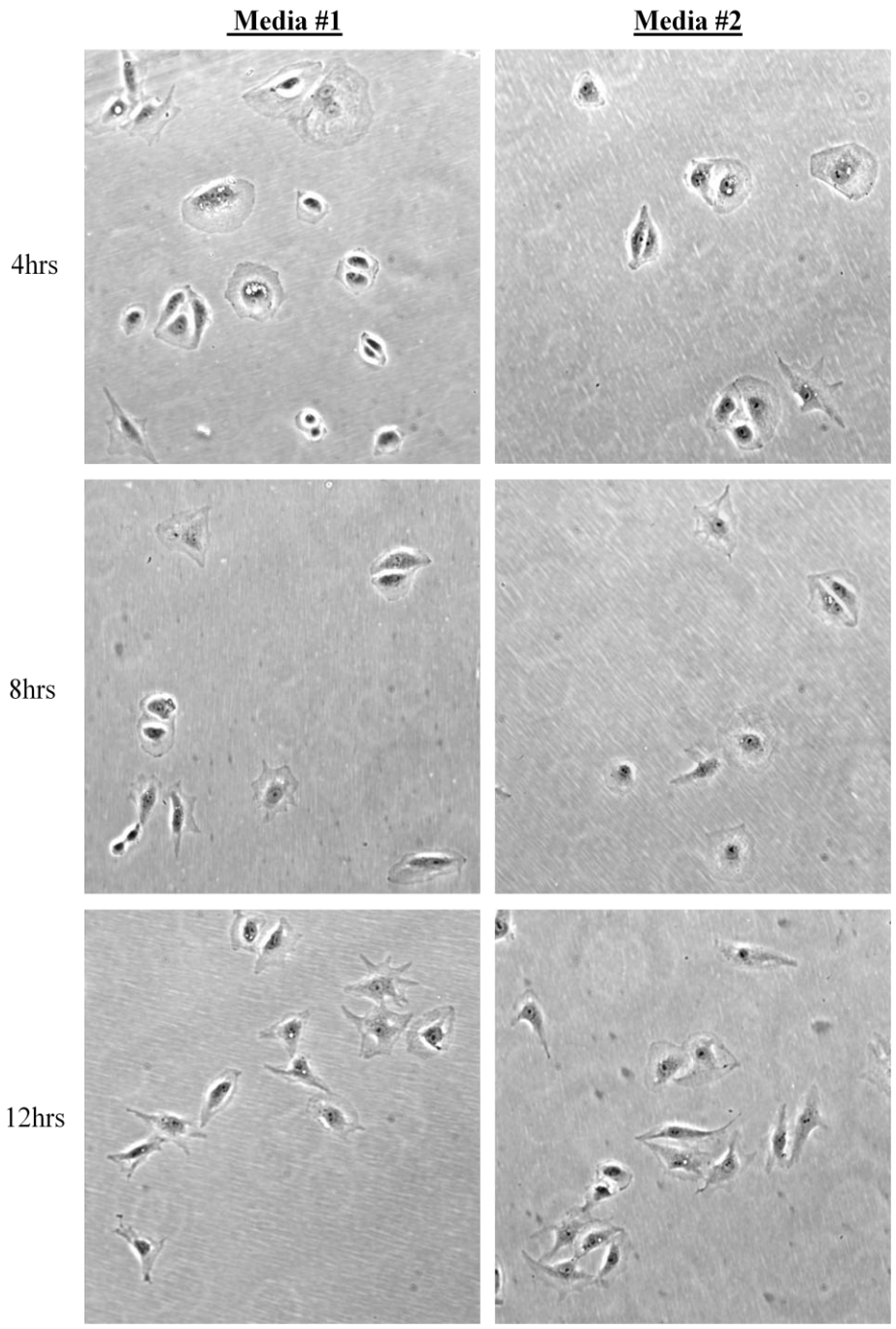

Figure 3.19 Bright field images (15x magnification) at 4, 8, and 12 hours showing the different morphologies of CV-1 cells incubated either in media #1 (optimal glucose/optimal glutamine; left panel) or in media #2 (no glucose/high glutamine; right panels).

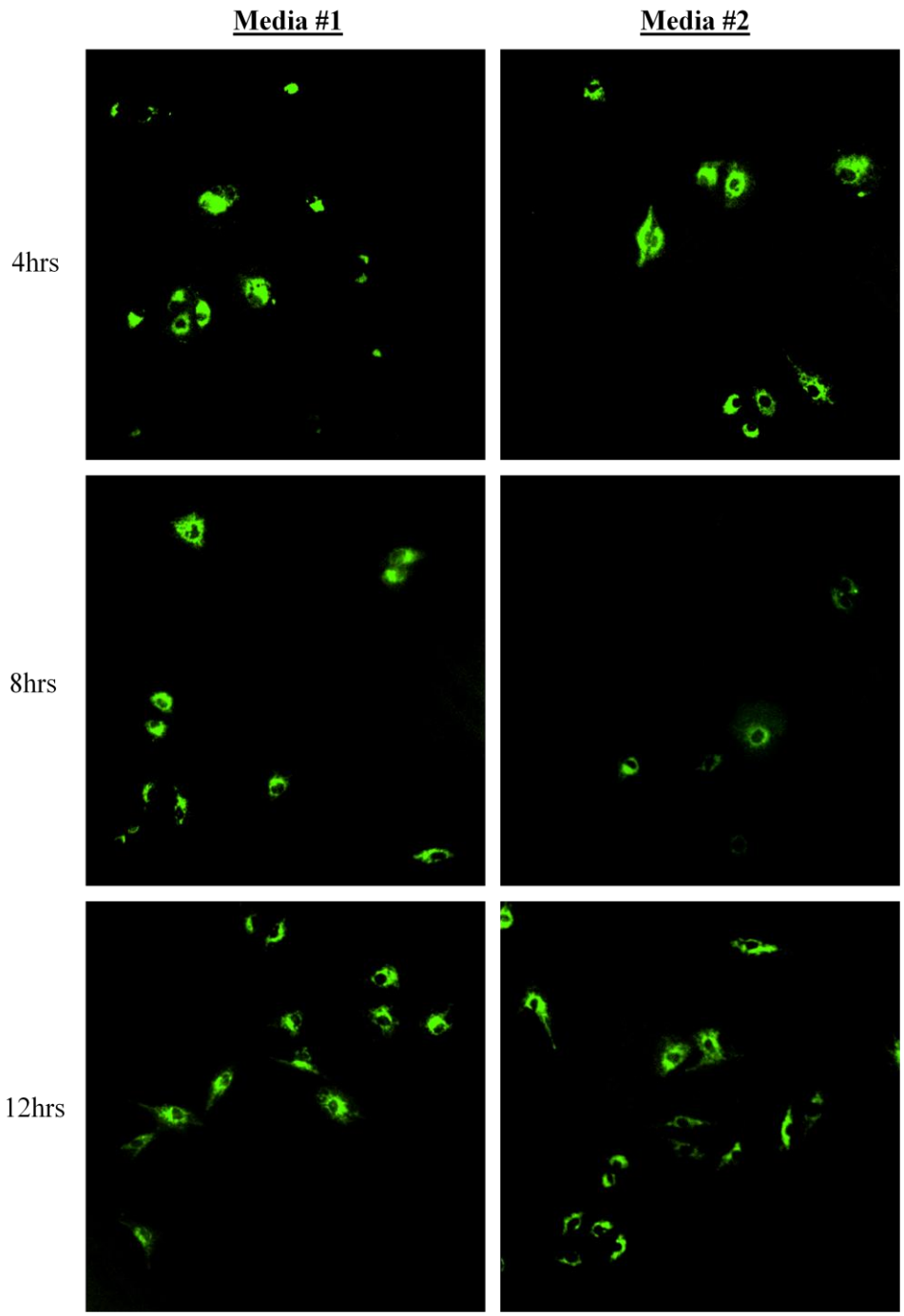

Figure 3.20 Fluorescence images (15x magnification) at 4, 8, and 12 hours of CV-1 cells incubated either in media #1 (optimal glucose/optimal glutamine; left panel) or in media #2 (no glucose/high glutamine; right panels).

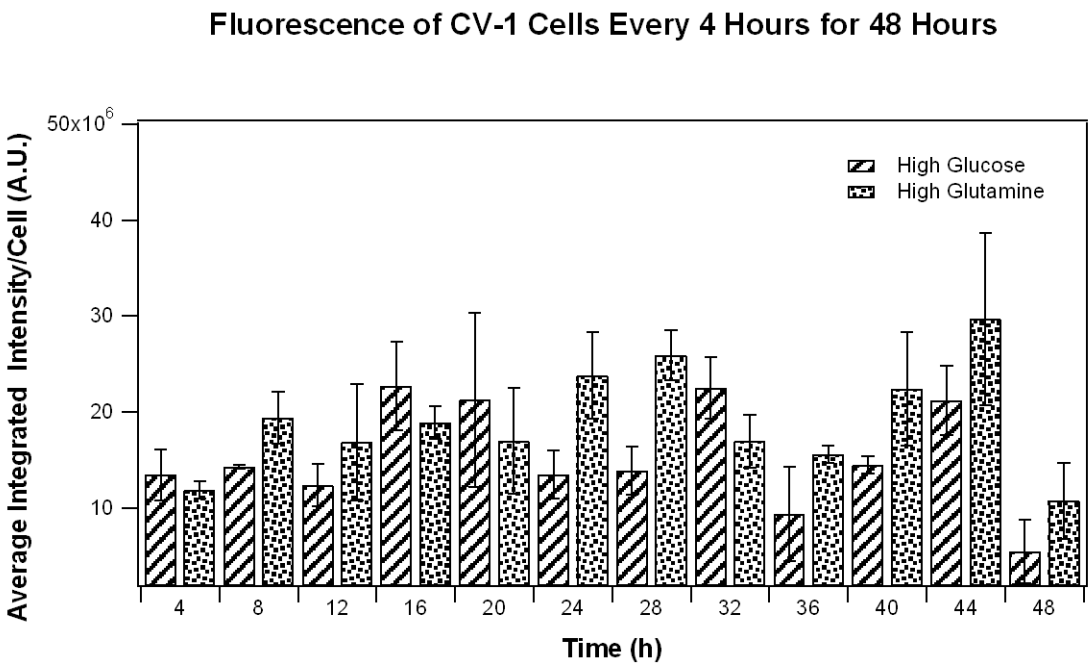

Figure 3.21 Average integrated fluorescence intensity comparison per CV-1 cell incubated either in media #1 (optimal glucose/optimal glutamine) or in media #2 (no glucose/high glutamine) every 4 hours for 48 hours.

is nearly the same under both growth conditions. Therefore, it is reasonable to infer that there is no difference in trend observed in cellular morphology or mitochondrial transmembrane potential in the first 12 hours when CV-1 cells are switched from media #1 to media #2.

Figure 3.22 shows the typical morphologies found in the cell culture at 16, 20, and 24 hours after switching from media #1 to media #2. In this figure, it can be seen that at each time interval all of the CV-1 cells are growing at comparable densities and there

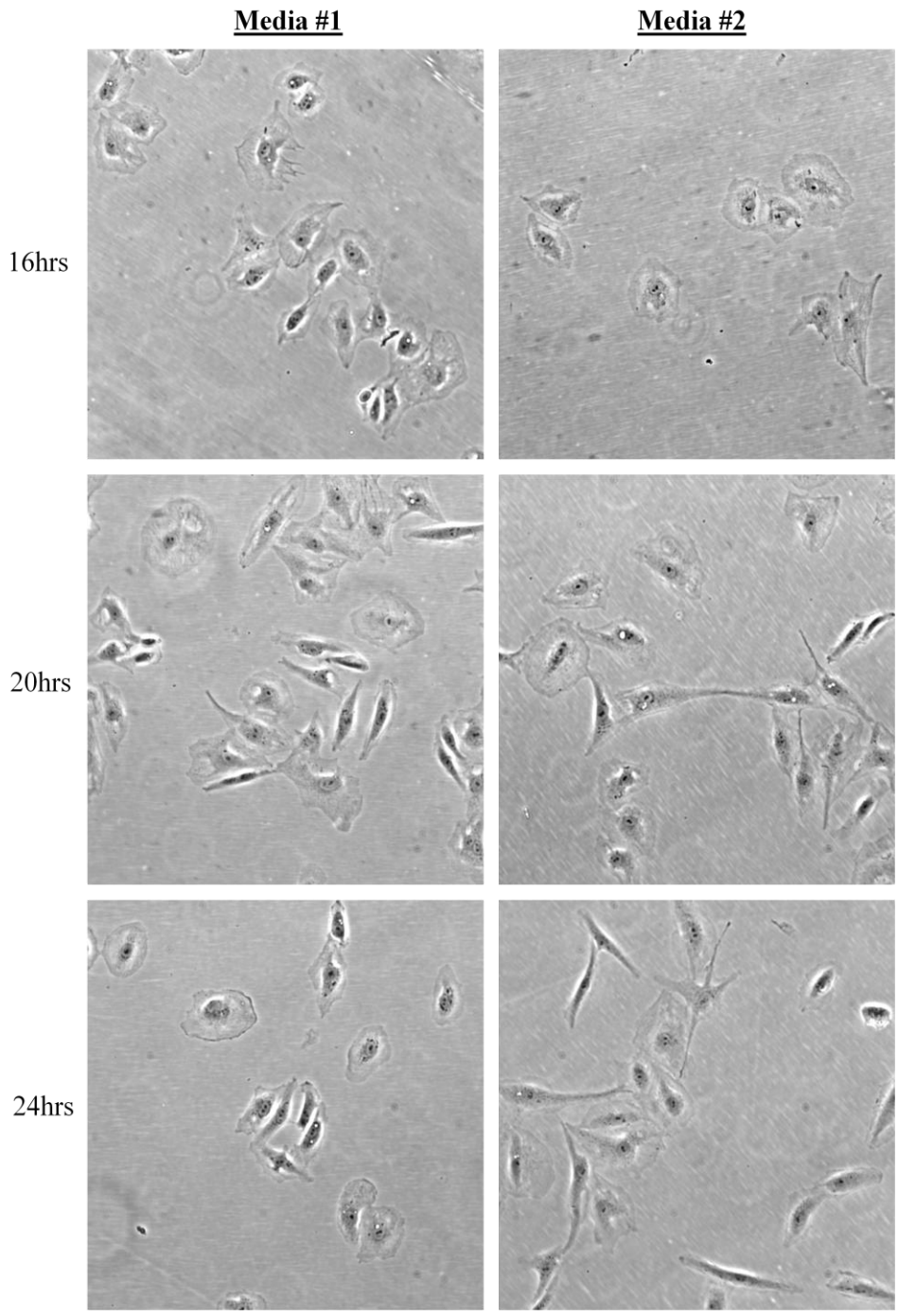

Figure 3.22 Bright field images (15x magnification) at 16, 20, and 24 hours showing the different morphologies of CV-1 cells incubated either in media #1 (optimal glucose/optimal glutamine; left panel) or in media #2 (no glucose/high glutamine; right panels).

are no obvious differences in the cellular morphology trend observed between the two growth conditions at 16 hours. However, it can be seen that at 20 hours the cells incubated in media #2 display an increase in the proportion of slightly elongated cells, also eminent at 24 hours. Furthermore, this increase in slightly elongated cells can be clearly seen in the fluorescence images (**Figure 3.23**) of the cells incubated in media #2 at both 20 and 24 hours. On the other hand, **Figure 3.21** reveals no detectable difference in trend observed between the two growth conditions at 16, 20, or 24 hours when the average integrated fluorescence intensity per cell is compared. Therefore, it is reasonable to infer that there is no enhancement of the mitochondrial transmembrane potential during the first 24 hours when the cells were switched from media #1 to media #2. However, there is a modest trend observed in cellular morphology change beginning at 20 hours after switching energy substrates from primarily glucose to primarily glutamine.

The same cell culture incubated in media #1 and media #2 was continually observed every 4 hours for an additional 24 hours. **Figure 3.24** shows the typical morphologies found under both conditions at 28, 32, and 36 hours. Here, there is an observable population of slightly elongated cells in the cell cultures comparative to those seen at 20 hours (**Figure 3.22**). There is no noticeable trend in the change in cellular morphology other than a small population of slightly elongated cells in media #2 after initially switching energy substrates from primarily glucose to primarily glutamine. Conversely, it can be observed that there is a small portion of slightly elongated cells which begin to appear in the cell culture incubated under control conditions (media #1) at 28 hours. Again, this distribution of observed cellular morphologies is made even more

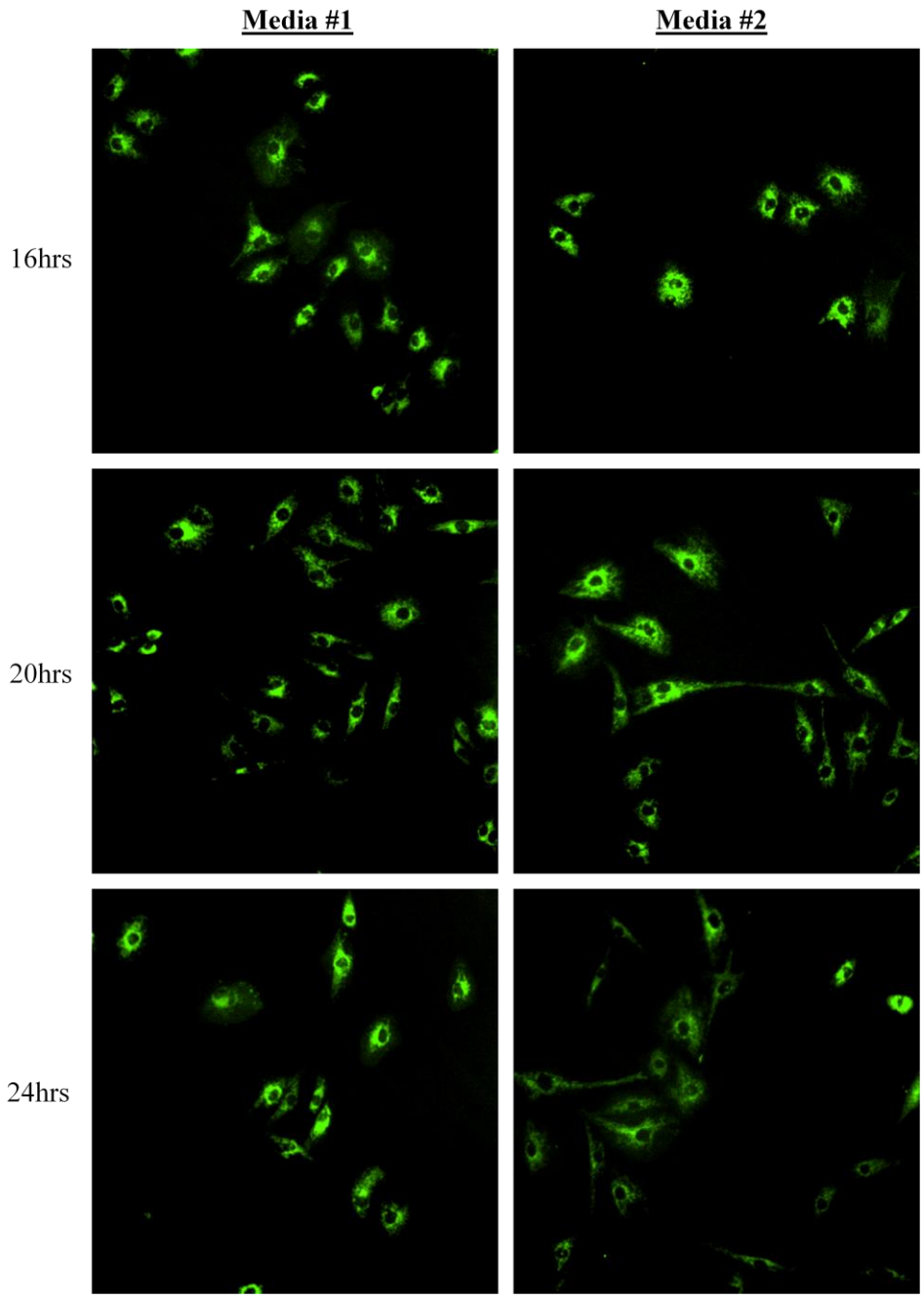

Figure 3.23 Fluorescence images (15x magnification) at 16, 20, and 24 hours of CV-1 cells incubated either in media #1 (optimal glucose/optimal glutamine; left panel) or in media #2 (no glucose/high glutamine; right panels).

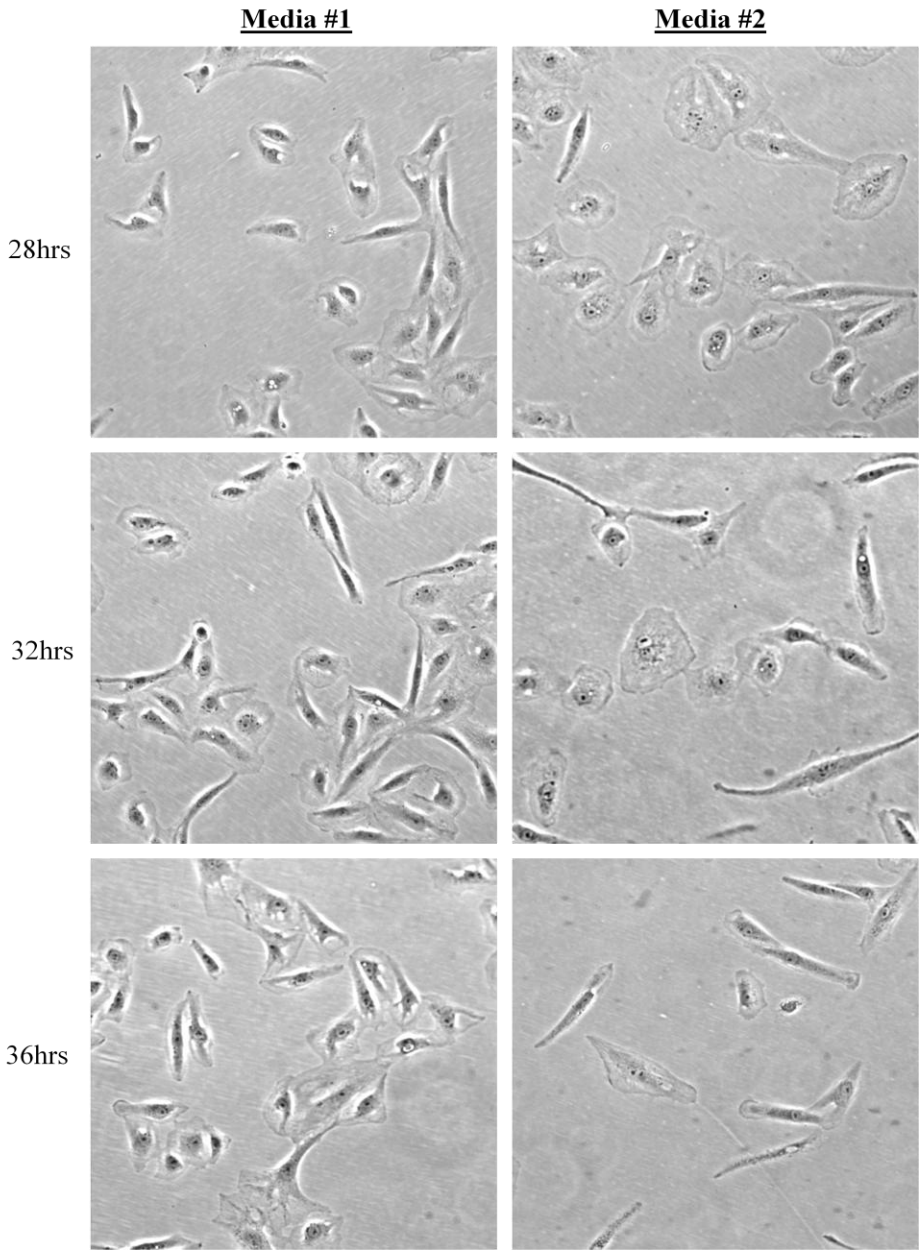

Figure 3.24 Bright field images (15x magnification) at 28, 32, and 36 hours showing the different morphologies of CV-1 cells incubated either in media #1 (optimal glucose/optimal glutamine; left panel) or in media #2 (no glucose/high glutamine; right panels).

evident when viewing the fluorescence images (**Figure 3.25**) of these cells. Furthermore, **Figure 3.26** shows that the morphologies found in the cells at 40, 44, and 48 hours are still displaying the same morphological trend noted at 36 hours (**Figure 3.25**) under both conditions. That is, there is still an increased population of slightly elongated cells observed in the cell culture incubated in media #2. Similarly, the observed morphologies are more evident when the mitochondrial transmembrane potential is probed employing the fluorescent dye, Rh-123 (**Figure 3.27**). Moreover, the average integrated fluorescence intensity per cell was acquired and plotted (**Figure 3.21**) with still no observable difference in trend within the initial 48 hours after the cells were switched from media #1 to media #2.

The results obtained here suggest that the enhanced mitochondrial transmembrane potential that is typically found in tumor cells cannot be induced in CV-1 cells within the first 48 hours by supplementing the growth media with copious amounts of glutamine, forcing these cells to use the anaplerotic pathway of glutaminolysis which is commonly employed by various tumor cell lines. Notably, there was an observable difference in the time interval in which the CV-1 cells start to display a slightly elongated morphology. In order to explore this effect in more detail, an additional experiment was designed and carried out in which the cellular morphology and mitochondrial transmembrane potential were monitored and compared for an additional 24 hour period of incubation.

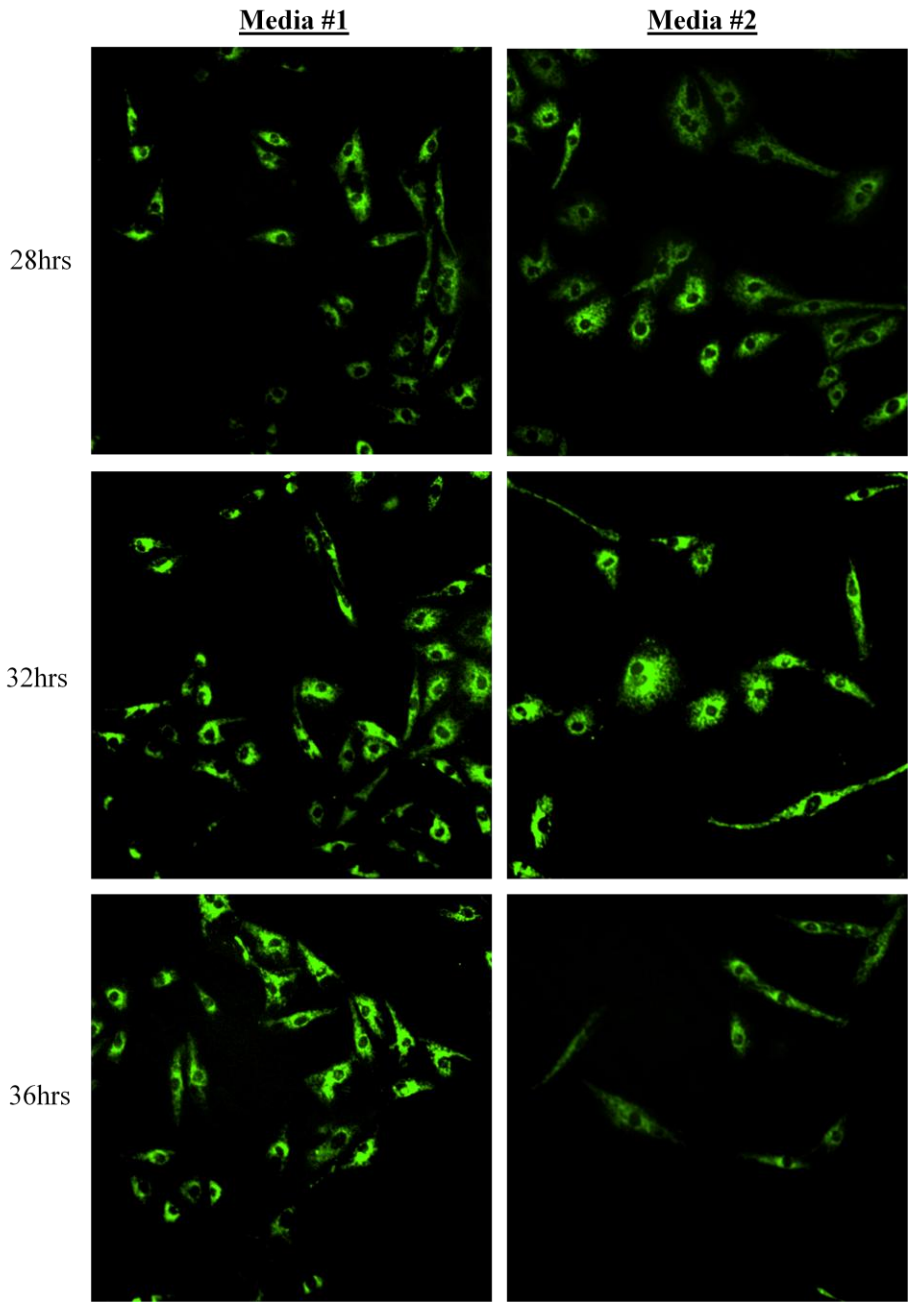

Figure 3.25 Fluorescence images (15x magnification) at 28, 32, and 36 hours of CV-1 cells incubated either in media #1 (optimal glucose/optimal glutamine; left panel) or in media #2 (no glucose/high glutamine; right panels).

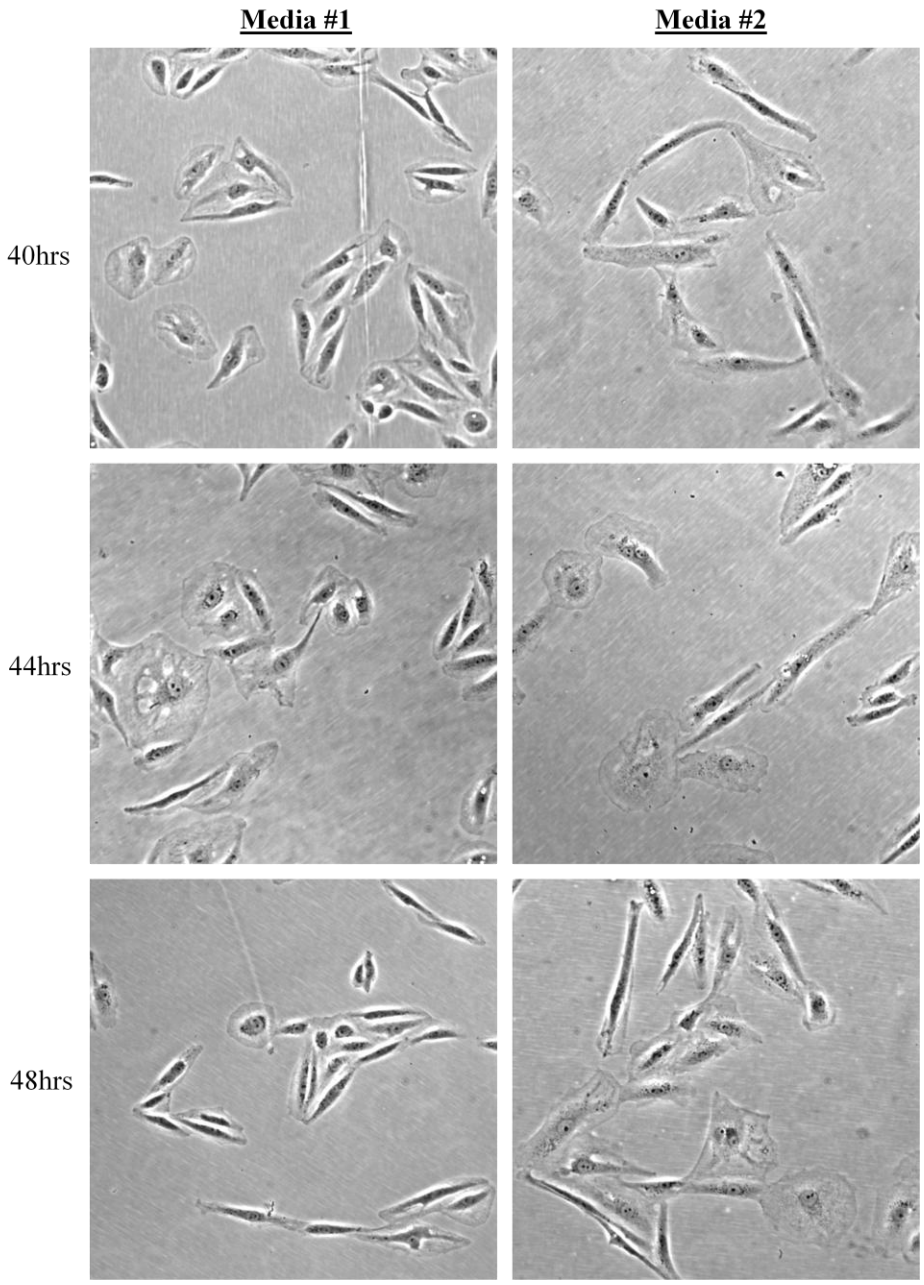

Figure 3.26 Bright field images (15x magnification) at 40, 44, and 48 hours showing the different morphologies of CV-1 cells incubated either in media #1 (optimal glucose/optimal glutamine; left panel) or in media #2 (no glucose/high glutamine; right panels).

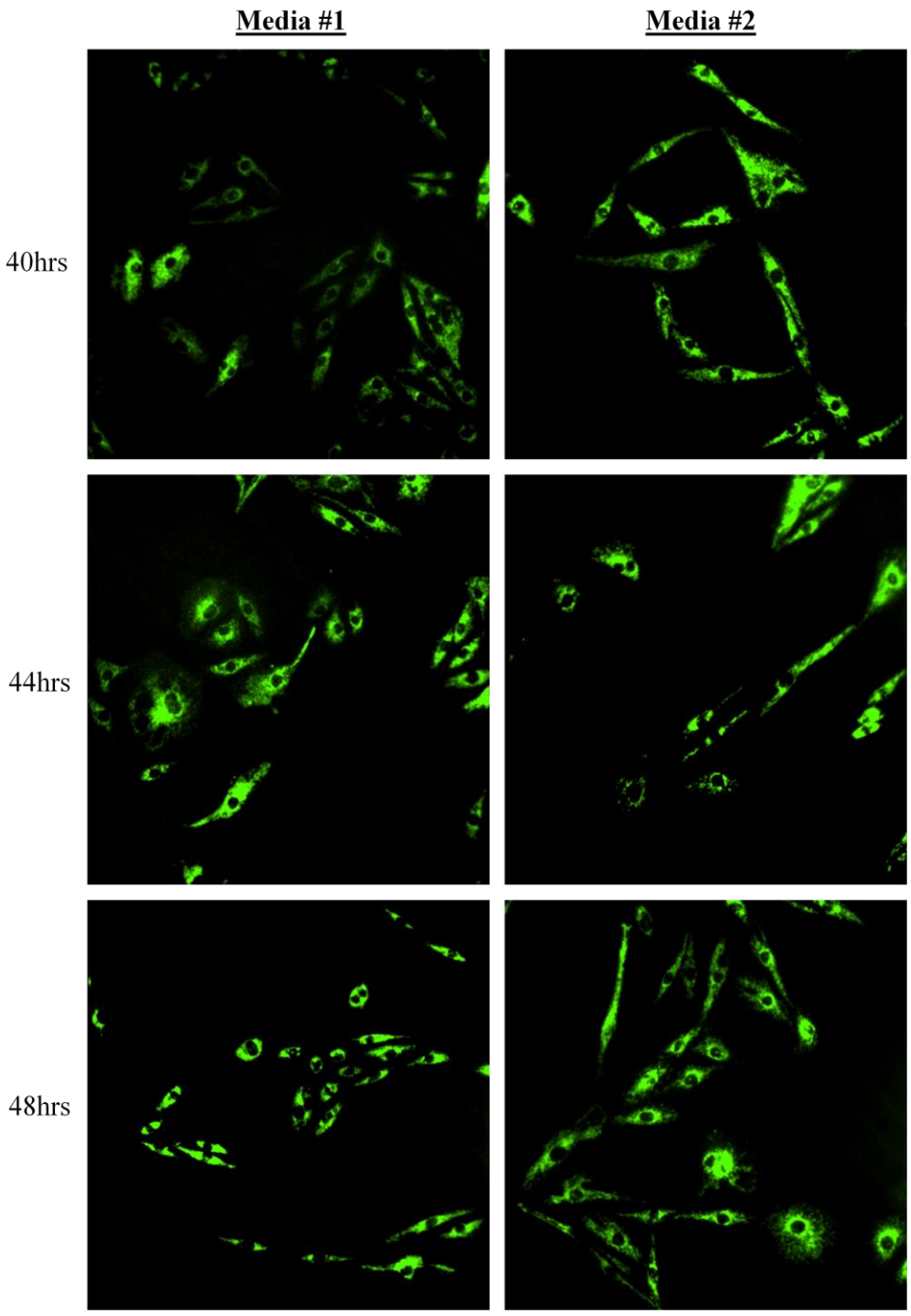

Figure 3.27 Fluorescence images (15x magnification) at 40, 44, and 48 hours of CV-1 cells incubated either in media #1 (optimal glucose/optimal glutamine; left panel) or in media #2 (no glucose/high glutamine; right panels).

3.3.2 Comparison of Changes in Cellular Morphology and Mitochondrial Transmembrane Potential in CV-1 Cells Every 12 Hours for 0-72 Hours

The study in 3.3.1 was repeated where CV-1 cells were switched from media #1 to media #2. However, in this study the cells were observed every 12 hours for 72 hours, an additional 24 hours than in part 3.3.1. This was done in order to determine if there were further changes in cellular morphology or enhancement of the mitochondrial transmembrane potential that could be observed in the first 72 hours. The same trend in cellular morphology was observed in the first 48 hours as in part 3.3.1. **Figure 3.28** shows the typical morphologies found in the cell culture at 60 and 72 hours after switching from media #1 to media #2. In this figure, it is observed that there is still an increase in the population of slightly elongated cells observed in the culture incubated in media #2 and a seemingly unequal distribution of this same morphology found in the cells grown in media #1. In addition, this morphology distribution can also be seen in the cellular fluorescence images (**Figure 3.29)**. The average integrated intensity was acquired from all the fluorescence images of the CV-1 cells incubated with Rh-123 and subsequently plotted for comparison. **Figure 3.30** shows that there is no clear trend observed when comparing the Rh-123 dye uptake of the CV-1 cells in the initial 72 hour period.

The difference in time intervals at which the CV-1 cells exhibit a slight change in cellular morpholgy observed in the previous experiment sparked interest in screening for any additional changes over a longer time period. Consequently, a study was set up in which CV-1 cell cultures could be monitored for any major changes in cellular morphology over a 36 day time period when grown in media #1 compared to media #2.

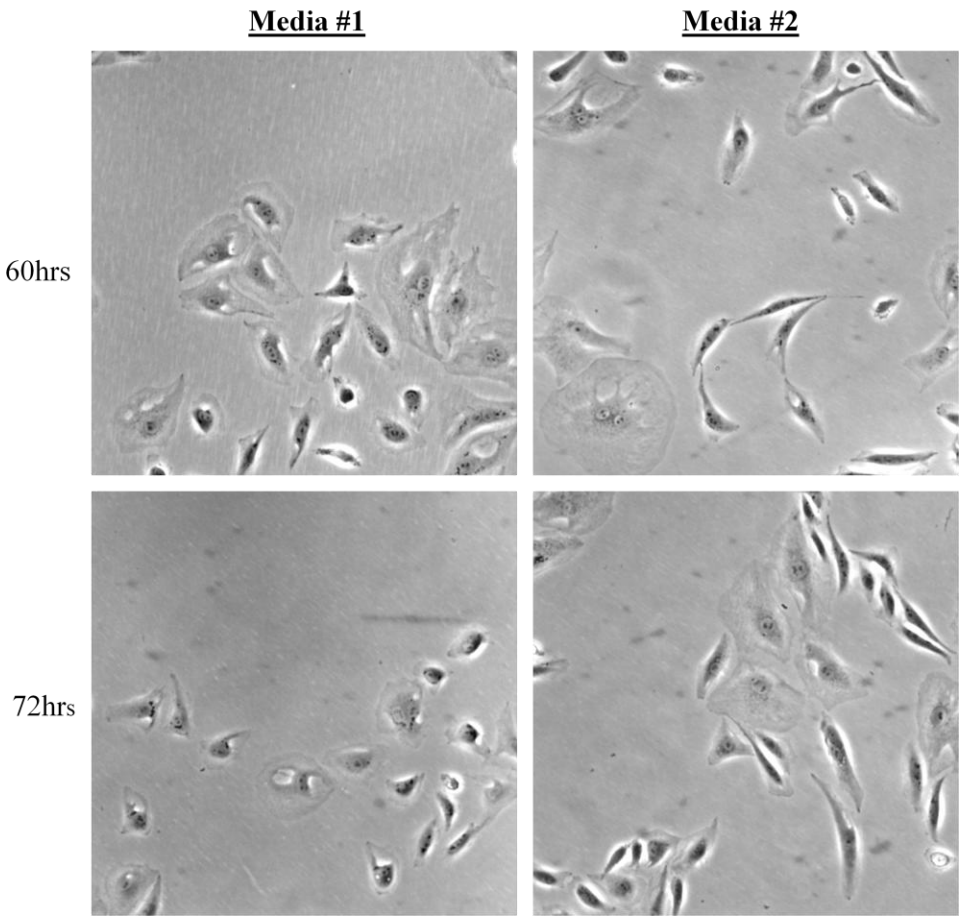

Figure 3.28 Bright field images (15x magnification) at 60 and 72 hours showing the different morphologies of CV-1 cells incubated either in media #1 (optimal glucose/optimal glutamine; left panel) or in media #2 (no glucose/high glutamine; right panels).

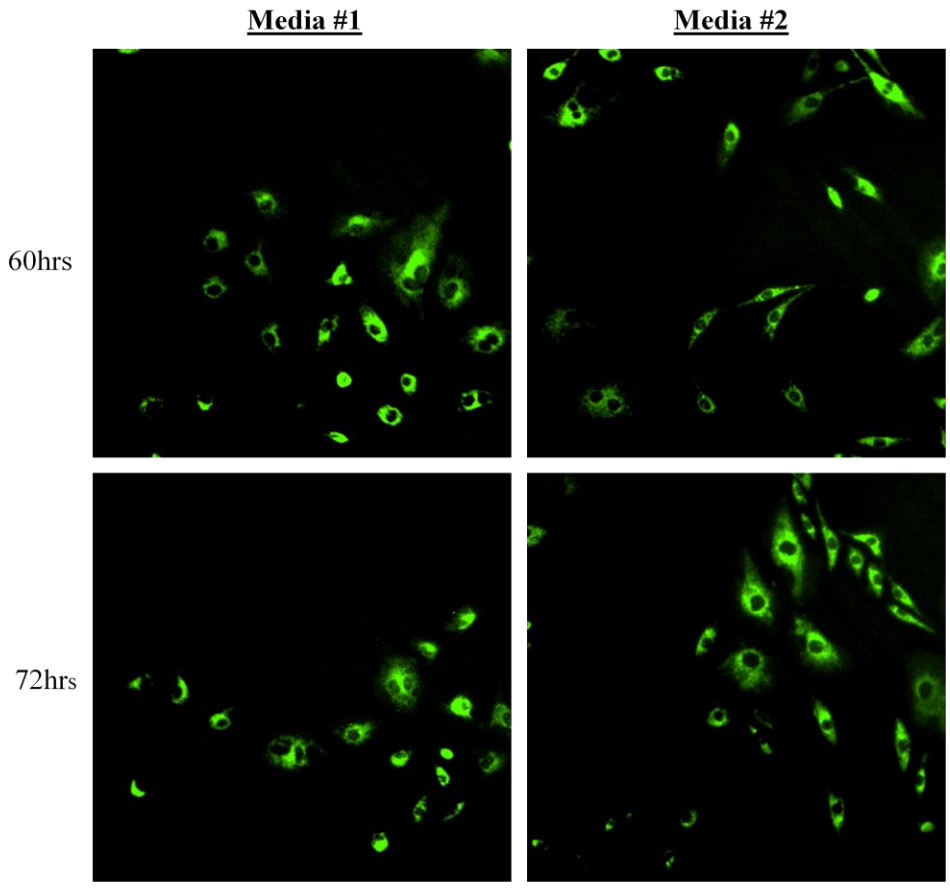

Figure 3.29 Fluorescence images (15x magnification) at 60 and 72 hours of CV-1 cells incubated either in media #1 (optimal glucose/optimal glutamine; left panel) or in media #2 (no glucose/high glutamine; right panels).

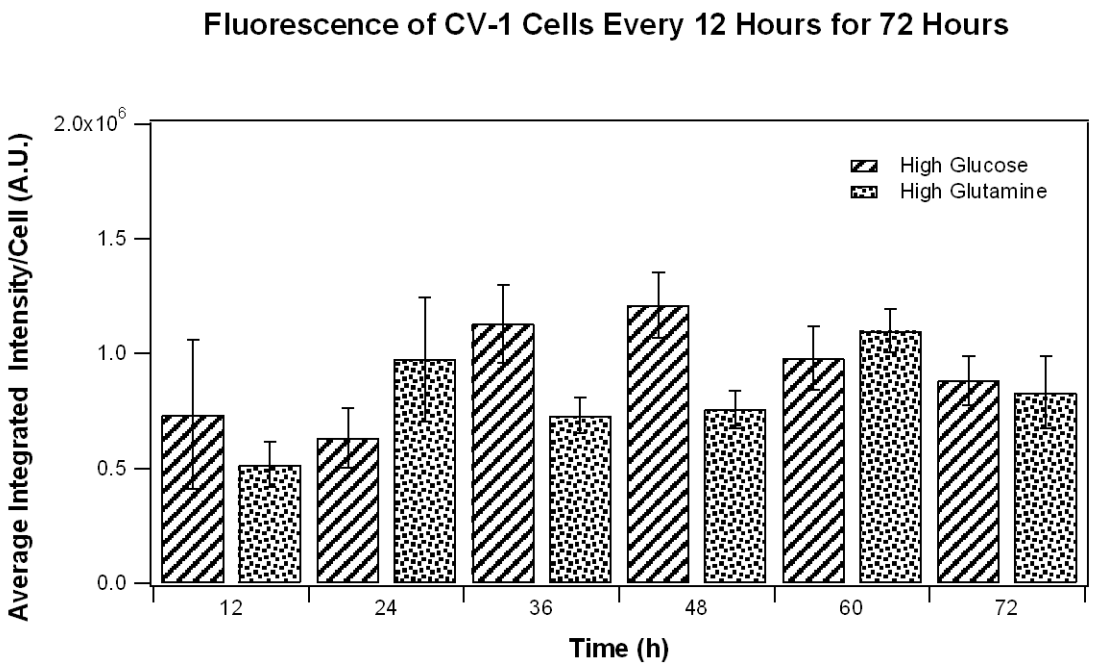

Figure 3.30 Average fluorescence intensity comparison per CV-1 cells incubated either in either media #1 (optimal glucose/optimal glutamine) or media #2 (no glucose/high glutamine) every 12 hours for 72 hours.

3.3.3 Comparison of Changes in Cellular Morphology in CV-1 Cells Over 36 Days

The morphology changes observed for long periods of incubation as shown in **Figures 3.31-3.32** were very pronounced. **Figure 3.31** shows the typical morphologies found in the above cell culture at 3, 9, and 12 days for the cells grown in media #1 and media #2. Comparatively, there appears to be a small population of slightly elongated cells in media #2 observed at 9 days. Interestingly, it can be seen that at 12 days there appears to be a remarkable difference in morphology between the two growth conditions. Here, the cells in media #1 are still growing in a normal, healthy manner typical of CV-1

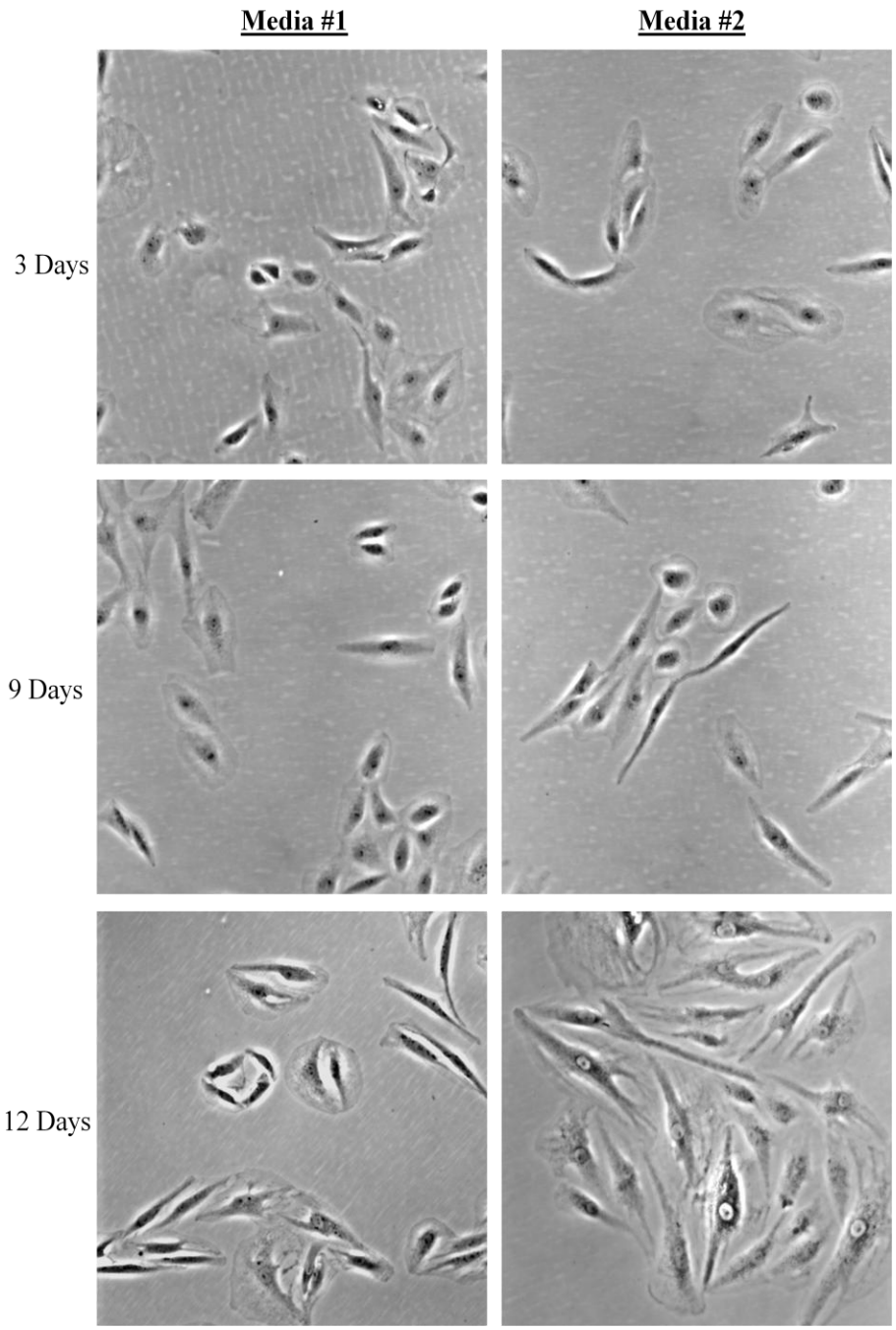

Figure 3.31 Bright field images (15x magnification) showing the different morphologies at 3, 9, and 12 days for CV-1 cells incubated either in media #1 (optimal glucose/optimal glutamine; left panel) or in media #2 (no glucose/high glutamine; right panels).

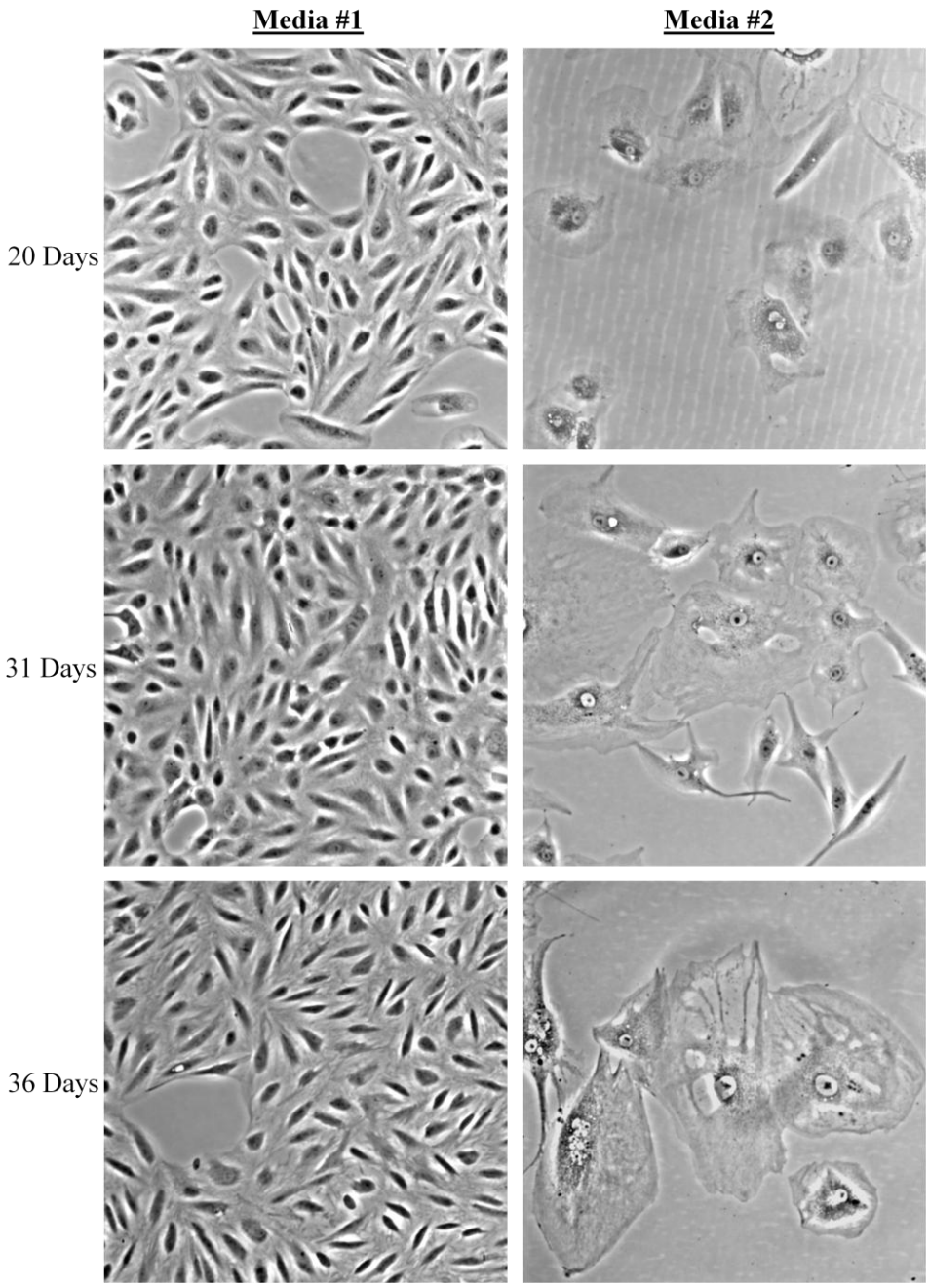

Figure 3.32 Bright field images (15x magnification) showing the different morphologies at 20, 31, and 36 days of CV-1 cells incubated either in media #1 (optimal glucose/optimal glutamine; left panel) or in media #2 (no glucose/high glutamine; right panels).

cells. On the other hand, the cells in media #2 emerge as visibly more granular and significantly larger in size. Additionally, in some cases the nucleus of the cells cultured in media #2 seems to be visibly larger. Also, there were no distinct differences in cellular morphology observed between the two growth conditions at 12 and 15 days (data not shown). **Figure 3.32** shows the typical morphologies found in the cell culture at 20, 31, and 36 days for the cells grown in media #1 to media #2. In this figure, it can be seen that all of the cells grown in media #1 at each time interval appear to be growing normal and in a healthy monolayer to near confluence, however, the cells in media #2 at 20 days appear to be slightly more round in shape distribution and do not appear to be growing in the same confluent pattern. This growth pattern and enlarged morphology can be observed at 31 days and persists until 36 days where the cells are significantly larger and unhealthy. These alterations in cellular morphology may be possibly attributed to autophagy, however, further testing using methods such as an autophagy detection kit would be needed in order to be certain (Mizushima et al. 2010). Overall, the results observed under the growth conditions at 12 days, and longer time periods, suggest that the over stimulation of the glutaminolysis pathway has a significant long-term effect on the growth of these cells.

Glutamine is a key metabolite needed by mammalian cells. It is known to donate its amide group in at least three enzymatic steps for purine synthesis and two steps in pyrimidine synthesis as well as contributing to the non-essential amino acid needs of the cell (Wise and Thompson 2010, Young and Ajami 2001, Ahluwalia et al. 1990). This contribution of glutamine to amino acid biosynthesis ascertains it as an essential factor for the protein translation needs of the cell, especially tumor cells because they typically

grow faster. Previous studies have shown that a significant amount of the glutamine taken up by certain cells is not used for anabolic metabolism (Nicklin et al. 2009). Rather, it may have many other important functions in various cellular pathways including the activation of protein translation and the inhibition macroautophagy in various cells (Wullschleger et al. 2006). Nonetheless, the late changes (i.e., 31+ days) in cellular morphology observed in the absence of glucose indicate that the CV-1 cells cannot sustain a close to normal growth pattern for long periods without glucose. Further experiments will be needed in order to better understand the determinants of the major morphological changes associated with long-term use of glutamine as the primary energy substrate in growth media.

3.3.4 Exploration of Cellular Morphology and Comparison of Mitochondrial Transmembrane Potential at 12 Days with Rh-123 and Rh-110

The previous experiments revealed that at 12 days there is a significant difference in cellular morphology observed between the cells cultured in media #1 compared to those in media #2. Although significantly enlarged, the cells in media #2 at this time period maintained a growing pattern typical of CV-1 cells. That is, they stretched and grew towards each other and cellular proliferation was observed. The over abundance of glutamine in the growth media is therefore thought to be responsible for the observable difference in cellular morphology. Recent studies suggest that glutamine is also the primary mitochondrial substrate and is needed for maintaining the mitochondrial transmembrane potential in mammalian cells (DeBerardinis et al. 2007). Moreover, some tumor cells are known to consume significant amounts of glutamine that exceed the cell's

use of glutamine for protein translation and nucleotide biosynthesis (Wise et al. 2008, DeBerardinis et al. 2007). Therefore, it was further hypothesized that the CV-1 cells displaying the noticeable change in cellular morphology at 12 days, presumably due to an increased glutamine metabolism, may also display an enhanced mitochondrial transmembrane potential similar to the one found in many tumor cells.

The subsequent experiment compared the dye uptake of cationic Rh-123 (exclusively mitochondrial) and zwitterionic Rh-110 (non-mitochondrial). Here, it is important to note that while the mitochondrial localization of Rh-110 under comparable experimental conditions is a slow process (Jeannot et al. 1997), the respective cell uptake in the cytosol is relatively fast as will be seen in the following figures. Therefore, incubation times of 1 hour and concentrations of 1 μM for both dyes were used in order to give the Rh-110 dye enough time to be taken up by the cells. **Figure 3.33** and **Figure 3.34** show the fluorescence and bright field images of Rh-123 and Rh-110, respectively. Both figures show a visual increase in fluorescence intensity for the cells cultured for 12 days in media #2. In addition, **Figure 3.35** and **Figure 3.36** show the bar graphs of the integrated fluorescence intensity per cell for the cells cultured in media #1 and media #2 for Rh-123 and Rh-110, respectively. Comparatively, the integrated fluorescence intensity per cell for those incubated in Rh-123 is nearly 40 times more for the cells cultured in media #2 compared to those cultured in media #1. Also, the integrated fluorescence intensity per cell for those incubated in Rh-110 it is nearly 13 times more for those cultured in media #2 compared to those cultured in media #1. Collectively, these observations suggest that the cells cultured in media #2 are taking up more Rh-123 and Rh-110 compared to those cultured in media #1. In order to further explore this

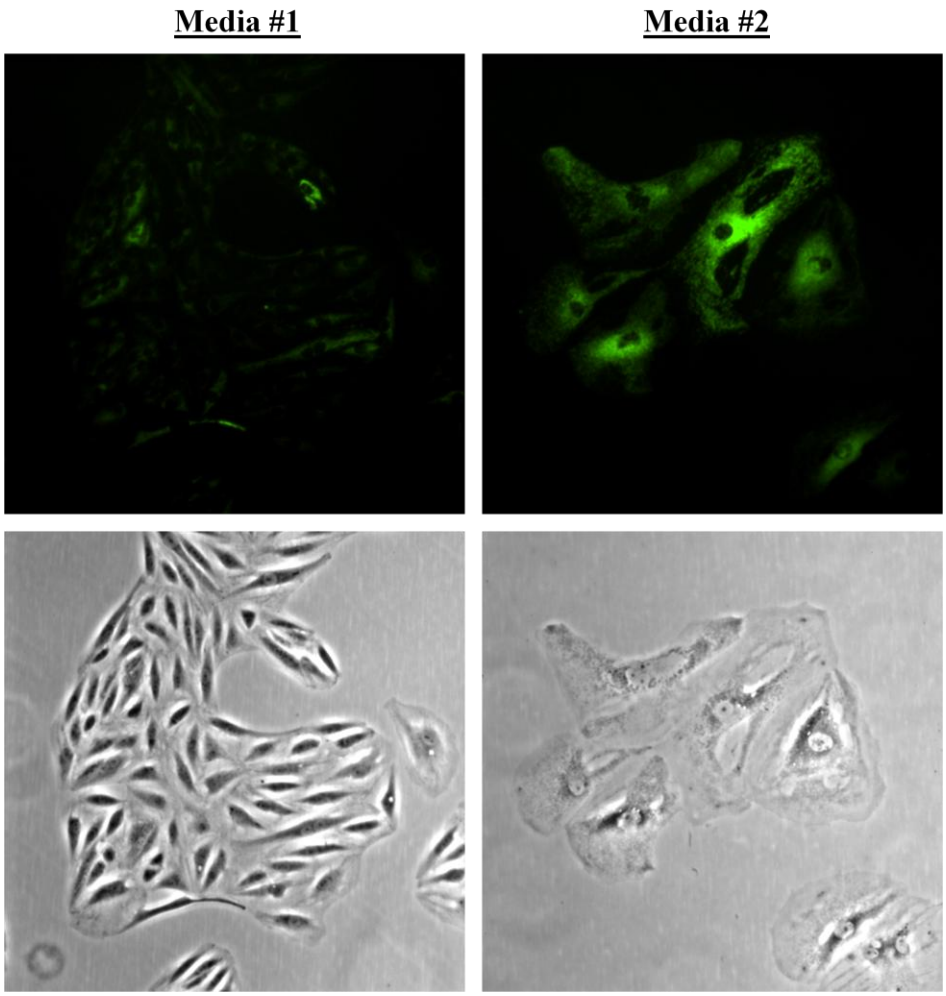

Figure 3.33 Top panels: visual comparison of fluorescence of CV-1 cells (15x magnification) incubated with 1μM Rhodamine-123 for 1 hour. Left: CV-1 cells previously grown for 12 days in media #1 (optimal glucose/optimal glutamine; left panel) and media #2 (no glucose/high glutamine; right panels). Lower panels: respective bright field images.

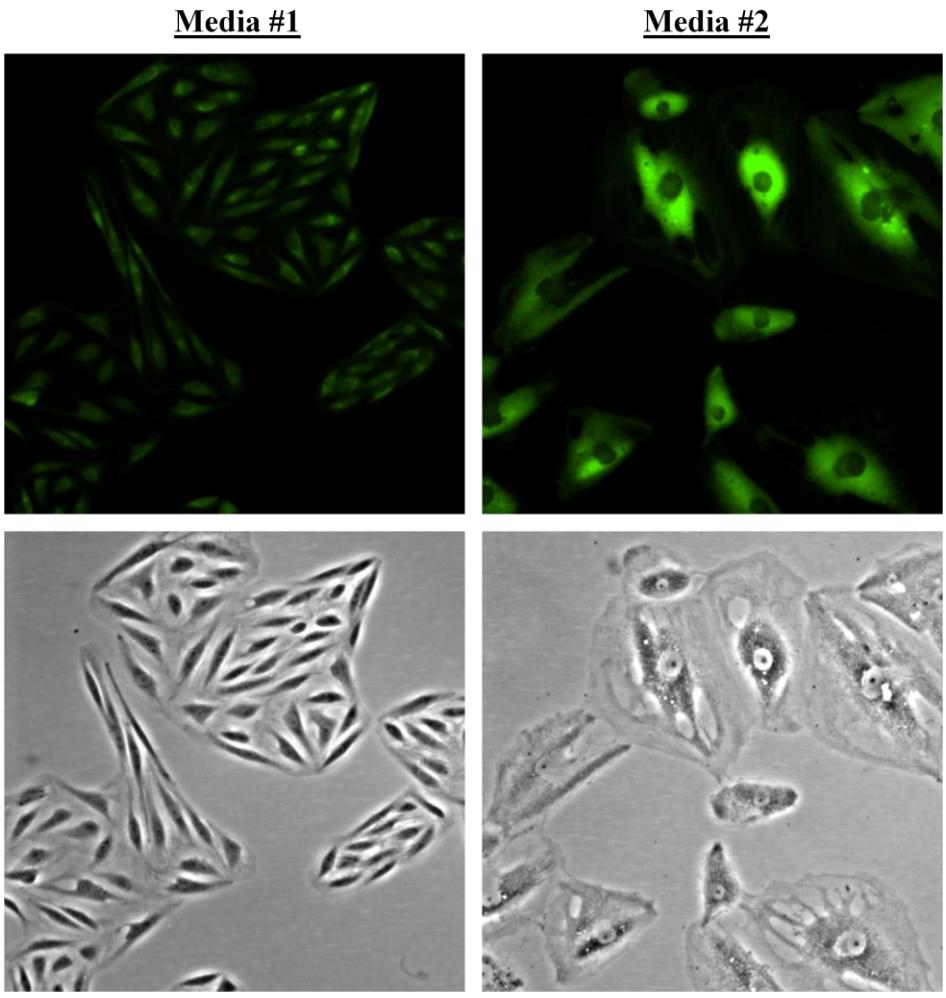

Figure 3.34 Top panels: visual comparison of fluorescence of CV-1 cells (15x magnification) incubated with 1μM Rhodamine-110 for 1 hour. Left: CV-1 cells previously grown for 12 days in media #1 (optimal glucose/optimal glutamine; left panel) and media #2 (no glucose/high glutamine; right panels). Lower panels: respective bright field images.

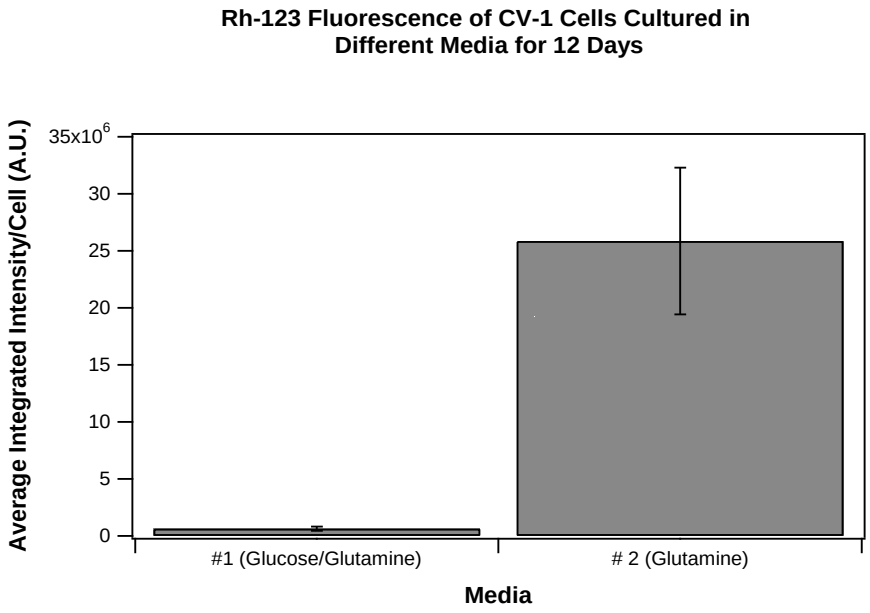

Figure 3.35 Average integrated fluorescence intensity comparison (1μM Rhodamine-123 for 1 hour) per CV-1 cell cultured either in media #1 (optimal glucose/optimal glutamine) and media #2 (no glucose/high glutamine) for 12 days.

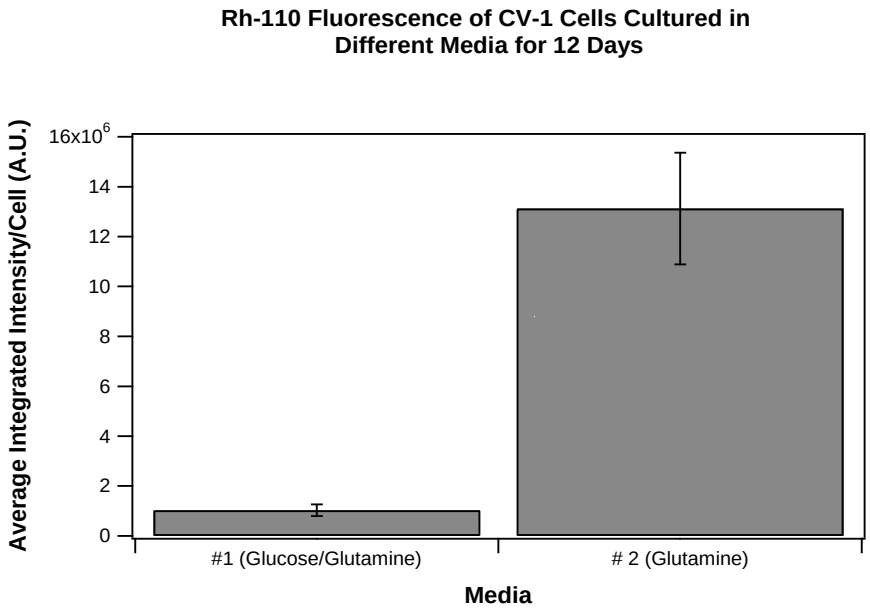

Figure 3.36 Average integrated fluorescence intensity comparison (1μM Rhodamine-110 for 1 hour) per CV-1 cell cultured either in media #1 (optimal glucose/optimal glutamine) and media #2 (no glucose/high glutamine) for 12 days.

phenomenon, the bar graphs displaying the integrated fluorescence intensity per cell were corrected for the enlargement in size of the cells cultured in media #2. **Figure 3.37** shows that the average area per cell for those incubated with Rh-123. Here, the average area per cell is 1 $\pm$ 0.2 units of area for those cells cultured in media #1 and the average area per cell is 13 $\pm$ 1 units of area for those cultured in media #2. Similarly, **Figure 3.38** shows that the average area per cell for those incubated with Rh-110. Here, the average area per cell is 1 $\pm$ .1 units of area for those cells cultured in media #1 and the average area per cell is 10 $\pm$ 0.9 units of area for those cultured in media #2. These average cell areas/sites (5 distinct images for each) were obtained using the sampling strategy described in section 2.2.11.1 of Materials and Methods. **Figure 3.35** and **Figure 3.36** were then corrected for the differences in size described in **Figure 3.37** and **Figure 3.38**. After correcting for size, the average fluorescence intensity per cell for those incubated in Rh-123 is nearly 3 times more for the cells cultured in media #2 compared to those the cells cultured in media #1 (**Figure 3.39**). In addition, the average fluorescence intensity per cell for those incubated in Rh-110 is only about 1.3 times higher for the cells cultured in media #2 compared to those cultured in media #1 (**Figure 3.40**). Initially, it was hypothesized that the CV-1 cells displaying the observed change in cellular morphology at 12 days would also display an enhanced mitochondrial transmembrane potential in analogy to what is found in many tumor cells. These experiments indicate that the cells cultured in media #2 are taking significantly more Rh-123 as compared to Rh-110 when switched from media #1 to media #2. The higher accumulation of Rh-123, as compared to Rh-110, suggests the possible enhancement of the mitochondrial transmembrane potential observed in the CV-1 cells cultured in media #2. Comparatively, there is not a significant

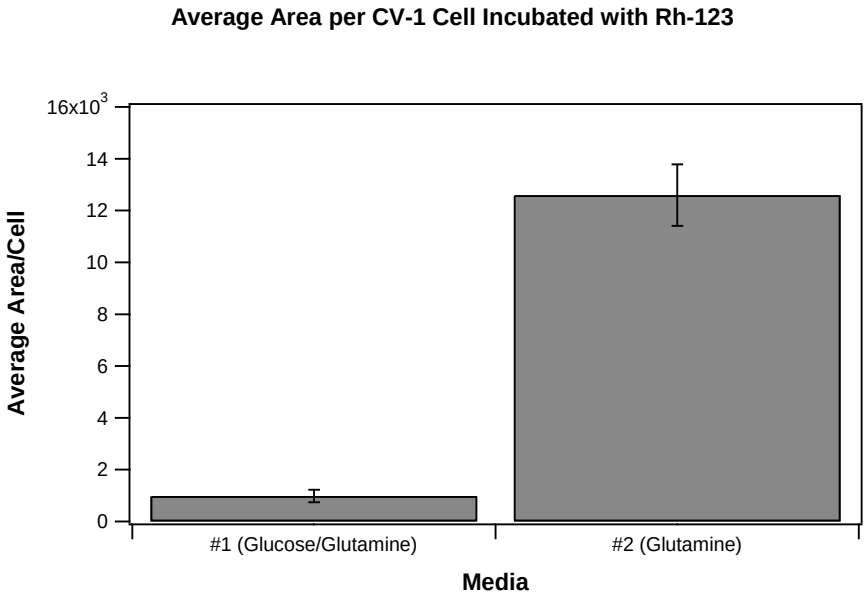

Figure 3.37 Average area comparison per cell of CV-1 cells previously grown in media #1 (optimal glucose/optimal glutamine) or in media #2 (no glucose/ high glutamine) for 12 days incubated in 1μM Rhodamine-123 for 1 hour.

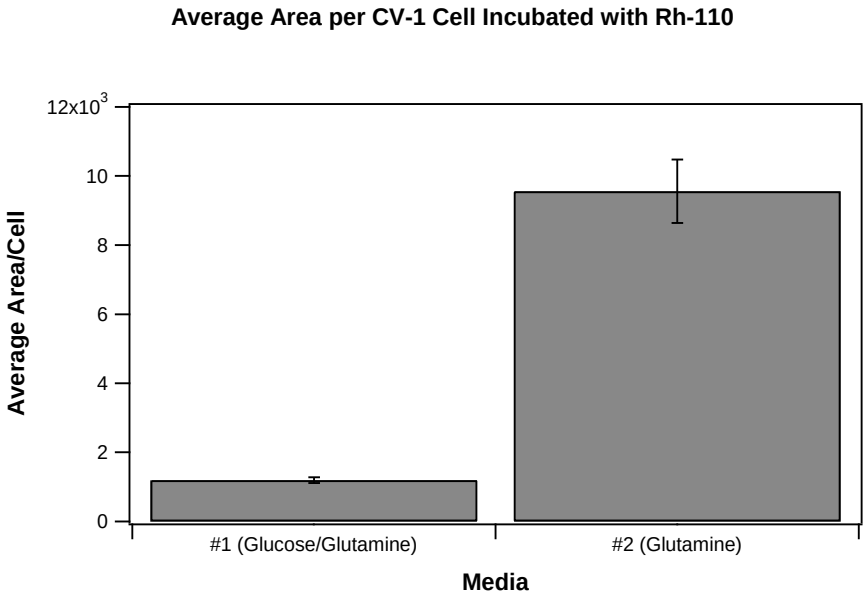

Figure 3.38 Average area comparison per cell of CV-1 cells previously grown in media #1 (optimal glucose/optimal glutamine) or in media #2 (no glucose/ high glutamine) for 12 days incubated in 1μM Rhodamine-110 for 1 hour.

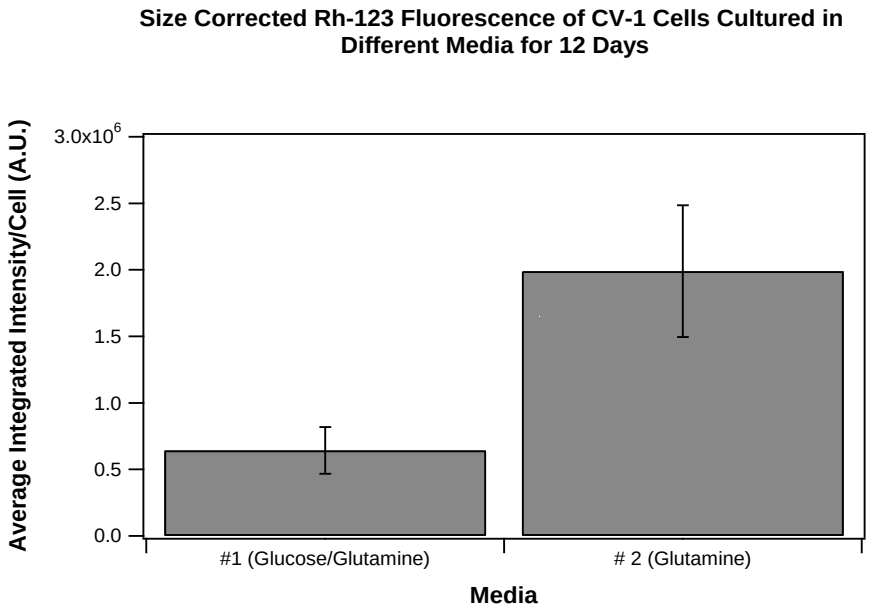

Figure 3.39 Size corrected fluorescence intensity comparison per cell of CV-1 cells previously grown media #1 (optimal glucose/optimal glutamine) or in media #2 (no glucose/ high glutamine) for 12 days incubated in 1μM Rhodamine-123 for 1 hour.

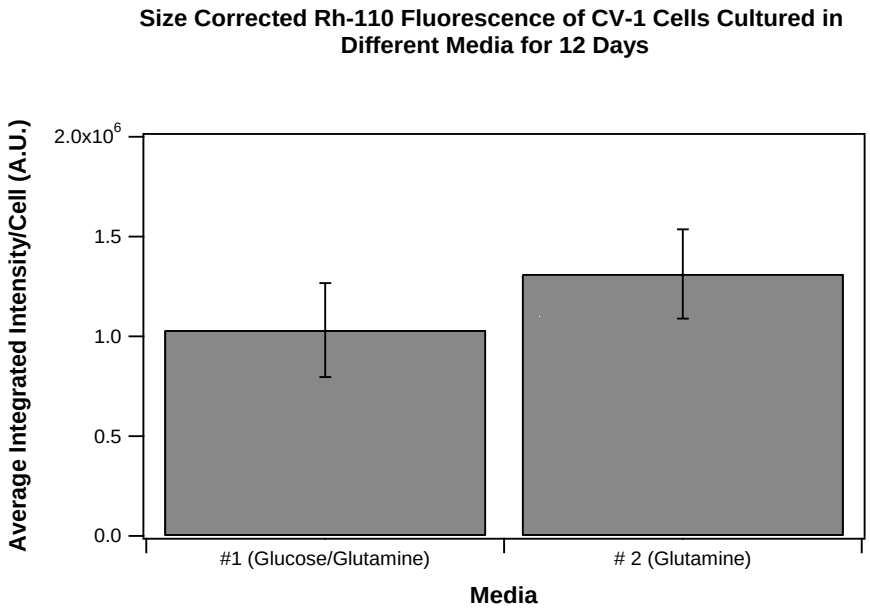

Figure 3.40 Size corrected fluorescence intensity comparison per cell of CV-1 cells previously grown in media #1 (optimal glucose/optimal glutamine) or in media #2 (no glucose/ high glutamine) for 12 days incubated in 1μM Rhodamine-110 for 1 hour.

difference in the cells cultured in media #2. Comparatively, there is not a significant difference in the lipophilicity between the two dyes; Rh-123 has one additional CH_3. However, at physiological pH, Rh-123 is a cation while Rh-110 is a zwitterion (pKa of its carboxylic group ~ 4.3 (Jeannot et al. 1997)). Our subcellular colocalization results as well as previous experiments have demonstrated that the rapid transmembrane transport process itself requires the protonated (cationic) form (Jeannot et al. 1997, Trapp and Horobin 2005, Horobin et al. 2007). An increase in pumping of protons to the intermembrane space in media #2 would potentially lead to an enhancement in the mitochondrial transmembrane potential and explain the enhanced uptake of Rh-123 observed in that media. The relatively small enhancement of Rh-110 uptake in media #2, as compared to media #1, is also in keeping with the idea that under our experimental conditions the transmembrane potential-driven mitochondrial localization of this zwitterionic dye is negligible. Therefore, the experimental results observed in these experiments suggest that the mitochondrial transmembrane potential may possibly have been enhanced by supplementing the growth media with an abundant supply of glutamine.

The above experimental results inspired another experiment in order to explore whether or not there would still exist an increase in Rh-123 uptake in the CV-1 cells cultured in a high glutamine media while also in the presence of optimal amounts of glucose. Here, a third media condition was introduced (media #3, optimal amounts of glucose and high amounts of glutamine) in which Rh-123 dye uptake could be compared for CV-1 cells cultured in media #1, media #2, and media #3 for 12 days. **Figure 3.41** and **Figure 3.42** show the size corrected fluorescence intensity comparison for those cells

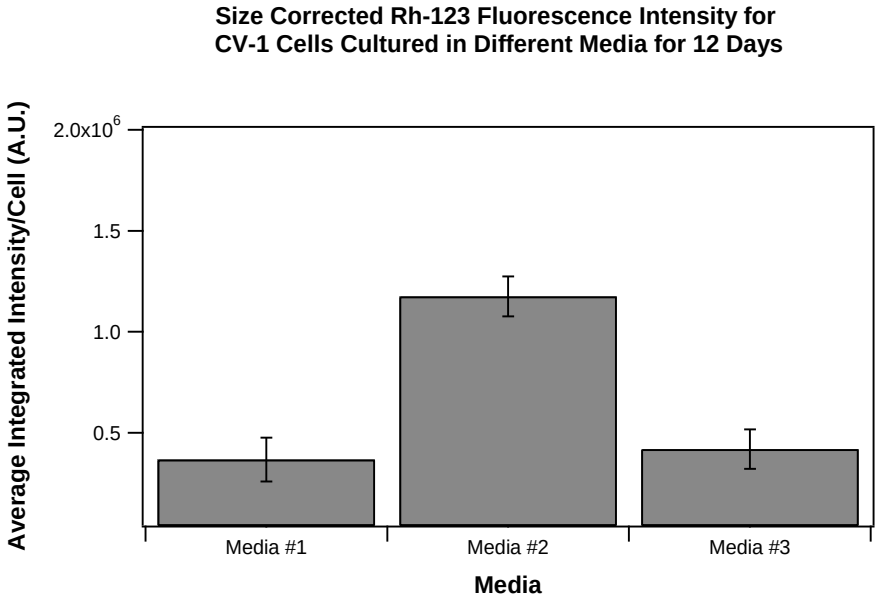

Figure 3.41 Size corrected fluorescence intensity comparison (1μM Rhodamine-123 for 1 hour) per CV-1 cell cultured in media #1 (optimal glucose/optimal glutamine), media #2 (no glucose/high glutamine), and media #3 (optimal glucose/high glutamine) for 12 days.

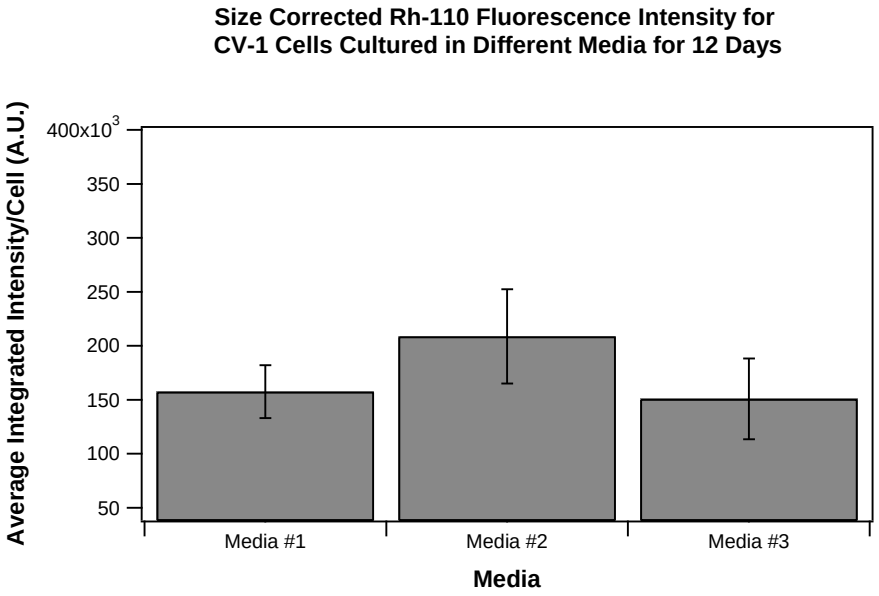

Figure 3.42 Size corrected fluorescence intensity comparison (1μM Rhodamine-110 for 1 hour) per CV-1 cell cultured in media #1 (optimal glucose/optimal glutamine), media #2 (no glucose/high glutamine), and media #3 (optimal glucose/high glutamine) for 12 days.

incubated with Rh-123 or Rh-110, respectively. After correcting for size, the average fluorescence intensity per cell for those incubated in Rh-123 was found to be nearly 3.2 times more for the cells cultured in media #2 compared to those cells cultured in media #1 and 1.1 times more for the cells cultured in media #3 compared to those cells cultured in media #1 (no statistically significant differences between media #1 and media #3). Likewise, in this experiment the average fluorescence intensity per cell for those incubated in Rh-110 is nearly 1.4 times more for the cells cultured in media #2 compared to those cultured in media #1 and only 1 times more for the cells cultured in media #3 compared to those cells culture in media #1 (also a result that does not appear to be statistically significant). The observed increase in dye uptake of both Rh-123 and Rh-110, for the cells cultured in media #2, confirms the trend observed in previous experiments. Interestingly, the cells cultured in a high glutamine media, also containing optimal amounts of glucose, did not display any significant increase in dye uptake. Therefore, it is reasonable to infer that the changes in cellular morphology and increase of dye uptake observed in media #2 can be satisfactorily attributed to the copious amounts of glutamine found in this last media, however, both phenomena (morphology changes and enhanced dye uptake) apparently only take place when the supply of glucose is limited.

3.3.5 Further Exploration of Glutamine Effects on the Cellular Morphology in CV-1 Cells

The changes in cellular morphology observed in the CV-1 cells cultures upon switching the growth media from one of optimal amounts of glucose and glutamine (media #1) to one of no glucose and high glutamine (media #2) inspired the design of

another two part experiment. The first was the effect on cellular morphology in CV-1 cells when the growth media was changed from media #1 to a media containing optimal amounts of glucose and no glutamine (media #4). The second was the effect on cellular morphology as well as the growth and proliferation of the significantly enlarged cells (previously grown in media #2 for 20 days) when switched back to optimal media (media #1) and subsequently cultured for 12 days. These experiments were carried out in order to gain a better understanding on how the amount of glutamine in the growth media can influence the growth and morphology of our CV-1 cells.

Figure 3.43 shows the typical morphologies of CV-1 cells at 1, 3, 6, 9, and 12 days when switched from media #1 to media #4. After 1 day, the cells were observed to be growing in a manner typical of the CV-1 cell line. In addition, no major changes in cellular morphology were observed. However, after 3 days the morphology of the cells appears to be slightly elongated and the cells are starting to stretch slightly. After 6 days, there was a significant amount of cell death observed in the culture. In addition, it seems that the cells exhibit an unhealthy, string-like appearance. This observation of increased cell death and string-like cellular morphology is present at 9 and 12 days as well. Furthermore, there was no major evidence of cellular proliferation observed at 6, 9, or 12 days. Therefore, the lack of glutamine in the cell culture media also results in a unique difference in cellular morphology in the CV-1 cells as well as well as increased cell death.

Keeping this in mind, it is reasonable to infer that glucose and glutamine are essential in maintaining a healthy cell culture over long periods of time. Both of these nutrients are needed to induce critical biosynthetic pathways and cell cycle regulators

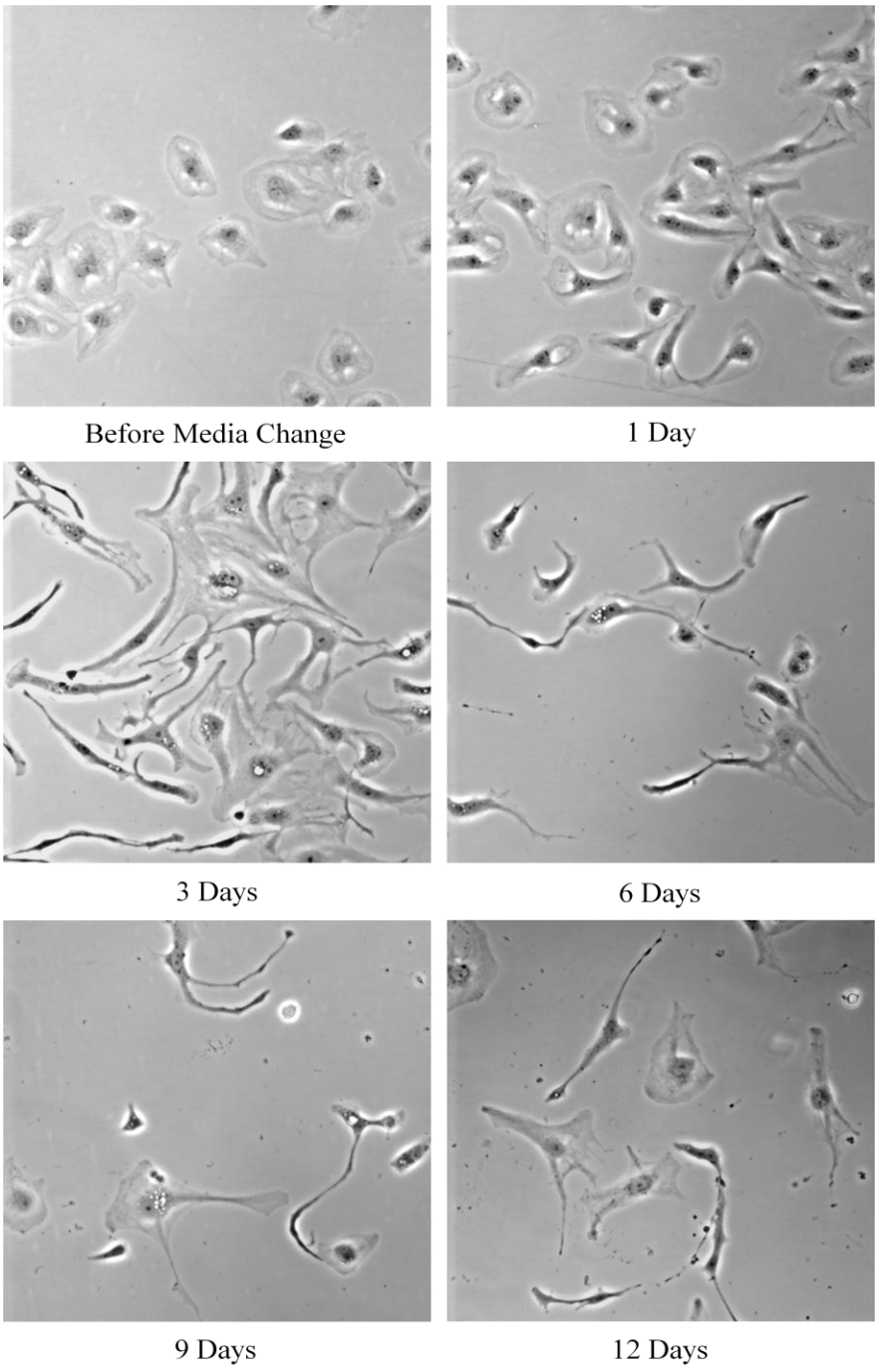

Figure 3.43 Bright field images (15x magnification) showing the different morphologies of CV-1 cells after being switched from media #1 (optimal glucose/optimal glutamine) to media #4 (optimal glucose/no glutamine) and cultured for 12 days.

which are required for cell division (Kaadige et al. 2009). In a series of experiments, Kaadige and colleagues demonstrated that both of these nutrients play independent roles in the induction of certain pathways and that the combination of both nutrients was found to induce multiple pathways which are required for cell division. Specifically, they found that cells grown in a media containing high amounts of glucose but lacking glutamine displayed low glucose uptake. Therefore, the results observed here further re-enforce the need for optimal amounts of both glucose and glutamine in order to maintain a healthy, proliferating cell culture.

Lastly, the effect on cellular morphology when switching the enlarged CV-1 cells, previously grown in media #2 for 20 days, back to media #1 (for 12 days) was investigated. **Figure 3.44** shows the distinctive morphologies that were observed after culturing the cells in media #2 for 20 days ("Before Media Change") as well as the morphologies seen at 5, 10, and 12 days when switched back to media #1. Before switching the growth media to media #1, they appear to be enlarged as well as very granular. After 5 days, in media #1 the cells were observed to be growing in a manner that is more common in a healthy CV-1 cell culture; the cells appear to be less granular as well as stretching near each other in a means of forming a monolayer. After 10 days, in media #1 it appears that there in an increased number of healthy cells in the culture as well as an increase in cellular proliferation with only a few of the enlarged cells remaining in the culture. After 12 days, it was observed that the cell culture appears to be similar to a normal, healthy CV-1 cell culture. Therefore, this experiment suggests that the morphology trend observed in the CV-1 cells cultured in media #2 could be reversed when switching the cells back to optimal media conditions. Furthermore, it can be

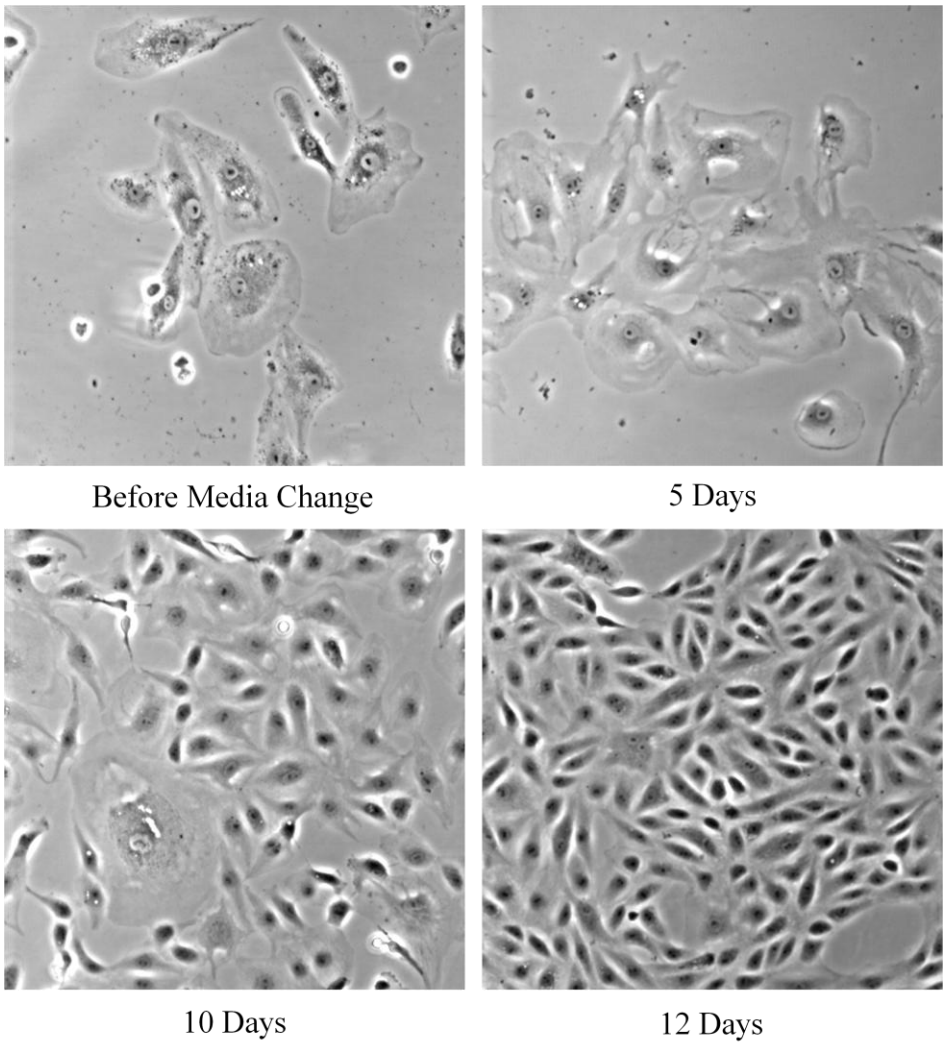

Figure 3.44 Bright field microscopy images showing the different morphology changes of CV-1 cells previously incubated in media #2 (no glucose/high glutamine) for 20 days and subsequently switched back to media #1 (optimal glucose/optimal glutamine).

concluded that the granular cells observed at 12 days in media #2 (part 3.3.3) are not senescent because the experimental results obtained here confirms that the enlarged cellular morphology observed at 12 days can be reversed.

The results observed here further re-enforces that optimal amounts of glucose and glutamine are needed for the normal cell growth and proliferation of CV-1 cells in culture. It is evident that there is a direct correlation between the addition of glucose to the growth media and the reversal of the cellular morphology observed in the cell culture previously incubated in media #2 for long time periods (20 days). In addition, this effect on cellular morphology does not appear to take place right away. That is, the cells previously grown in media #2 for 20 days started to reverted back to a normal growing pattern after 3 days when switched back to a media consisting of optimal amounts of glucose and glutamine (media #1). Therefore, the effect on cellular morphology observed when a lack of the appropriate amounts of glucose and glutamine were provided to the CV-1 cells, further supports the hypothesis that both glutamine and glucose are needed in combination in order to maintain a normal, healthy growing pattern in CV-1 cells for long time periods.

In summary, we have observed that there is a direct effect of the energy substrate availability on cellular morphology, and apparently also mitochondrial transmembrane potential in CV-1 cells. Our results indicate that there is a dramatic change in cellular morphology as well as an increase on Rh-123 and Rh-110 dye uptake evident at 12 days when removing all glucose from the growth media and supplementing it with excess glutamine. In addition, this change in cellular morphology can be reversed over time when the availability of glucose is restored. Lastly, we have demonstrated that glutamine,

in combination with glucose, is also needed by CV-1 cells in order to maintain a healthy growing pattern over long time periods. Overall, this pilot study has provided us with information on whether or not CV-1 cells could potentially be used as a single-cell model in which the effects of the mitochondrial transmembrane potentials on selective cell kill could be explored. Apparently, they cannot be used for that purpose. The observed changes in Rh-123 uptake are still modest (~3 fold) when compared to the typically observed (and/or predicted) 10 fold increase between normal and tumor cells. In addition, the morphology of CV-1 cells change continuously upon exposure to media #2, making it difficult to clock experiments so that all comparisons are made with cells showing the same morphology.

4. Conclusions

In this study we have performed a systematic evaluation on (i) how, and to which extent, the molecular structure of a series of rhodamine dyes affects the IR spectroscopic properties and fluorescence quantum yields, (ii) how molecular structure and charge affects the selectivity with which these dyes localize in energized mitochondria, and (iii) the extent to which substrate availability affect both cell morphology and dye uptake when using CV-1 cells as a model non-transformed cell line. Here, we have determined which structural modifications have the greatest impact on the fluorescence quantum yields of these dyes as well as the effect that these modifications have on mitochondrial localization. We have also determined that the availability of glucose or glutamine alone has a direct correlation on cellular morphology in CV-1 cells. Furthermore, we have observed that the stimulation of the anaplerotic pathway of glutaminolysis leads to a more pronounced increase in Rh-123 uptake as compared to Rh-110 uptake. These last experimental results provide an initial line of evidence suggesting that the mitochondrial transmembrane potential of normal (non-transformed) cells can be significantly affected by the composition of the media used to grow the cells.

First, our experimental results have indicated that there is a direct correlation between the molecular structure of our selected rhodamine dyes and their respective spectroscopic properties and fluorescence quantum yields. We have observed that there is a slight decrease in the fluorescence quantum yields as well as a small red shift in the wavelength of maximum dye absorption and the wavelength of maximum fluorescence emission upon the alkyl substitution of the carbonyl group of the respective free acid dyes (Rh-110, Rh6gFA, and RhB). In the same manner, it was observed that there was a

modest increase in the fluorescence quantum yields as well as a small blue shift in the wavelength of maximum dye absorption and the wavelength of maximum fluorescence emission upon the removal of the alkyl group from the ester linkages (Rh6gFA, RhBEE). In addition, our experimental results indicate that the fluorescence quantum yields decrease upon the increasing degree of alkylation of the amino groups of the respective parent dyes. Moreover, the substitution of bromine atoms of the rhodamine dyes, Rh-123 and Rh-Oct, results in a characteristic red shift in the wavelength of maximum absorption and the wavelength of maximum fluorescence as well as a significant decrease in the respective fluorescence quantum yields.

Second, we have addressed how molecular structure and charge affect the selectivity with which our selected rhodamine dyes localize in energized cell mitochondria. Here, our experimental results confirm the cationic requirement of rhodamine dyes for rapid and effective mitochondrial localization. In addition, we were able to confirm that the lipophilic character associated with our selected rhodamine dyes was low enough to preclude any competitive phenomenon of lipophilic partitioning on subcellular localization. Furthermore, our results indicate that any cationic (and cationic only) analog of the ideal mitochondrial localizing dye, Rh-123, (showing appropriate lipophilicity) is likely to localize in the energized cell mitochondria of CV-1 cells with great specificity. Therefore, any PDT agent with structural features and lipophilic character comparable to that of the prototypical cationic mitochondrial marker, Rh-123, should also localize in energized cell mitochondria with great specificity and subsequently induce targeted cell kill with a high degree of selectivity.

Lastly, we have explored the extent to which distinct energy substrate availability

in the cell culture media affects both cell morphology and dye uptake when using CV-1 cells as model normal (non-transformed) cells. Our experimental results indicate that optimal amounts of the main energy substrates, glucose and glutamine, are needed in combination for long-term growth and proliferation in CV-1 cells. We have observed that when either glucose or glutamine is limited, CV-1 cells display abnormal changes in cellular morphology and a decrease in cellular proliferation over long time periods. Moreover, our experimental results indicate that the change in cellular morphology observed when the supply of glucose is limited is reversible when the supply of glucose is restored. In addition, we have demonstrated that when the anaplerotic pathway of glutaminolysis is stimulated, there is a preferential increase in Rh-123 uptake as compared to Rh-110 uptake. The larger dye uptake effects observed for the cationic rhodamine (Rh-123) represents a first line of evidence suggesting that mitochondrial transmembrane potentials may be significantly affected by glutaminolysis when the cells experience glucose starvation.

5. References

Ahluwalia, G.S., J.L. Grem, Z. Hao, D.A. Cooney. "Metabolism and action of amino acid analog anti-cancer agents." *Pharmacol. Ther.* 46 (1990): 243-271.

Arbeloa, F.L., T. L. Arbeloa, M.J. Tapia Estevez, I.L. Arbeloa. "Photophysics of rhodamines. Molecular structure and solvent effects." *J. Phys Chem.* 95 (1991): 2203-2208.

Arbeloa, F.L., I. U. Aguirresacona, I.L. Arbeloa. "Influence of the Molecular Structure and the Nature of the Solvent on the Absorption and Fluorescence Characteristics of Rhodamines." *Chemical Physics* 130 (1989): 371-378.

Bartlett, J. "Chemical aspects of mitochondrial targeting in photodynamic therapy."*Doctor of Philosophy thesis, University of Wisconsin-Madison.* (2002).

Belostotsky, I., S.M. Silva, M.G. Paez, G.L. Indig. "Mitochondrial targeting for photochemotherapy. Can selective tumor cell killing be predicted based on n-octanol/water distribution coefficients?" *Biotechnic & Histochemistry*. 86 (2011): 302-314.

Bergmann, F., H. Stepp, R. Metzger, U. Rolle, A. Johannson, H. Till. "In vitro and in vivo evaluation of photodynamic techniques for the experimental treatment of human hepatoblastoma and neuroblastoma: preliminary results." *Pediatric Surg Int.* 24 (2008): 1331-1333.

Bernal, S.D., T.J. Lampidis, R.M. McIsaac, L.B. Chen. "Anticarcinoma activity in vivo of rhodamine 123, a mitochondrial-specific dye". *Science.* 222 (1993): 169–172.

Brasseur, N., I. Menard, A. Forget, R. El Jastimi, R. Hamel, N.A. Molfino NA, J.E. van Lier. "Eradication of multiple myeloma and breast cancer cells by TH9402-mediated photodynamic therapy: implication for clinical ex vivo purging of autologous stem cell transplants". *Photochem.Photobiol*. 72 (2000): 780–787.

Chen, L. B. "Fluorescent labeling of mitochondria." *Methods Cell Biol.* 29 (1989): 103-123.

Chen, L. B. "Mitochondrial membrane potential in living cells." *Ann. Rev. Cell Biology*. 4 (1988): 155-181.

Davis, S., M. J. Weiss, J. R. Wong, T. J. Lampidis, L. B. Chen. "Mitochondrial and plasma membrane potentials cause unusual accumulation and retention of rhodamine 123 by human breast adenocarcinoma-derived MCF-7 cells." *J. Biol. Chem.* 260 (1985): 13844-13850.

DeBerardinis, R. J., A. Mancuso, E. Daikhin, I. Nissim, M. Yudkoff , S. Wehrli , C.B. Thompson. "Beyond aerobic glycolysis: Transformed cells can engage in glutamine metabolism that exceeds the requirement for protein and nucleotide synthesis." *Proc. Natl. Acad. Sci.* 101 (2007): 19315-19350.

Demas, J. N. and G.A. Crosby. "The measurement of photoluminescence quantum yields. A review." *J. Phys. Chem.* 75 (1971): 991-1024.

Dolmans, D.E.J.G.J., D. Fukumura and R.K. Jain. "Photodynamic therapy for cancer." *Nature.* 3 (2003): 380-387.

Dougherty, T. J., "Photochemistry in the treatment of cancer". *Adv. Photochem.* 17 (1992): 275-311.

Dougherty, T. J., H.R. Withers, L.J. Peters . "Photodynamic therapy." *Medical Radiology - Innovations in Radiation Oncology.* (1988): 175-188.

Dougherty, T. J., J. E Kaufman, A. Goldfarb, K. R Weishaupt, D. Boyle and A. Mittleman. "Photoradiation therapy for the treatment of malignant tumors". *Cancer Res.* 38 (1978): 2628–2635.

Duxbury, D. F., "The photochemistry and photophysics of triphenylmethane dyes in solid and liquid media". *Chem. Rev.* 93 (1993): 381-433.

Eagle H. "Nutrition needs of mammalian cells in tissue culture". *Science* 122 (1955):501-504.

Eigenbrodt, E. and S. Mazurek. Metabolic Database. http://www.metabolicdatabase.com /html/glutaminolysis_energy_scheme.html (September 13, 2011).

Ferlay, J., H.R. Shin, F. Bray, D. Forman, C. Mathers and D. M. Parkin. " Estimates of worldwide burden of cancer in 2008." *GLOBOCAN 2008. International Journal of Cancer*. 127 (2010): 2893–2917.

Horobin, R.W., D. Trapp, V. Weissig. "Mitochondrictropics: a review of their mode of action, and applications for drug and DNA delivery to mammalian mitochondria." *J. Control. Rel.* 121 (2007) 125–136.

Huang, H.F., Y.Z. Chen, Y. Wu, P. Chen. "Purging of murine erythroblastic leukemia by $ZnPcS_2P_2$-based-photodynamic therapy." *Bone Marrow Transplantation*. 37(2006): 213-217.

Indig, G. "Mechanisms of action of cationic dyes in photodynamic therapy of tumors." Recent Res. Devel. Pure & Applied Chem., 3 (1999): 9-19.

Indig, G.L., G.S. Anderson, M.G. Nichols, J.A. Bartlett, W.S. Mellon, F. Sieber. "Assessment of crystal violet and other triarylmethane dyes as photosensitizers for purging of autologous bone marrow grafts from residual tumor cells". *J. Pharm. Sci.* 89 (2000): 88-99.

Jeannot, V., J.M. Salmon, M. Deumie, P. Viallet. "Intracellular accumulation of rhodamine 110 in single livingcells" *J. Histochem. Cytochem.* 45 (1997): 403-412.

Johnson, L. V., M. L. Walsh, B. J. Bockus, L. B. Chen. "Monitoring of relative mitochondrial membrane potential in living cells by fluorescence microscopy." *J. Cell Biol.* 88 (1981): 526-535.

Kaadige, M.R., R.E. Looper, S. Kamalanaadhan, D.E. Ayer. "Gluamine-dependant anapleurosis dictates glucose uptake by regulating MondoA transcriptional activity." *Proc. Natl. Acad. Sci.* 106 (2009): 14878-14883.

Kandela, I. K., J. A. Bartlett, G. I. Indig. "Effect of molecular structure on the selective phototoxicity of triarylmethane dyes toward tumor cells." *Photochem. Photobiol. Sci.* 1 (2002): 309-314.

Kandela, I.K., W. Lee, G.L. Indig. "Effect of the lipophilic/hydrophilic character of cationic triarylmethane dyes on their selective phototoxicity toward tumor cells." *Biotech. & Histochem.* 78 (2003) 157–169.

Kasha, M., H. R. Rawls. "Correlation of orbital classification of molecular electronic transitions with transition mechanism: the aromatic amines." *Photochem. Photobiol.* 7 (1968): 561-569.

Kessel, D., and NL. Oleinick. "Initiation of Autophagy by Photodynamic Therapy." *Methods Enzymol*. 453 (2009): 1-16.

Khan, A. U., T. Wilson. "Reactive oxygen species as cellular messengers." *Chem. and Biol.* 2 (1995): 437-445.

Kovacevic, Z. and J.D. McGivan. "Mitochondrial metabolism of glutamine and glutamate and its physiological significance". *Physiological Reviews*. 63 (1983): 547-605.

Lacerda, S. H. D., B. Abraham, T. C. Stringfellow, G. L. Indig. "Photophisical, photochemical, and tumor-selectivity properties of bromine derivatives of Rhodamine 123." *Photochem. Photobiol.* 81 (2005): 1430-1438.

Lampidis, T. J, C. Salet, G. Moreno, L. B. Chen. "Effects of the mitochondrial probe rhodamine 123 and related analogs on the function and viability of pulsating myocardial cells in culture." *Agents Actions.* 44 (1984): 751-757.

Lipson, R.L., E.J. Baldes and A.M. Olsen. "The use of an derivative of hematoporphyrin in tumor detection." *J. Natl Cancer Inst.* 26 (1961): 1-11.

Maeda, H. "The enhanced permiability and retention (EPR) effect in tumor vasculature: the key role of tumor-selective macromolecular drug targeting". *Advan. Enzyme Regul.* 41 (2001): 189-207.

Mchedlov-Petrossyan, N.O., I.V. Kukhtik, I.V. Alekseeva. " Ionization and tautomerism of fluorescein, rhodamine B, N,N-diethylrhodol and related dyes in mixed and nonaqueous solvents " *Dyes and Pigments* 24 (1994): 11-35.

Matsuno, T., T. Satoh, H. Suzuki. "The pathway of glutamate oxidation in isolated mitochondria from the avian hepatomatous growth induced by MC-29 virus. " *J. Cell Physiol* 130 (1987): 171.

Mitchell, P. "Coupling of phosphorylation to electron and hydrogen transfer by a chemi-osmotic type of mechanism". *Nature* 191 (1961): 144–148.

Mizushima, N., T. Yoshimori, B. Levine. "Methods in mammalian autophagy research." *Cell*. 140 (2010): 313.

Moan, J. and K. Berg. "The photodegradation of porphyrins in cells can be used to estimate the lifetime of singlet oxygen." *Photochem Photobiol*. 53 (1991): 549–553.

Moan, J. and Q. Peng. "An outline of the history of PDT". In Thierry Patrice. *Photodynamic Therapy* . Comprehensive Series in Photochemistry and Photobiology. 2 (2003) 1–18.

Modica-Napolitani, J.S. and J.R. Aprille. "Delocalized lipophilic cations selectively target the mitochondria of carcinoma cells." *Adv. Drug Delivery Rev.* 49 (2001): 63-70.

Morgan, J., Whitaker J.E. and A.R. Oseroff. "GRP78 induction by calcium ionophore potentiates PDT using the mitochondrial targeting dye Victoria Blue BO." *Photochem Photobiol.* 67 (1998): 155-164.

Nelson, D.L. and M.L Cox. " Lehninger: Princliples of Biochemistry." *W.H. Freeman and Company.* (2008).

Nicklin, P., P. Bergman, B. Zhang, E. Triantafellow, H. Wang, B. Nyfeler, H. Yang, M. Hild, C. Kung, C. Wilson, V. E. Myer, J. P. MacKeigan, J.A. Porter,Y. K. Wang, L.C. Cantley, P.M. Finan, L. O. Murphy. "Bidirectional Transport of Amino Acids Regulates mTOR and Autophagy." *Cell.* 136 (2009): 521-534.

Osseroff, A.R., D. Ohuoha, G. Ara, D. McAuliffe, J. Foley, L. Cincotta. "Intramitochondrial dyes allow selectivein vitro photolysis of carcinoma cells." *Proc. Natl. Acad. Sci.USA.* 83 (1986): 9729-9733.

Pal, P., H. Zeng, G. Durocher, D. Girard, T. Li, A. K. Gupta, R. Giasson, L. Blanchard, L. Gaboury, A. Balassy, C. Turmel, A. Laperriere, L. Villeneuve. "Phototoxicity of some bromine substituted rhodamine dyes: synthesis, photophisical properties and applications as photosensitizers." *Photochem. Photobiol.* 63 (1996): 161-168.

Remington's Pharmaceutical Sciences, E, Gennaro, A. R., Chase, G. D., Marderosian, A. D., Harvey, S. C., Hussar, D. A., Medwick, T., Rippie, E. G., Schwartz, J. B., Swinyard E. A., Gilbert Z. L., Eds., *Mack Publishing Company*, Easton, PN, 1990.

Rossignol, R., R. Gilkerson, R. Aggeler, K. Yamagata, S.J. Remington, R.A. Capaldi. "Energy Substrate Modulates Mitochondrial Structure and Oxidative Capacity in Cancer Cells." *Cancer Research.* 64 (2004): 985-993.

Schastak, S., B. Handzel, R. Hermann, P. Wiedemenn. "Improved photoinactivation of gram-negative and gram-positive methicilline-resistant bacterial strains using a new near-infrared absorbing meso-tetrahydroporphyrin: a comparative study with a chlorine e6 photosensitizers." *Methods Find. Exp. Clin. Pharmacol.* 30 (2008): 129-133.

Shea, C. R., N. Chen, T. Hasan. "Dynamic aspects of rhodamine dye photosensitization in vitro with an argon-ion laser." *Laser in Surgery and Medicine* 9 (1989): 83-89.

Sikder, S., J.M.G. Reyes, C.S. Moon, O.S. Apichon, J.H. Elisseeff, R.S. Chuck. "Noninvasive mitochondrial imaging in live cell culture." *Photochem. Photobiol.* 81 (2005): 1569-1571 .

Sorokina, M. "A comparative study on triarylmethane, phenothiazine and rhodamine dyes as potential photosencitizers for antibacterial photodynamic therapy." *Master's thesis, University of Wisconsin-Milwaukee.* (2009).

Soukos, N. S., M. Wilson, T. Burns, P. M. Speight. "Photodynamic effects of toluidin blue on human oral keratinocytes and fibroblasts and Streptococcus sanguis evaluated in vitro." *Lasers Serg. Med.* 18 (1996): 253-259.

Stewart, F., P. Baas, W. Star. "What does photodynamic therapy have to offer radiation oncologists (or their cancer patients)? ". *Radiother Oncol.* 48 (1998): 233-48

Summerhayes, I.C., T.J. Lampidis, S.D. Bernal, J.J. Nadakavukaren, K.K. Nadakavukaren, E.L. Shepherd, L.B. Chen. "Unusual retention of rhodamine 123 by mitochondria in muscle and carcinoma cells." *Proc. Natl. Acad. Sci.* 79 (1982): 5292-5296.

Tappeiner, H. von, and H. Jesionek. "Therapeutische Versuche mit fluoreszierenden Stoffen". *Munch. Med. Wschr.* 50 (1903): 2042–2044.

Tardivo, J. P., A. Del Giglio, L. H. Paschoal, A. S. Ito, and M. S. Baptista. "Treatment of melanoma lesions using methylene blue and RL50 light source." *Radiodiagn. Photodyn. Ther.* 1 (2004): 345-346.

Trapp, S. and R.W. Horobin. "A predictive model for the selective accumulation of chemicals in tumor cells." *Eur. Biophys. J.* 34 (2005): 959-966.

Turro N.J. "Modern Molecular Photochemistry." *Benjamin/Cummings.* (1978): 185–195.

Villeneuve, L. "Ex vivo photodynamic purging in chronic myelogenous leukaemia and other neoplasias with rhodamine derivatives". *Biotechnol. Appl. Biochem.*30 (1999): 1–17.

Vogel, M, and W. Rettig. "Efficient intramolecular fluorescence quenching in triphenylmethane dyes involving excited states with charge separation and twisted conformations " *J. Phys. Chem.* 89 (1985): 962-968.

Wise, D. R., R. J. DeBerardinis , A. Mancuso , N. Sayed , X. Zhang , H.K. Pfeiffer , I. Nissim , E. Daikhin , M. Yudkoff , S.B. McMahon , C. B. Thompson . "Myc regulates a transcriptional program that stimulates mitochondrial glutaminolysis and leads to glutamine addiction." *Proc. Natl. Acad. Sci.* 105 (2008): 18782-18787.

Wise, D.R. and C.B. Thompson. "Glutamine addiction: a new therapeutic target in cancer." *Trends Biochem Sci.* 35 (2010): 427-433.

Young, V.R. and A.M. Ajami. "Glutmaine: the emperor or his clothes?" *J. Nutr.* 131 (2001): 2449-2459.

Woislawski, S. "The spectrophotometric determination of ionization constants of basic dyes". *J. Am. Chem. Soc.* 75 (1953): 5201-5203.

Wullschlrger, S., R. Loewith, M.N. Hall. "TOR signaling in growth and metabolism." *Cell*. 124 (2006): 471-484.